NOVA SCHOOL OF SCIENCE & TECHNOLOGY

UNIVERSIDADE DE ÉVORA

DEPARTMENT OF EARTH SCIENCES

BORA AGBULUT

BSc in Geological Engineering

PALYNOSTRATIGRAPHY OF THE EARLY CRETACEOUS (HAUTERIVIAN-BARREMIAN) MUNK MARL BED OF THE NORTH SEA

MASTER IN PALEONTOLOGY

NOVA University Lisbon

NOVEMBER, 2023

NOVA SCHOOL OF SCIENCE & TECHNOLOGY

DEPARTMENT OF EARTH SCIENCES

PALYNOSTRATIGRAPHY OF THE EARLY CRETACEOUS (HAUTERIVIAN-BARREMIAN) MUNK MARL BED OF THE NORTH SEA

BORA AGBULUT

BSc in Geological Engineering

Adviser: Lígia Castro
Assistant Professor, NOVA School of Science and Technology

Co-adviser: Manuel Vieira
Doctor Senior Stratigrapher, Aker BP, ASA

Examination Committee:

Chair: Paulo Legoinha,
Full Professor, NOVA School of Science and Technology

Rapporteurs: Gil Machado,
Doctor, Chronosurveys, Lda

Adviser: Ligia Castro,
Assistant Professor, NOVA School of Science and Technology

MASTER IN MSC PALEONTOLOGY

NOVA School of Science and Technology
November, 2023

Palynostratigraphy of the Early Cretaceous (Hauterivian-Barremian) Munk Marl Bed of North Sea, Norway

"The supreme guide in life is science."

(Mustafa Kemal ATATURK)

ACKNOWLEDGMENTS

I would like to express my gratitude to my supervisor Prof. Lígia Castro for all her support and help from the beginning to the end of my thesis process. I would also like to express my gratitude and appreciation to my Co-Supervisor Doctor Manuel Vieira, who shaped and shaped my thesis with his interest and guidance from the very beginning of my thesis and also provided the necessary specimens and palynological slides for my thesis and sent us the specimens from Norway.

I would also like to express my gratitude to Mr. Bruno Camilo Silva, director of the Sociedade de História Natural, who has been very supportive both technically and morally during my thesis process.

This study was supported by Aker BP with the provision of samples and help with laboratory treatment.

''Believe it, but suspect it.''

Tamerlane (Amir Temur).

ABSTRACT

This study aims to provide a comprehensive palynostratigraphic overview of the Munk Marl Bed (part of the Åsgard Formation), highlighting key findings and contributions to the field. The results discussed herein offer valuable insights into the depositional environment, fossil assemblages, and paleoclimatic conditions of the Early Cretaceous North Sea region. In this study, 19 core samples were selected and prepared from 1918 m to 1925 m of the 16/2-21 well, to evaluate in detail an Early Cretaceous section in the Utsira High area (North Sea, Norway). The examination and analysis of the palynofloral assemblage, including the identification of key diagnostic palynomorphs and their stratigraphic distribution in relation to an established reference zonation scheme, was conducted to infer the biostratigraphy and paleoenvironmental reconstruction of the studied section along the Åsgard Formation. On the other hand, this study also evaluates the application of machine learning and deep learning methods to the automatic detection and recognition of dinoflagellate cysts using the specie *Batioladinium longicornutum* as an example. A large dataset of images (1453) of species was collected representing various classes of the target variable. These images were used to train a deep-learning model implemented in Python using the Tensorflow library. The overall focus is to interpret the biostratigraphy of the Hauterivian-Barremian interval of the Munk Marl Bed from North Sea region.

Keywords: Palynology, Early Cretaceous, North Sea, Munk Marl Bed

RESUMO

Este estudo tem como objetivo fornecer uma visão global da palinostratigrafia do Munk Marl (parte da Åsgard Formation) com novas contribuições para a área de palinologia. Este estudo permitiu fornecer informações valiosas sobre o ambiente deposicional, a associação de fósseis e as condições paleoclimáticas da região do Mar do Norte durante o Cretácico Inferior. Neste estudo, foram selecionadas e preparadas 19 amostras da sondagem 16/2-21 (1918-1925 m), para avaliar em pormenor uma secção do Cretácico Inferior na zona de Utsira High (Mar do Norte, Noruega). A associação de palinomorfos, incluindo a identificação dos palinomorfos diagnósticos e a sua distribuição estratigráfica relativamente à zonação de referência estabelecida permitiu inferir a reconstituição biostratigráfica da secção estudada ao longo da Formação Åsgard. Por outro lado, este estudo também avalia a aplicação de métodos de *machine learning e deeplearning* na deteção e reconhecimento automático de dinoquistos, utilizando como exemplo a espécie *Batioladinium longicornutum*. Foi recolhido um conjunto de 1453 imagens, representando várias classes da variável alvo, que permite distinguir a espécie alvo, o seu estado de conservação e algumas características morfológicas únicas. As imagens foram utilizadas para treinar um modelo de *deeplearning* implementado, em Python, com recurso à biblioteca Tensorflow. O objetivo geral é interpretar a biostratigrafia do intervalo Hauteriviano-Barremiano do Munk Marl Bed da região do Mar do Norte.

Palavras-chave: Palinologia, Cretácico Inferior, Mar do Norte, Munk Marl Bed

CONTENTS

LIST OF FIGURES

ACRONYMS

BP – British Petroleum.

CNN – Convolutional Neural Network

NATO – North Atlantic Treaty Organization.

NPD – Norwegian Petroleum Directorate

1

INTRODUCTION

Marine sedimentary deposits offer unique opportunities for utilizing palynostratigraphy to characterize geological formations and achieve high resolution age-dating (Nohr-Hansen et al., 2020). The Early Cretaceous MMB (Munk Marl Bed) is a key marker bed across the North Sea region, defined by organic-rich, laminated fine-grained sediments bounded by bioturbated organic-poor mudstones, marlstones, or marly chalks (Jeremiah, 2000; Copestake et al., 2003). It is a condensed interval, part of the Åsgard Formation, composed by dark, laminated claystone facies believed to be of transgressive nature and represent a maximum flooding surface in some areas (Garrett et al., 2000). The occurrence of this bed has attracted significant attention from researchers seeking to understand the paleoenvironmental and paleoecological conditions during this period. The Munk Marl is not always easy to define in wireline logs or composite well logs due to the similar or locally higher gamma marls, so the biostratigraphy plays an important role to help geologists understand the subsurface in higher detail (Dalseg et al., 2016; Oosting et al., 2006).

This thesis aims to provide a comprehensive overview of previous studies conducted on the MMB, highlighting key findings and contributions to the regional biostratigraphy. The studies discussed herein offer valuable insights into the depositional environment, fossil assemblages, and paleoclimatic conditions of the Early Cretaceous in the North Sea region.

In this study, 19 core samples (9 of them poorly preserved) were selected and prepared from 1918 m to 1925 m of the 16/2-21 well, to evaluate in detail an Early Cretaceous section from the Åsgard Formation in the Utsira high area (North Sea, Norway). The examination and analysis of the palynofloral assemblage, including the identification of key diagnostic palynomorphs and their stratigraphic distribution in relation to an established reference zonation scheme, was conducted to infer the biostratigraphic and paleoenvironmental reconstruction of the studied section along the Åsgard formation.

1.1 Locality of the Study

For this study the well 16/2-21 (58° 46' 40.76'' N, 2° 36' 38.77'' E) was selected, drilled in the Norwegian Continental Shelf during the appraisal of the Johan Sverdrup field in the Utsira High area (Fig.1). The Johan Sverdrup oil field represents a significant discovery in the North Sea, with reserves estimated at several billion barrels of oil. It is operated by Equinor and its partners are Petoro, Aker BP and Total Energies.

The well was sampled over the depth interval of 1918 m to 1925 m comprising the previously interpreted Munk Marl interval, part of the regional Early Cretaceous Åsgard Formation.

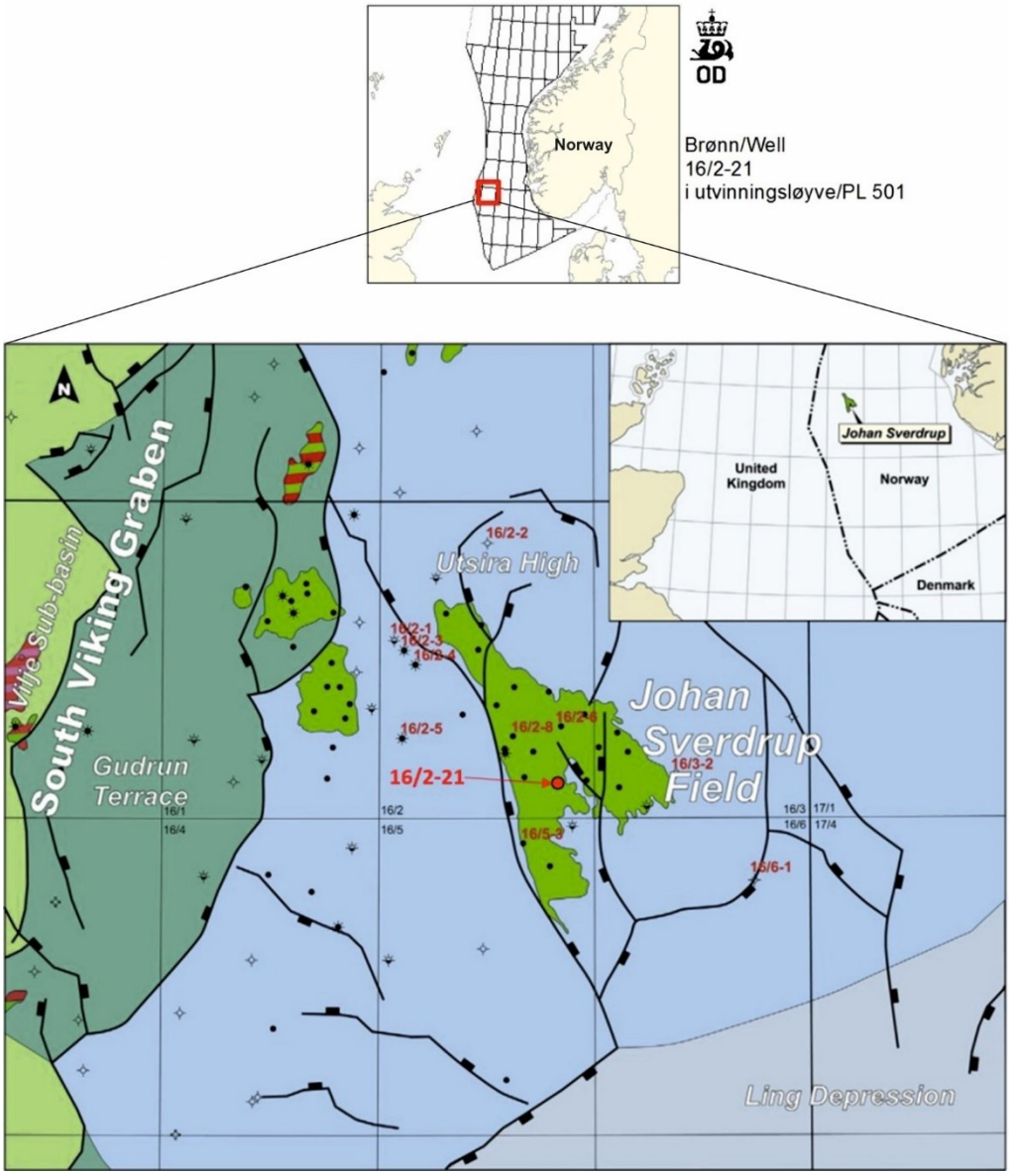

Figure 1. Location of the studied well. Modified from (NPD, 2016; Olsen et al., 2017)

1.2 Study Objectives

The aim of the study is to describe in detail the palynoflora of the MMB using core samples. This type of samples provides a reliable source of data when compared with traditional analyses using drilling cuttings.

- The main objective is also to identify all the different types of palynomorphs: dinoflagellate cysts, pollen and spores and acritarchs. By using these finds, it is aimed to create a high resolution palynostratigraphy of this stratigraphic interval and to facilitate correlations with other oil wells in the region and similar formations.

- To infer the palynostratigraphic reconstitution of the studied section along the Åsgard Formation and, more specifically, in the MMB.

- 19 samples were collected and analyzed from borehole 16/2-21 (1918-1925m), Lower Cretaceous of the Åsgard Formation, in the Utsira High area.

Evaluated the application of deep learning models with convolutional neural network (CNN) architectures in Python to create prediction models for the key marker species *Batioladinium longicornutum*, with the aim of improving correlation for further studies from the region.

2

GEOLOGICAL CONTEXT

The North Sea region is a geologically complex area, with a long and varied history. The oldest rocks in the region date back to the Precambrian era whichconstitute the basement of the sedimentary fill.. The sedimentary rocks in the North Sea region were deposited over a period from the Silurian to the Quaternary. These rocks are divided into a several different groups and formations, each of which has its own unique characteristics (Fig.2). In this study the focused interval is the Early Cretaceous of Norwegian North Sea defined by the Cromer Knoll lithostratigraphic Group in the Utsira High area. The Utsira High is a relatively young geological feature, dating back to the Late Jurassic epoch. It is located in the central North Sea (Stanley Duxbury, 1977; Isaksen & Tonstad, 1989; Mutterlose & Harding, 1987).

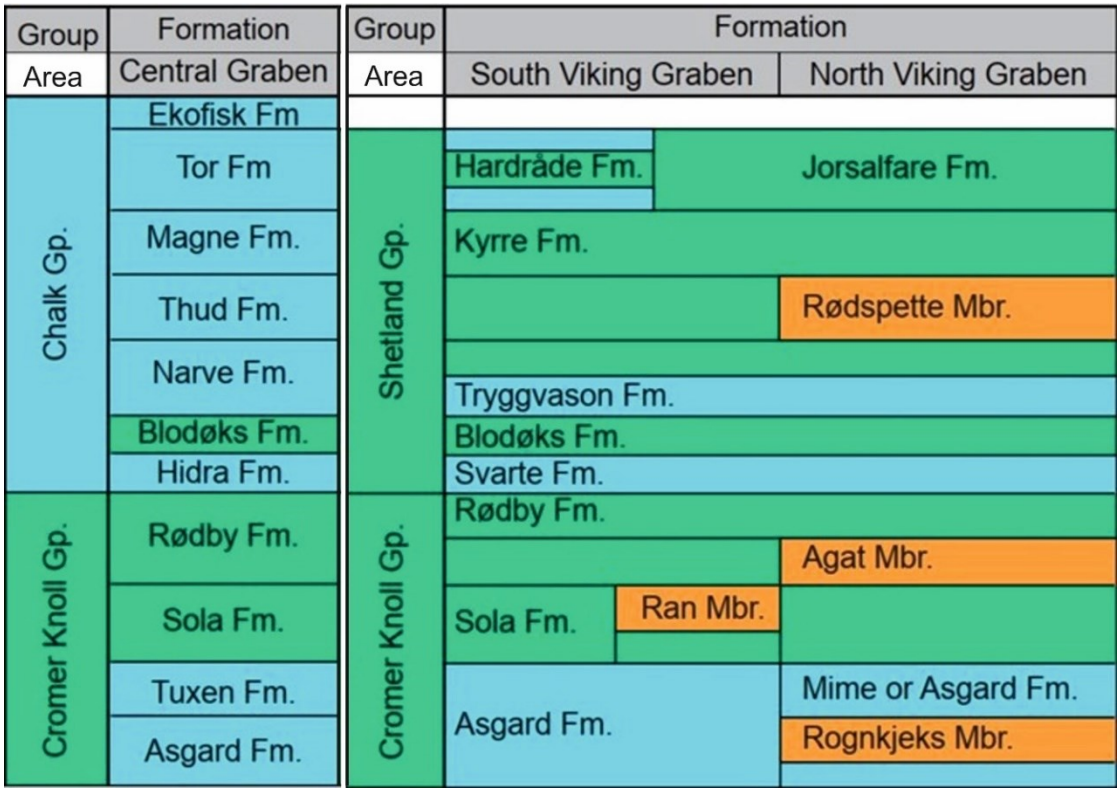

Figure 2. General lithostratigraphy of the Cromer Knoll Group, Shetland Group and Chalk Group cross three areas of the Norwegian North Sea (modified from NPD, 2020).

2.1 Cromer Knoll Group

The Cromer Knoll Group is a Lower Cretaceous sedimentary rock unit that spans most of the North Sea area across the UK and Norwegian continental shelf. It is widely distributed and consists mainly of fine-grained, argillaceous, marine sediments with a varying content of calcareous material. Calcareous claystones, siltstones and marlstones dominate, but subordinate layers of limestone and sandstone occur (Petersen, et al., 2022). The group was deposited in an open marine environment, with generally low energy. In the studied area the Cromer Knoll is divided into six formations: the Åsgard, Tuxen, Mime, Sola, Rødby and Agat formations. The Cromer Knoll Group is thought to have been deposited from the Berriasian to Albian/Early Cenomanian stages of the Cretaceous period. The group provides insights into the geological history of the North Sea region and the potential for hydrocarbon deposits (Bøe et al., 2010; Rønnevik et al., 2017; Van Buchem et al., 2018).

Above the Cromer Knoll Group we find the Late Cretaceous Chalk or the Shetland groups. During the Late Cretaceous the southern part of the North Sea Basin formed a shallow marine basin allowing the deposition of chalk facies, which consists of chalky limestones, limestones, marls, and calcareous shales and rarer mudstones forming the Chalk Group, but this laterally changes to a more mudstone dominated environment toward the north defining the Shetland Group.

2.2 Åsgard Formation

The Åsgard is the oldest formation of the the Cromer Knoll Group. It is typically around 100 meters thick but can be as thick as 200 meters in some places. The formation is composed of a variety of sedimentary rocks, including fine-grained to medium-grained sandstones, dark gray to black mudstones, and grey to green shales (Fig.3). The sandstones are often cross-bedded, while the mudstones are often organic-rich, and the shales are often thinly bedded. The Åsgard Formation is thought to have been deposited in a shallow marine environment, possibly a deltaic setting, according to the pointed crossbedding structures during the late Hauterivian to early Barremian stages of the Lower Cretaceous (Jensen et al., 1986). The Åsgard Formation is an important geological unit in the North Sea, as it contains hydrocarbon deposits in some areas (Graversen, 2016; Martinsen & Dreyer, 2001; Zwaan, 2019).

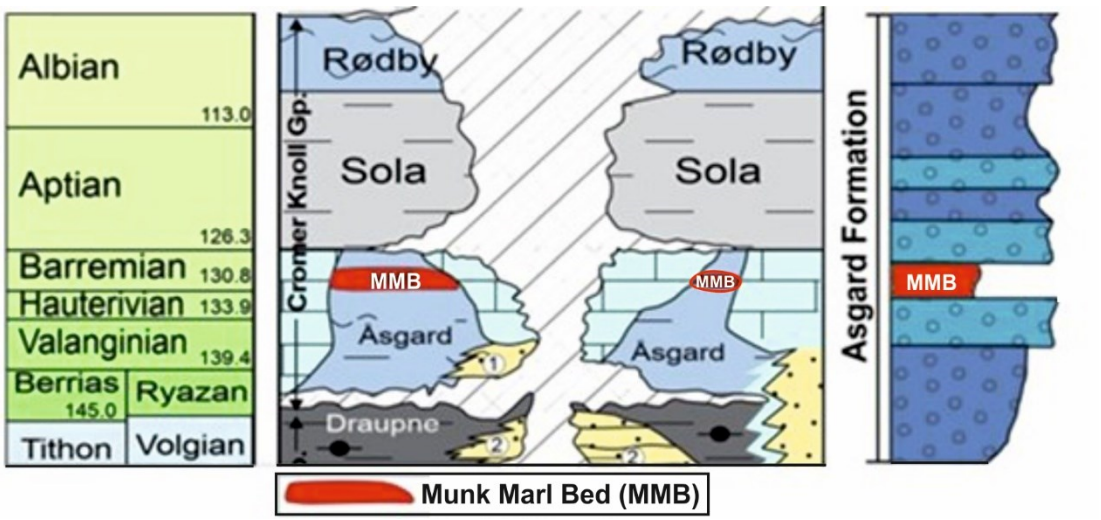

Figure 3. Lithostratigraphy of the Munk Marl Bed from the North Sea Utsira High. Stratigraphic column section is not to scale and represents the region of the drilling well (modified from Lundin, 2017; van Buchem et al., 2017).

2.3 Munk Marl Bed

Jensen et al. (1986) described a 0.3 to 1 m thick black, laminated, pyritic shaly bed of claystone with algal-rich organic matter content (Jensen et al., 1986), which they named the MMB. They proposed the MMB as a new key bed in the Danish North Sea.

Crittenden et al. (1991) equated the MMB with the Blätterton facies of the early to mid-Barremian of north-west Germany.

Garrett et al. (2000) agreed with Crittenden et al. (1991) that the MMB represents a period of maximum regional flooding. They also suggested that the MMB may have been deposited during the 'latest' Early Barremian, contemporaneous to a major transgressive pulse that led to anoxic, locally dysaerobic, bottom waters.

(Ainsworth et al., 2000) concurred with the findings of Jensen et al. (1986), Crittenden et al. (1991), and Garrett et al. (2000). They also noted that the MMB is a significant stratigraphic marker in the Danish North Sea.

It is important to note that the MMB is a relatively new discovery, and there is still some debate about its exact age and origin. However, the research conducted by Jensen et al. (1986), Crittenden et al. (1991), Garrett et al. (2000), and Ainsworth et al. (2000) has helped to shed light on this important stratigraphic unit. The MMB is better defined in the Danish North Sea region. In that area it is part of the Tuxen Formation, which was also deposited during the Early Cretaceous epoch (Jelby et al., 2022). The Tuxen Formation consists of a

sequence of mudstones, siltstones, and sandstones that were deposited in a shallow marine environment, (Glad et al., 2022).

The MMB is particularly rich in fossils, including foraminifera, dinoflagellates, and calcareous nannofossils, which have been extensively studied (Jelby et al., 2022). The dinoflagellates found in the MMB have been used to refine the biostratigraphy of the Barremian, particularly in the North Sea region (Lauridsen et al., 2022).

The Åsgard Formation is also rich in macrofossils, including ammonites, belemnites, bivalves, and brachiopods (Ineson, Petersen, et al., 2022). The formation has been extensively studied for its paleoenvironmental and paleogeographic implications, particularly in relation to the breakup of the supercontinent Pangaea and the subsequent opening of the Atlantic Ocean (Nohr-Hansen et al., 2020).

2.4 Lithology

The MMB is mainly composed of laminated, organic-rich mudstones and shales with abundant dinoflagellate cysts and foraminifera (Lauridsen et al., 2022). The authors also report the occurrence of thin sandstone layers with bioturbation and trace fossils. Jelby et al. (2022) described the MMB as a sequence of dark grey to black mudstones and shales with intercalated thin sandstone beds.

The Åsgard Formation consists of dark organic-rich mudstones and shales with varying biogenic silica and carbonate content, occasionally featuring thin layers of siltstones and sandstones (Glad et al., 2022). The formation is rich in organic matter, with TOC values ranging from 1 to 12 (Rønnevik et al., 2017). Common fossils include dinoflagellate cysts and foraminifera, and phosphatic nodules have been reported (Lauridsen et al., 2022).

According to (Blok et al., 2022), (Mutterlose, 2013; Surlyk, 2020) the Tuxen Formation in the Danish Central Graben is mainly composed of white to greyish-pink, calcareous claystones and marlstones, with subordinate dark grey to black, laminated mudstones with abundant organic matter. The formation terminates vertically upwards with a chalk sequence containing subordinate marlstone layers. The chalk is white to pale orange or yellowish grey, occasionally greenish and reddish. The marlstones are generally light grey to greenish-grey or olive-grey but may be reddish-brown in some wells. A 0.3-1 m thick, radioactive,

marlstone bed is frequently encountered within the Tuxen Formation in the Danish sector where it is defined as the MMB. The Tuxen Formation (Fig.4) also contains locally occurring phosphatic nodules (Jelby et al., 2022).

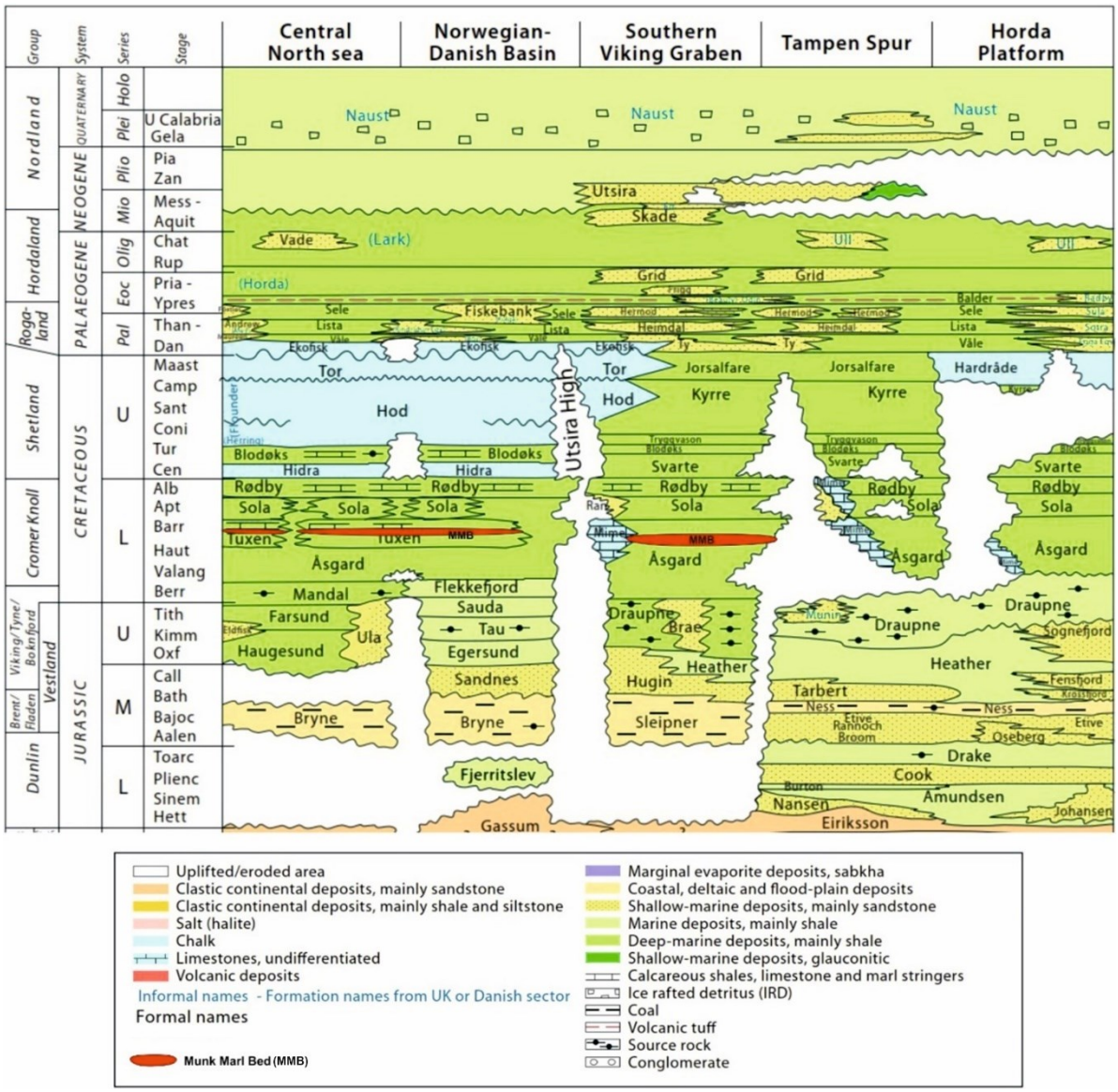

Figure 4. General lithostratigraphic units of the area (modified from Peter, 1998).

Several studies have investigated the geochemical and mineralogical characteristics of these formations. For instance, (Jelby et al., 2022) analyzed the mineralogy of the MMB and found that it is dominated by smectite, illite, and quartz, with minor amounts of calcite, pyrite, and feldspar. They also noted that the organic matter in the marl is relatively immature and composed of mainly type III kerogen. The Åsgard Formation is enriched in organic carbon,

with total organic carbon (TOC) values ranging from 0.5 to 5.5 wt.%. Studies also noted that the mudstone is rich in iron sulfides, particularly pyrite, which is an indicator of anoxic depositional conditions. In addition, studies found that the sandstone is enriched in quartz and feldspar, with minor amounts of heavy minerals, such as garnet, zircon, and tourmaline (Horikx et al., 2014; Jakobsen et al., 2004; Oosting et al., 2006).

2.5 Anoxic Conditions

The MMB is known for its unique stratigraphic and lithological characteristics. One of the most significant features of this formation is the occurrence of anoxic conditions, which has led to various geological problems in the region (Ottesen et al., 2022). Anoxic conditions are defined as the lack of oxygen in aquatic environments. In the case of the MMB, the anoxic conditions were caused by the restricted circulation of seawater in the basin, which prevented the introduction of oxygen into the sediments. The lack of oxygen created an environment where anaerobic bacteria could thrive, resulting in the deposition of organic-rich sediments (Olsen et al., 2017; Wesenlund, 2016). One of the main problems associated with anoxic conditions in the MMB is the production of hydrogen sulfide (H_2S) gas, which is toxic to marine life and can also corrode well casings and production equipment (Mutterlose & Harding, 1987) . Additionally, the organic-rich sediments can be a source of hydrocarbons, but the presence of H_2S gas can make it difficult and dangerous to extract oil and gas from the source rock (Rønnevik et al., 2017). The anoxic conditions also have implications for the stratigraphy of the MMB. The deposition of organic-rich sediments has led to the formation of laminated black shales, which are distinctive lithologies that can be used to identify the formation (Ottesen et al., 2022). However, despite the anoxic conditions, bioturbation, which involves the mixing of sediment layers by organisms like burrowing worms and clams, has not been lost. (Jelby et al., 2022). This lack of bioturbation has made it difficult to determine the depositional environment of the sediments and to interpret the stratigraphy of the formation (Gowland et al., 2018). According to Ineson et al., 2022, the MMB has the potential to produce significant amounts of oil and gas. The study found that the formation contains high levels of organic matter, which is the source of hydrocarbons.

2.6 Stratigraphy and Depositional Setting

The MMB has been the focus of several studies aimed at understanding its stratigraphy and significance. The lithostratigraphical reappraisal by Blok et al., (2022) and Ottesen et al., (2022)provided valuable insights into the lithostratigraphic characteristics of the MMB, helping to establish its stratigraphic position and regional correlation. Furthermore, Bøe et al. (2010) addressed the biostratigraphic markers within the MMB, refining the correlation and dating of the boundary between the Upper Jurassic and Lower Cretaceous (Fig.5). The MMB contains important fossil assemblages that aid in biostratigraphic correlations. These fossils can be used to highlight the significance of biostratigraphic markers within the formation, providing insights into the age and correlation of the MMB (Lauridsen et al., 2022; Mutterlose, 2013). Chemostratigraphic analysis can also play a role in understanding the MMB. Pearce et al., (2020) concluded that the geochemical signatures of the MMB can provide insights into the depositional conditions and paleoclimate during its deposition. Specifically, the same author reported that the MMB was deposited in a shallow marine environment with restricted circulation. The climate during the deposition of the marl was interpreted as warm and arid, with high evaporation rates.

The MMB's depositional environment has been inferred through sedimentological and paleontological evidence. Lauridsen et al., (2022) discussed the lithological characteristics and interpreted the paleobathymetry, water depth, and circulation patterns during the deposition. Sea-level fluctuations and their influence on the depositional environment were also considered (Bøe et al., 2008).

This geological formation offers invaluable insights into the regional geology and the prevailing environmental conditions during its depositional period. It can also be used for correlations across numerous well sites in the central and northern North Sea, and its similarity with other organic-rich intervals has been well-documented. (Blok et al., 2022; Jelby et al., 2022; Ottesen et al., 2022).

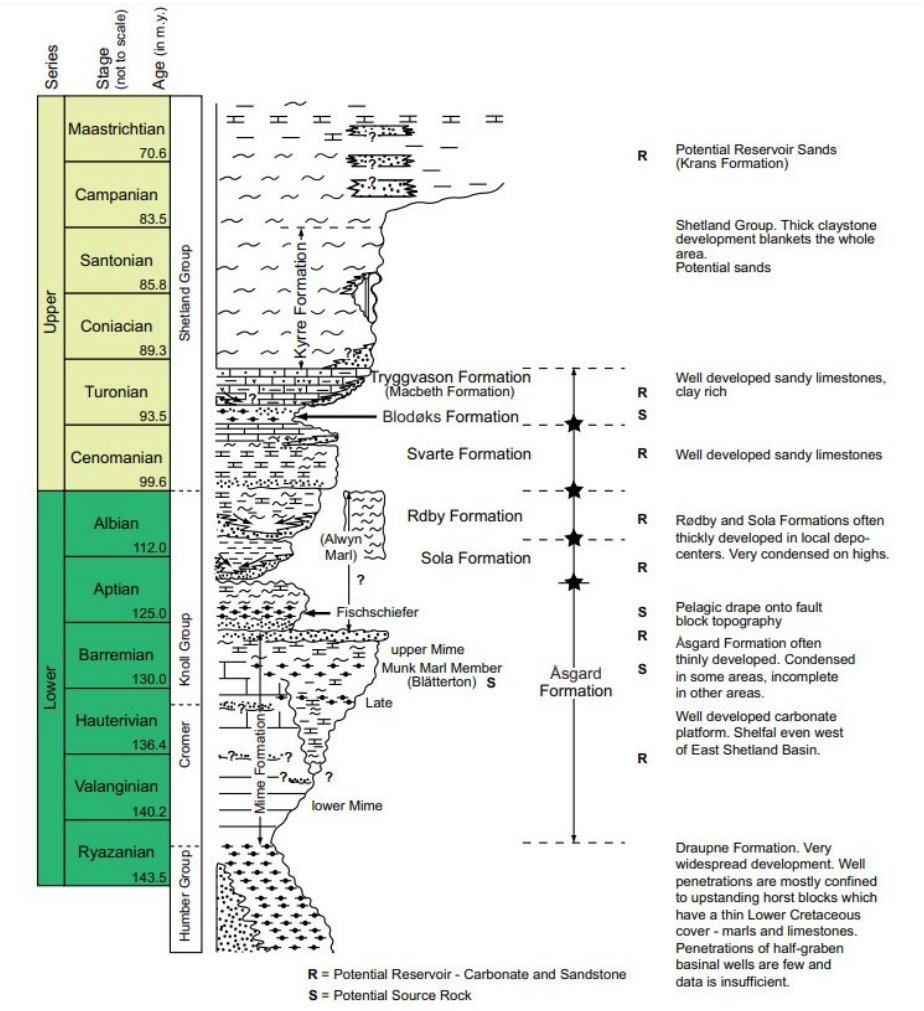

Figure 5. Schematic stratigraphic and facies transect of the Cretaceous strata, west margin of north Viking Graben and East Shetland Basin (modified from Isaksen & Tonstad, 1989).

3

MATERIALS AND METHODS

3.1 Sample collection

The selection of the well and core to be studied was performed in collaboration with the Norwegian oil company Lundin Energy in 2022, before the merge with Aker BP. In October of 2022 Lundin Energy ceased to exist so all the following permissions and communications have been conducted with Aker BP where one of the supervisors works.

The selected well, 16/2-21 is located offshore Norway, in the Johan Sverdrup field (Utsira High area).

For this study, 19 core samples were selected and prepared from the depth interval between 1918 m to 1925 m to evaluate in detail an Early Cretaceous section in the Åsgard Formation with special focus on the MMB (Fig.6). The sampling targeted primarily the dark marl levels, characteristic lithology of the Munk Marl, but also some samples in the reddish-white marls above and below for stratigraphic control and comparison. The fossil recovery in the Munk Marl was expected to be good due to the known high amounts of organic mater preserved.

The sample collection was performed at Stratum Reservoir core store in Stavanger, Norway. The sediment collected was weighted, bagged, and marked properly before being shipped to the Applied Petroleum Technology (APT) Palynology Laboratory in Oslo.

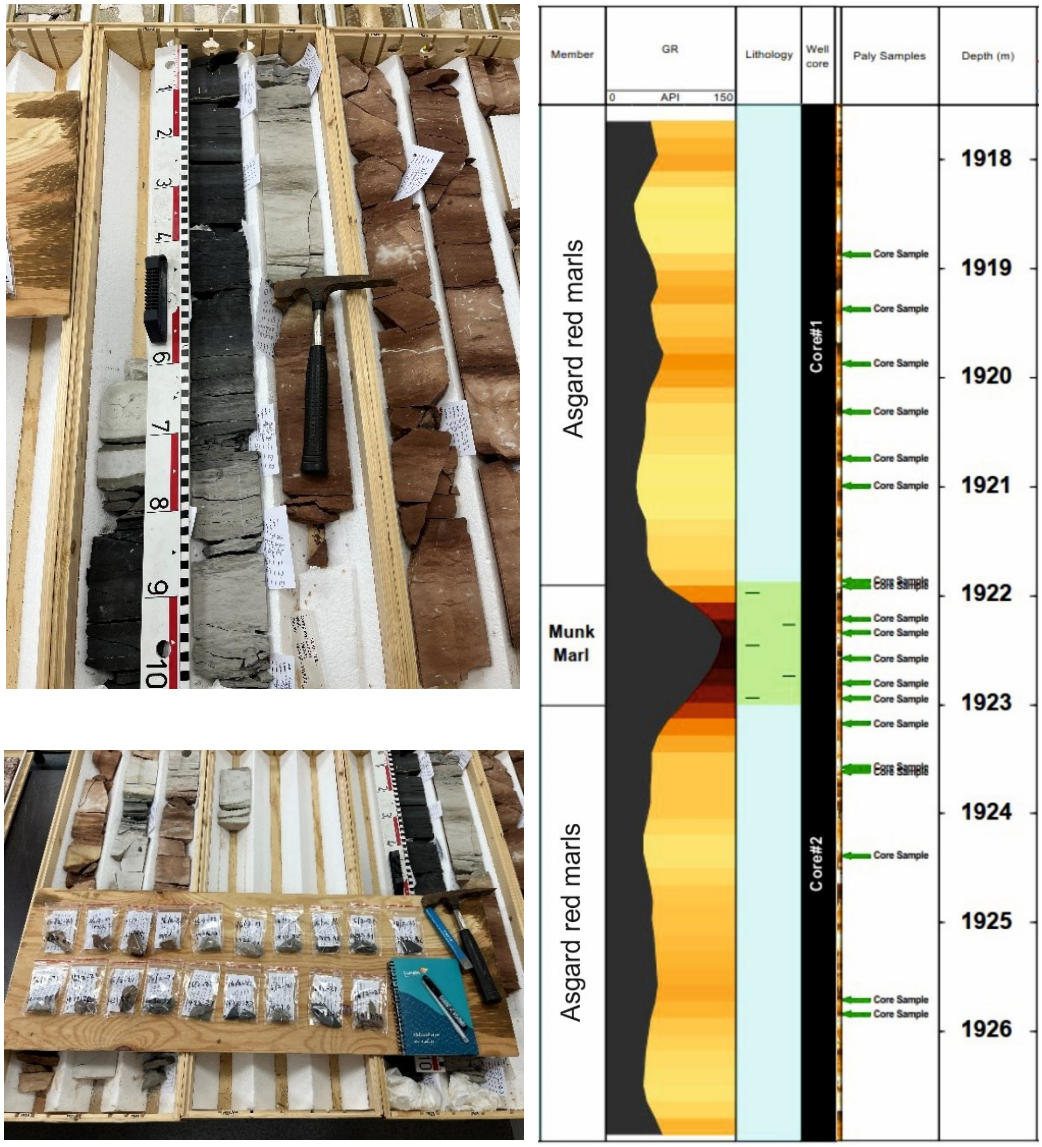

Figure 6. General stratigraphic column of the drilling core and selected samples.

3.2 Laboratory processes

The samples collected underwent standard palynological laboratory treatment to separate palynomorphs from minerals, involving the removal of carbonates and silicates through chemical treatments (using 37% HCl and 45-55% HF). The process involved crushing the rock samples and washing them to remove impurities. Hydrochloric acid (HCl) was used to dissolve carbonates, with methanol added to minimize gas production. Neutralization was carried out to counteract the effects of HCl. Hydrofluoric acid (HF) was then applied to dissolve silicates, followed by another round of neutralization. Ultrasonic bath and centrifugation were employed to facilitate sieving and remove heavy minerals. A diluted solution of nitric acid (HNO_3) was used to oxidize and eliminate organic matter, which produces cleaner slides for palynological analysis.

In cases where mineral residues still remain on the samples after the initial reaction phase in the laboratory treatments, it becomes necessary to repeat the HF reaction. Therefore, a revisiting of the reaction step may be required, as indicated in Fig.7.

The size of the processed palynomorphs usually ranges between 20 to 90 μm (Traverse, 2007). The remaining organic fraction was sieved through 15 μm and 125 μm nylon sieves to concentrate the kerogen. The residues were then mounted on glass slides using Petropoxy 154 resin as permanent mounts. The use of Petropoxy 154 resin gives the slides higher durability when stored for many years without decomposing of the palynomorphs. Two slides have been mounted for each sample to ensure having enough material to analyse in detail. Each slide was appropriately labeled with relevant sample information. The slides were stored in slide boxes or cabinets to protect them from damage and environmental factors (e.g. Traverse, 2007; A. Bercovici & Vellekoop, 2017).

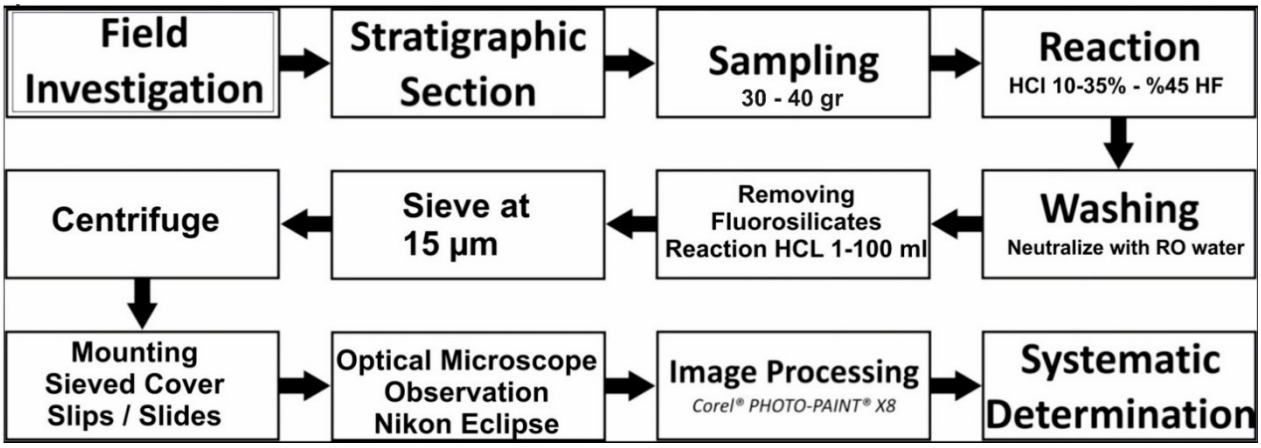

Figure 7. A) Office work processes at the DCT/FCT/UNl. B) Slide view from the microscope camera with 20x magnification. C) Slide view from the microscope objection with 20x magnification

3.3 Sample observation and analyses

The palynological slides were prepared at APT Palynological Laboratory in Oslo, then packed and shipped from Norway to Lisbon to get analyzed at the Department of Earth Sciences at the NOVA School of Science and Technology (DCT/FCT/UNL). The palynological slides received by the Earth Sciences Department underwent an initial assessment, where slides abundant in fossils and with a higher proportion of organic matter were promptly scanned and categorized. In total, 38 slides, representing 19 samples, were meticulously examined one by one using a Nikon Eclipse optical microscope at DCT/FCT/UNL. Following this detailed observation, samples with significantly low fossil content were identified, and

from these, 10 specific samples were carefully chosen to serve as the primary focus of the study. The stratigraphic column section was used during the selection of the 10 samples.

In the initial phase, a crucial photographic process was conducted before the counting procedure, as taxonomic identification of some palynomorphs was uncertain. All the photographs were taken using the Nikon Eclipse E600 optical microscope's built-in microscope camera. All slides were quickly scanned for photography and a total of 1490 palynomorph photographs were captured. To prepare these images for taxonomic analyses and systematic comparisons, CorelDraw 2018 software was employed for their modification. As the microscope camera lacked an integrated scale, manual scales were used in the microscope images. For scaling, custom-made micrometers cardboard rulers were placed under the microscope, and photographs were taken to establish scales at 20x, 40x, and 60x corresponding to the magnification ratios of each microscope objective. This scaling process was executed using Corel Draw software, simplifying the subsequent integration of scales onto the palynomorph photographs. Following these procedures, the gathered photographs were categorized into distinct groups: Spore and Pollen, Acritarch, and Dinoflagellates cysts. For each group, comprehensive catalogues were meticulously compiled. Taxonomic assessments were then conducted using these catalogues as references. On the other hand, all the photographs in these catalogues from 10 samples 2 slides of each and specifically the photographs of the *Batioladinium longicornutum* species were applied to machine learning using the Tensorflow library in Python software to create deep learning models. The details of this study will be given in Chapter 8. Notably, the website Dinoflaj3 and other references played a crucial role in the systematic examination. Upon completing the taxonomic identification, the palynomorphs were counted. During this step, the captured photographs were utilized to methodically count and document each individual species. In total, systematic counting and recording yielded 1877 specimens, representing 14 distinct taxa of Spores and Pollen. Following the taxonomic identification, the Dinoflagellates were also subjected to careful counting. A thorough examination of the slides resulted in the diligent counting of 1783 dinoflagellate cysts, representing 26 distinct species and 17 genus. On completion of the counting process, the numerical data was used to produce informative charts and tables to support the the biostratigraphic and paleoenvironmental interpretation. Both Excel and Google Sheets were used to produce these visual aids during the counting phase. The compiled data from these Excel and Google Sheets records were then imported

into the Stratabugs software. This enabled the creation of intricate and detailed biostratigraphic charts (Fig.8).

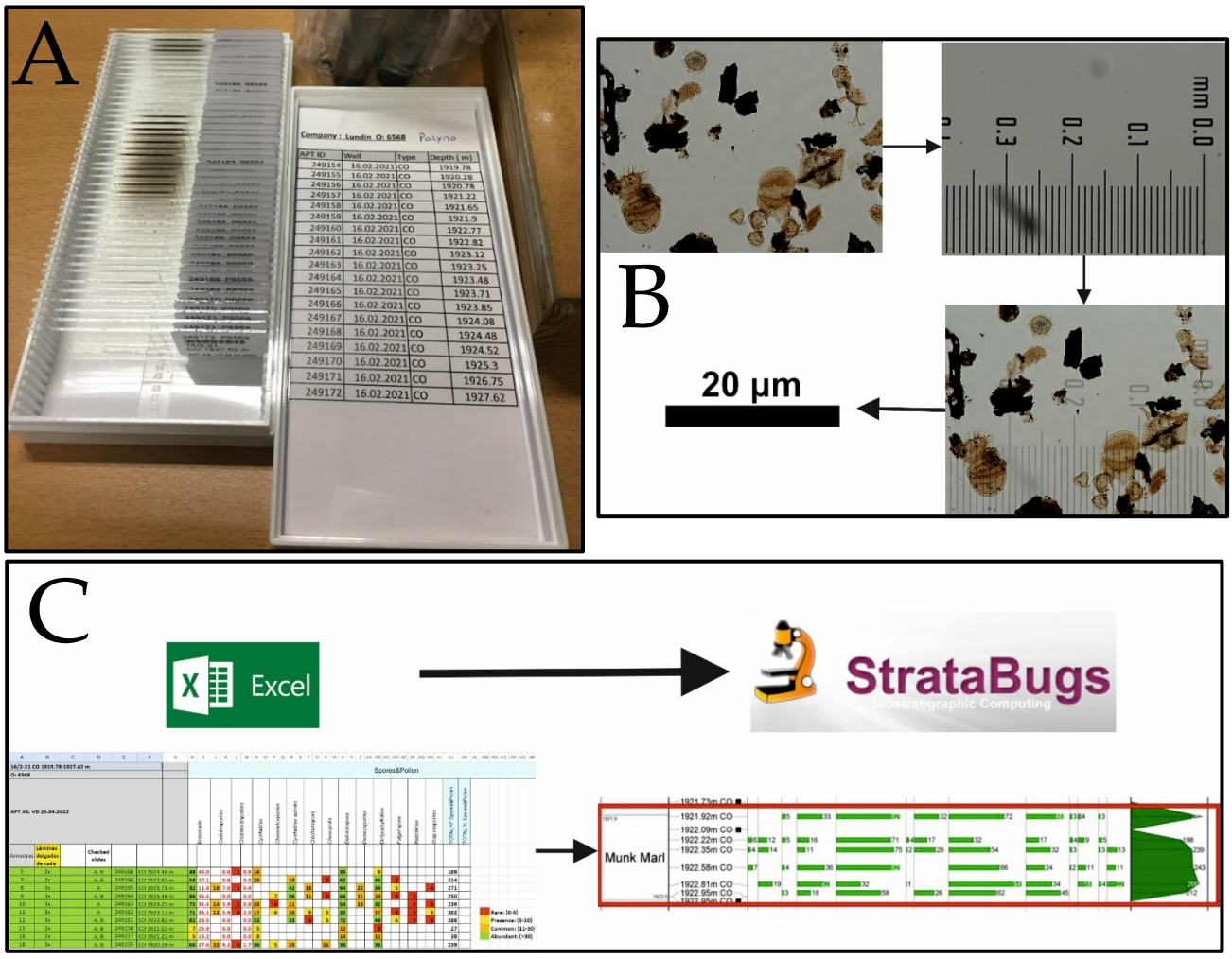

Figure 8. Flowchart of the software implementation: A) Office work processes at the DCT/FCT/UNL; B) Slide view from the microscope camera with 20x magnification; C) Slide view from the microscope objection with 20x magnification.

4

PALYNOLOGICAL CONTENTS

All the organic residues were mainly composed of dark brown to black opaque organic particles, are divided by different groups (Fig.9). This chart illustrates the main groups of palynomorphs and their first occurrence through the geological time scale (Tyson, 1995).

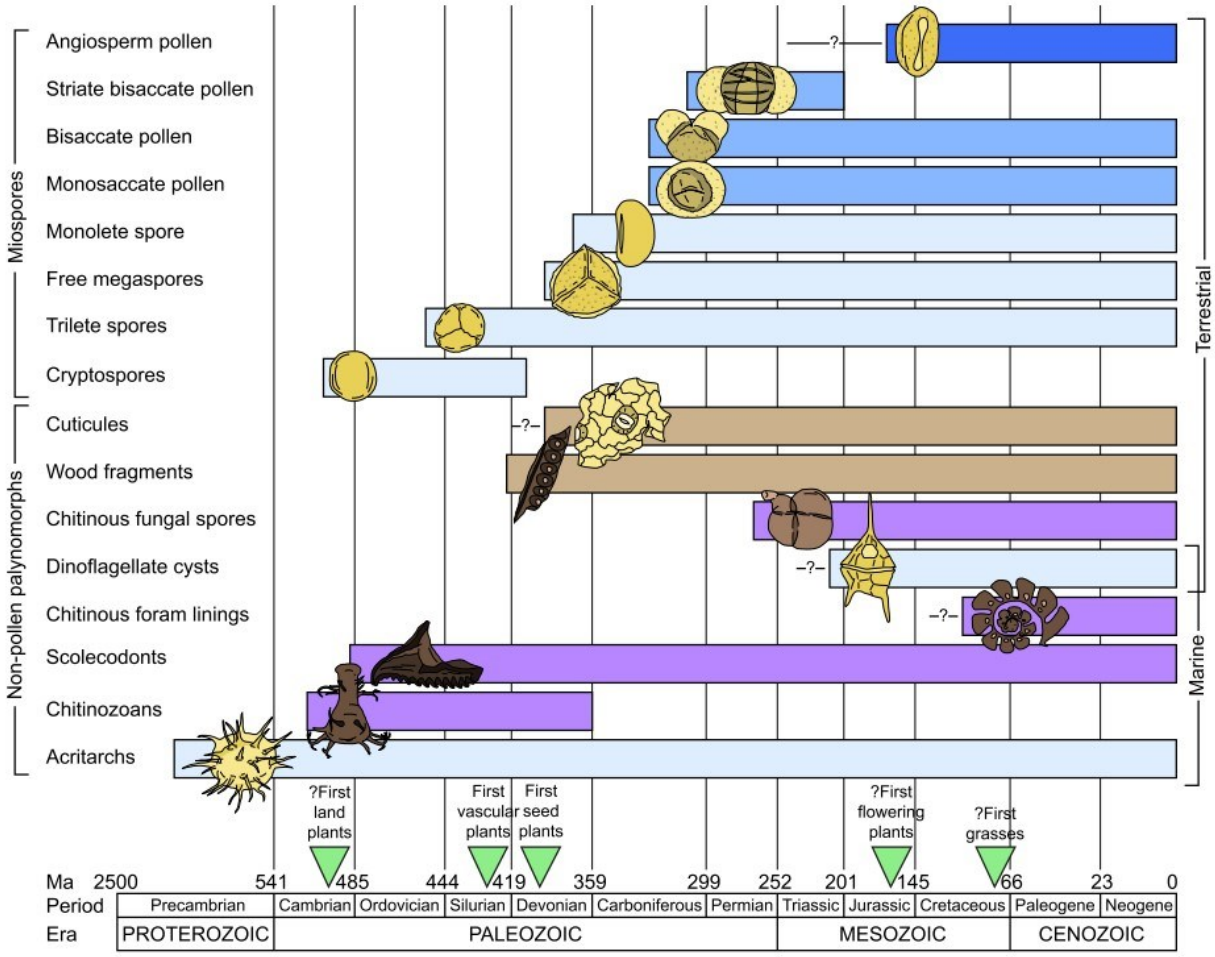

Figure 9. Stratigraphic range chart of the major groups of palynomorphs (Bercovici & Vellekoop, 2017 in Traverse, 2007)

4.1. Cuticles and Wood Fragments

Cuticles and wood fragments are commonly found in terrestrial palynological assemblages. Cuticles are the waxy coatings that cover the epidermal cells of leaves. They can provide valuable information about plant taxonomy and paleoenvironment, as they contain anatomical features such as epidermal cell walls, stomata, guard cells, and hair bases. Stomatal density in cuticles can serve as a record of atmospheric composition throughout Earth's history (Barclay et al., 2007).

Wood fragments, which are derived from lignified tissues of vascular plants, are also prevalent in palynological preparations. They can indicate transport and erosion processes and may be preserved as charcoal fragments resulting from wildfires. Charcoal fragments have been particularly useful in studying early flowers and other aspects of paleobotany (Retallack, 2001).

These different components contribute to our understanding of plant evolution and paleoenvironments. For example, the presence of cuticles with a high stomatal density can indicate a warm and humid climate, while the presence of charcoal fragments can indicate a fire-prone environment. By studying the different components of terrestrial palynological assemblages, we can gain a better understanding of the history of plant life on Earth and the environmental conditions that have shaped it (Upchurch, 1995).

In addition, the presence of cuticles and wood fragments in the MMB can be used to help identify the plant communities that were present in the area at the time of deposition. This information can be used to reconstruct the paleogeography of the area and to understand how the plant communities have changed over time (Barclay et al., 2007; Retallack, 2001).

4.2. Phytoclasts

Phytoclasts are plant-derived, fragmentary, resistant-walled particles that indicate terrestrial input. These organic particles can be subdivided based on their different stages of oxidation, degradation, and shape (Traverse, 2007). Cuticles, mostly derived from leaves, are translucent phytoclasts with clear cellular structures that are easily deteriorated. Vitrinite is translucent, with a color range from pale orange to dark brown. Through thermal maturation, the original color will become darker (Tyson, 1985). Semi-opaque dark brown vitrinite particles can be confused with inertinite. Inertinite is opaque up to edge, oxidized wood of terrestrial origin. Vitrinite and inertinite can present biostructuration. Heavily degraded phytoclasts commonly maintain their sharp edges. This characteristic allows their differentiation from Amorphous organic matter (AOM), which has an irregular outline (Hughes, 1989; Traverse, 2007; Tyson, 1985). The presence of phytoclasts in the MMB can be used to infer the paleoenvironment of the deposit (Tyson, 1985). Phytoclasts in Munk Marl samples indicate terrestrial runoff during deposition, transporting plant fragments into the marine environment. Initially considered deltaic, the MMB deposition involves sediment from rivers entering the ocean.(Jelby et al., 2022; Jensen et al., 1986; Skupien & Mohamed, 2008; Tyson, 1985). This sediment can be rich in organic matter, including phytoclasts. Additionally, the MMB is an organic-rich deposit, meaning that it contains a high concentration of organic matter, which can be seen by the dark color of the sediment in cored sections. This organic matter would have provided a good environment for the preservation of phytoclasts (Glad et al., 2022; Hughes, 1989; Ineson, Lauridsen, et al., 2022; Traverse, 2007).

4.3. Amorphous Organic Matter

Amorphous organic matter (AOM) is a heterogeneous material that can contain inclusions and has diffuse edges. It can have either terrestrial or marine origin. In marine environments, AOM can represent plankton fecal pellets, larger bacterially degraded mats, or marine organic matter that has been degraded by bacteria. In the studied samples (Fig.10), the AOM was dark brown to black, which suggests that it was of marine origin. This is because terrestrial AOM is typically lighter in color (A. Bercovici & Vellekoop, 2017). Additionally, all the structureless particles with sharp edges were considered to be degraded phytoclasts,

which are plant-derived organic particles. This leaves the dark brown to black AOM as the only possible source of the amorphous organic matter in the samples (Tyson, 1995).

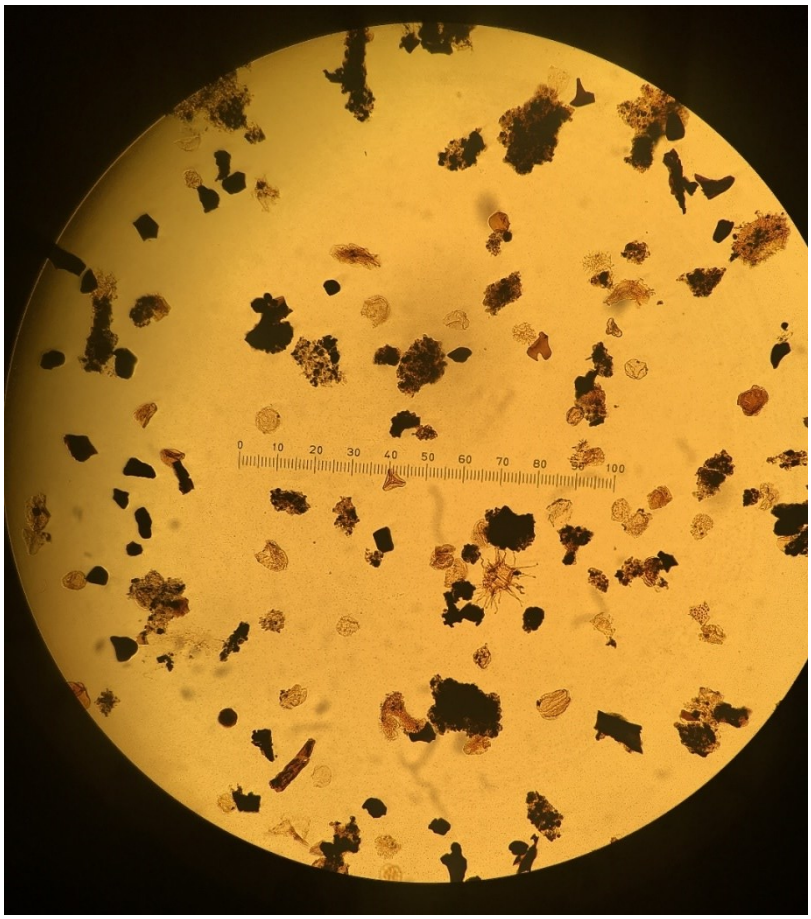

Figure 10. Microscope view of the slide from Munk Marl sample (249155).

Samples dominant by the AOM materials and sporomorphs (Microscope objection is 20x as a scale in this picture).

4.4. Sporomorphs

Terrestrial-derived spores and pollen are both produced by plants, but they have different functions and morphological features. Spores are produced by lower plants known as cryptogams, including bryophytes (mosses, liverworts, and hornworts) and pteridophyte vascular plants (ferns, lycopsids, and horsetails); are frequently found as fossils from Silurian to recent times (Traverse, 2007). They have a resistant wall (exine) that is variable in thickness and ornamentation. Trilete spores have three pronged marks (laesurae) that

resemble an upper-case "Y", while monolete spores have one laesurae (Traverse, 2007). Stratigraphically they range from late Devonian to recent times and is defined functionally as the microspore wall of seed plants, plus the microgametophyte that develops within the wall. Pollen is produced by seed plants, including gymnosperms (conifers and their ancient relatives) and angiosperms (flowering plants) (Moore et al., 1991). Pollen has a more complex structure than spores and has a variety of morphological features that can be used to identify different plant groups (Hughes, 1989). Prepollen is a transitional form between spores and pollen. It has the morphological features of spores (e.g. trilete laesurae) but functions as pollen. Prepollen represents the stage at which microspores still germinated proximally (A. Bercovici & Vellekoop, 2017; Traverse, 2007).

Pollen and spores are microscopic and highly resilient structures that have biostratigraphic potential (Kemp & Cook, 1997). They are produced by land plants (embryophytes) but can occasionally be found in nearshore marine deposits. Pollen and spores are useful indicators of paleoecology and paleoenvironment and can be used to correlate terrestrial and marine deposits.

The outer wall of pollen and spores, known as the exine, is composed of sporopollenin, one of the most chemically inert and durable biopolymers. This makes pollen and spores highly resistant to degradation, even in harsh environments. Pollen and spores are dispersed by animals, wind, or water, and can travel long distances. This makes them valuable biostratigraphic markers, as they can be used to correlate deposits from different locations (Faegri & Iversen, 2000).

When linked to their parent plants and associated ecological information, pollen and spores can be used to reconstruct paleoenvironments. For example, the presence of certain types of pollen can indicate the presence of specific plant communities, which can in turn be used to infer climate conditions. Pollen and spores have a long fossil record, dating back to the colonization of land by the first terrestrial plants. This makes them a valuable tool for studying the evolution of plant life. The identification of pollen and spores can be challenging, as they are often disconnected from their parent plants. However, there are several techniques that can be used to identify pollen and spores, including anatomical comparisons, chemical analysis, and DNA sequencing.

The spores and pollen found in the MMB provide evidence of the plant life that existed in the area surrounding the basin during the Early Barremian. The presence of trilete spores

indicates that bryophytes and ferns were common. The presence of bissacate pollen in a marine environment could indicate that the area was transitioning from a spore-producing plant community to a pollen-producing plant community, but it could also be due to the presence of sporomorphs that were carried from land into the marine environment (Jelby et al., 2022; Vieira and Jolley, 2020). Spores and pollen diversity was abundant in the Munk Marl Bed levels of the section. Shape can be found in (Fig.11).

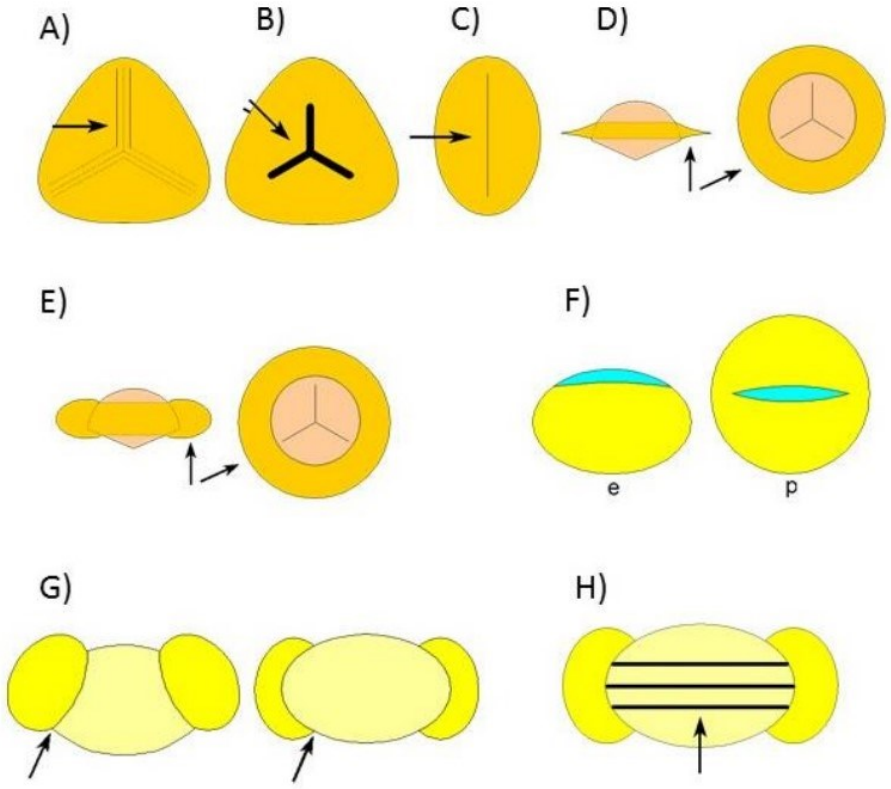

Figure 11. Spores and Pollen morphological features Modified from (Punt et al. 2007)

A) Laesura: Refers to the arm of a fissure or scar found in spores. Trilete spores possess three laesura, whereas monolete spores have only one. B) Trilete mark (Y-mark): Exhibits the characteristic Y-shaped mark found on spores. C) Monolete mark: Occurs rarely on pollen grains and represents a single mark. D) Zona: Refers to the thin outer structure of a spore projecting at the equator. However, it does not extend over the distal or proximal face. E) Cingulum: Represents a thick outer structure of a spore projecting at the equator. It also does not extend over the distal or proximal face. F) Sulcus: Describes an elongated latitudinal ectoaperture located at either the distal or proximal pole of a pollen grain. G) Bisaccate pollen grains: These grains exhibit sacci that appear discontinuous with the outline of the corpus (the main body). As a result, they give the impression of consisting of three distinct parts. H) Taenia: Depicts one or more strap-like structures, resembling parallel strips on the corpus of pollen grains (e.g., Striatites) (Miljeteig, 2016; Punt et al., 2007)

4.5 Acritarchs

Acritarchs are organic-walled microfossils with uncertain biological origins. They can be found in rocks ranging from the mid-Precambrian Era to recent times (Evitt, 1985). While many acritarchs are believed to be the cysts or resting stages of marine phytoplanktonic algae, their exact biological affinity remains unknown. Some forms have been tentatively assigned to the division Prasinophyta of green algae based on their morphology (Martin, 1993). Informal groupings have been defined using morphology, which are helpful for Precambrian and Paleozoic biostratigraphy as well as paleobiogeography (Downie, 1973). Acritarchs were most abundant during the Paleozoic Era and are predominantly associated with marine environments, although they can also occur in non-marine settings (Downie, 1973). Only a single taxon was identified in the MMB samples.

4.6 Dinoflagellates

Dinoflagellates are unicellular eukaryotes algae characterized by their motility through a pair of flagella. They play a crucial role in marine phytoplankton and have been present and exist since the Mesozoic era. While many dinoflagellates undergo photosynthesis, some are mixotrophic, combining photosynthesis with heterotrophic feeding. They primarily inhabit marine environments, but certain species can also thrive in brackish and freshwater habitats. Dinoflagellates exhibit intriguing traits such as the presence of carotenoid pigments like dinoxanthin and peridinin, which contribute to their vibrant red coloration and bioluminescence (Hughes, 1989; Taylor, 1991).

Dinoflagellate blooms, commonly known as "red tides," occur when these organisms undergo rapid population growth, resulting in water discoloration due to high algal cell concentrations. These blooms have significant ecological and economic implications since some dinoflagellates produce toxins that can be harmful to fish, invertebrates, and even humans through the consumption of contaminated filter-feeders. Dinoflagellates have a complex life cycle that involves the formation of resting cysts, allowing them to remain dormant on the sea floor during unfavorable conditions, such as winter. These cysts can remain inactive for several decades until favorable conditions trigger their escape and

resumption of motility (Antoine Bercovici, 2017). Fossilized dinoflagellates are primarily preserved as cysts, although only a small percentage of living dinoflagellate species are known to encyst following sexual reproduction. Some dinoflagellate taxa produce cysts made of a resilient organic material called dinosporin, which has the potential to be preserved in the fossil record. These organic-walled dinoflagellate cysts are referred to as " dinoflagellate cysts." In contrast, certain dinoflagellates produce non preservable resting cysts that quickly decay after excystment (Traverse, 2007). Taxonomic classification of dinoflagellates in biological studies relies on the examination of living motile cells, while the fossil record primarily relies on the identification of resting cysts. As a result, determining the specific species corresponding to a particular dinoflagellate cyst morphology often poses a challenge. To address this, a separate taxonomic system based on form taxa has been developed for dinoflagellate cysts. This system utilizes morphological traits such as size, shape, wall structure, surface features, and the presence of an archaeopyle to classify and identify dinoflagellate cysts. The arrangement of sutural features on the cyst, known as "paratabulation," is a crucial aspect of dinoflagellate cyst taxonomy. The Kofoid system, introduced by Kofoid in 1907, is a classification scheme based on paratabulation (Bujak & Foundation, 2018; Kofoid, 1907).

The fossil record has revealed more than 4,400 identified species of fossil dinoflagellate cysts, demonstrating the abundance and diversity of dinoflagellates in the more recent past. This extensive fossil record makes dinoflagellates a significant subject of study for palynologists, particularly in understanding the dynamics of Mesozoic and Cenozoic oceans. Dinoflagellate cysts have proven valuable for biostratigraphy, correlation, and paleoenvironmental reconstruction due to their sensitivity to factors such as water temperature, salinity, and depth. For example, the relative abundance ratio between two major dinoflagellate groups, Gonyaulacaceae and Peridiniaceae, are commonly utilized as an indicator of productivity and nutrient availability in surface waters (Evitt, 1985; Hughes, 1989; Nohr-Hansen et al., 2020).

In the majority of dinoflagellates, the cell is divided into an upper (epi-) and a lower (hypo-) portion by a structure called the *cingulum*. The ventral side of the cell is defined by another structure known as the *sulcus* (Fig.12).

However, it's important to note that some *taxa*, such as podolampids, do not possess a depressed cingulum. In species that have both cingulum and sulcus, the flagellation follows

a dinokont pattern, where the transverse and longitudinal flagella align with the transverse and longitudinal furrows or grooves, respectively. On the other hand, in prorocentroids, the flagellation exhibits a desmokont pattern, where the typical dinoflagellate flagellation is not associated with grooves. (Hoppenrath, 2017).

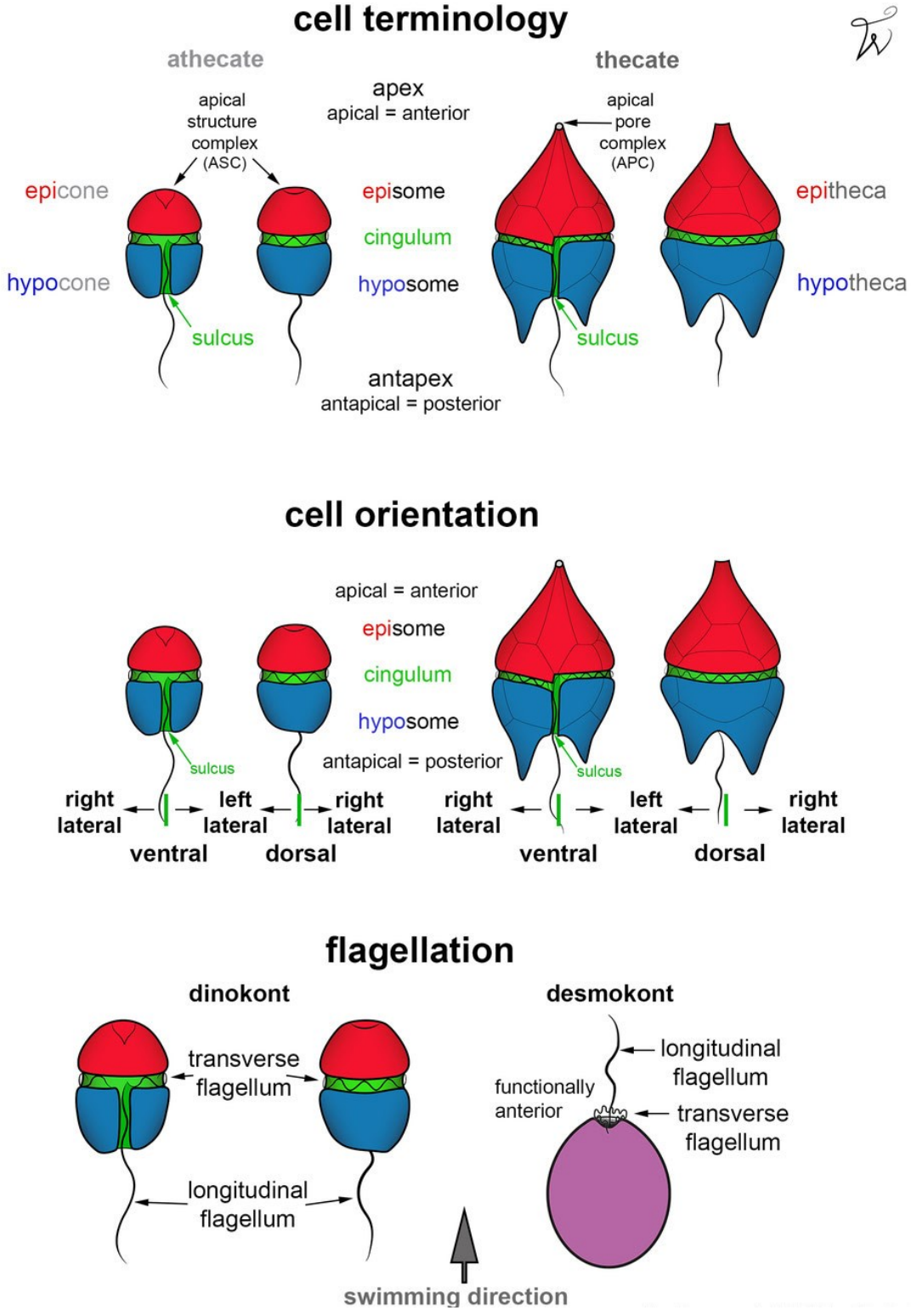

Figure 12. Dinoflagellate morphology (modified from Hoppenrath, 2017).

4.6.1 Kofoid System

The "Kofoid System" is a widely used convention for naming and numbering the plates in dinoflagellates. It follows a specific pattern where plates are numbered from left to right, starting from the plate closest to the midventral position. Primes ('), (''), ('''), and (''''') are used to indicate the apical, precingular, postcingular, and antapical plates, respectively (Fig. 13). This notation is used when labeling plates on figures and creating plate formulas, which provide the total count of plates in each series for a species or genus (Hoppenrath, 2017; Kofoid, 1907). Different plates are represented by letters: C for cingulars, S for sulcals, a for anterior intercalaries, and p for posterior intercalaries. Additionally, there is a transitional plate called the t plate, which is located between the cingulars and sulcals. In peridinioids, it is found at the proximal end of the girdle, while in gonyaulacoids, it is located at the distal end. Peridinioids commonly have plate combinations like 2–3a, 7'', 5''', 2'''', whereas gonyaulacoids typically have combinations like 6'', 6''', 1p, 1'''' (Hoppenrath, 2017).

Although the general trend is for peridinioids to exhibit bilateral symmetry and gonyaulacoids to display torsion, exceptions can occur due to suture loss or plate subdivision (Kofoid, 1907; Evitt, 1985).

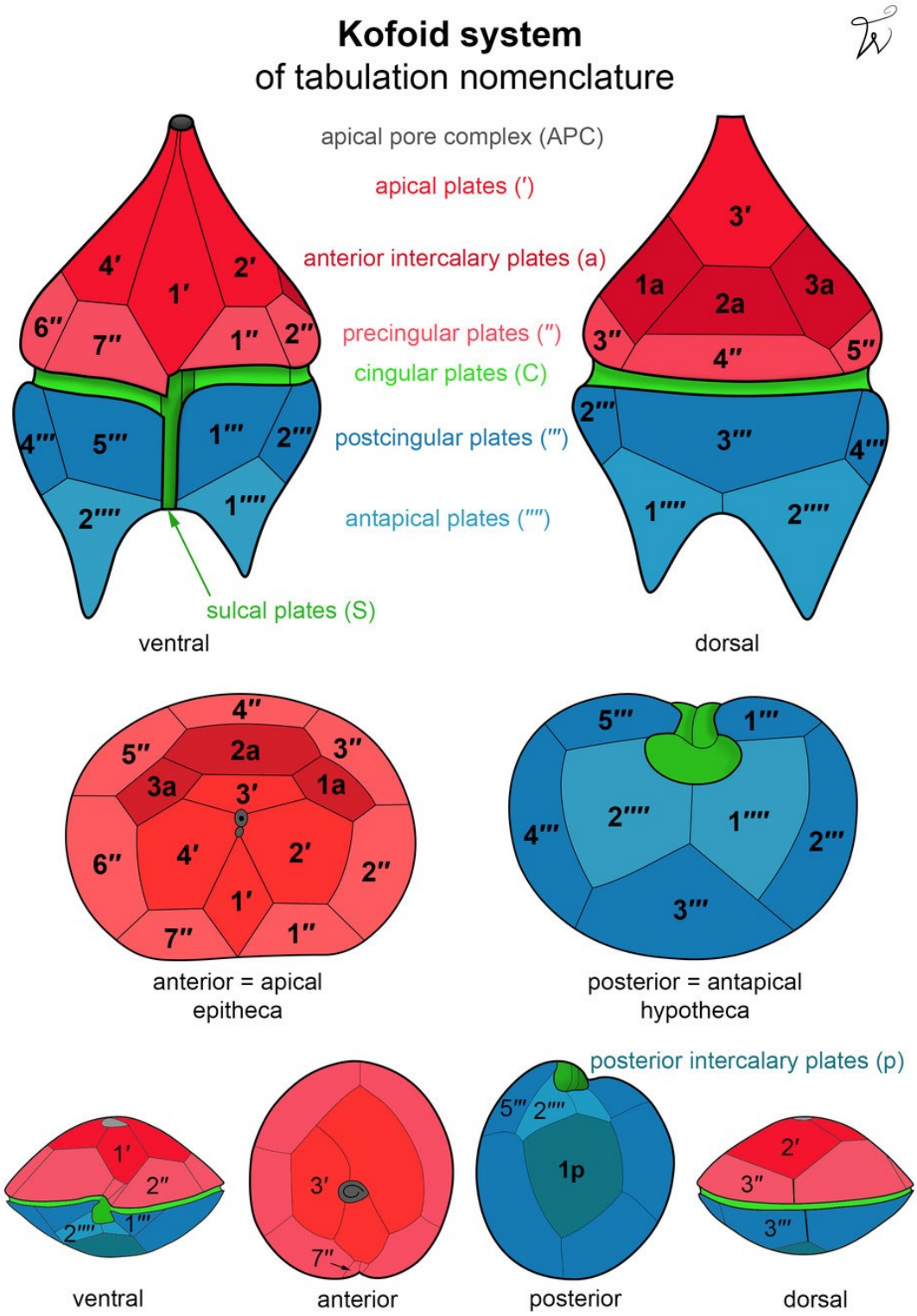

Figure 13. Kofoid system for morphological features of Dinoflagellates (modified from Hoppenrath, 2017).

5

SYSTEMATICS & TAXONOMY

In this section, we focus on *taxa* that are commonly found or dominant, including those that have been previously discussed, those awaiting classification, might newly discovered ones, or those found in new locations beyond their known stratigraphic range. A total of 17 genera of dinoflagellate cysts from the samples are represented based on their morphological characteristics. Additionally, we have identified specimens belonging to 26 formally established species.

5.1 Acritarchs

Division **Acritarcha**

Genus ***Micrhystridium*** Deflandre, 1939

***Micrhystridium* sp.**

Plate 4, Fig. m

Description and remarks: *Micrhystridium* sp. is a relatively small acritarch, with a diameter of typically around 10 μm. It has a spherical or ovoid shape, and its surface is covered in small spines or tubercles. The interior of the acritarch is divided into two chambers by a wall called the septum.

5.2 Dinoflagellate Cysts

For a comprehensive list of all formal nomenclatural changes related to the taxonomic entities mentioned here, refer to the Lentin & Williams Index of Fossil Dinoflagellates (Williams et al., 2017). We have employed the Kofoid Tabulation System for plate identification and we used Palsys website for taxonomic informations. The geometric archaeopyle terminology follows the original proposal by Bujak & Davies (1983), while other descriptive morphological terminology adheres to that of (Lentin and Fensome, 1998; Riding et al., 2012).

Division **Dinoflagellata** (Bütschli, 1885) Fensome et al., 1993

Class **Dinophyceae** Pascher, 1914

Family **Pareodiniaceae** Gocht 1957

Genus ***Batioladinium*** Brideaux, 1975

Species ***Batioladinium longicornutum*** **(**Brideaux, 1975) Pourtoy (1988)

Plate 3, Fig. a

Age: early Hauterivian-latest Barremian.

Description: Species presents a cyst characterized by a cornucavate, elongate, and ellipsoidal form with a fusiform shape. Its equatorial section is circular, emphasizing an oblong structure. The epicyst features an exceptionally long, slender apical horn, while the hypocyst showcases extremely elongated dextral and sinistral antapical horns. These antapical horns may either curve outward or possess short forked or branched terminations. The cyst measures between 241 to 298 μm in overall length and 32 to 38 μm in width, distinguishing itself within the dinoflagellate group due to its unique, elongated morphology and the specialized structures of its horns.

Remarks: According to (Davey, 2001), the first occurrence of *B. longicornutum* corresponds to the middle part of the lowermost Hauterivian *Endomoceras amblygonium* ammonite Zone. This correlation is based on dinoflagellate cyst analysis and its relationship to lower Hauterivian ammonite stratigraphy at Speeton, East England. Nøhr-Hansen (1994) indicates that *B. longicornutum* appears for the first time in the upper Barremian Stage.

Family **Gonyaulacaceae** Lindemann, 1928

Genus ***Cassiculosphaeridia*** Davey, 1969

Species ***Cassiculosphaeridia magna*** **(**Davey, 1974) Harding (1990)

Plate 1, Fig. g

Age: Barremian.

Description: *Cassiculosphaeridia magna* is a robust, thick-walled cyst with a subspherical to ovoidal shape, featuring a surface that ranges from smooth to lightly pitted and forms intertwining crests supported by stout processes, giving a slightly wrinkled appearance. The

cyst's defining features include a well-defined *cingulum*, an apical archaeopyle with a simple polyplacoid operculum, and an ambital oblate to subcircular shape. The hypocyst is notably half as long again as the epicyst, displaying moderate dorso-ventral compression. Septa, occasionally fenestrated and reaching up to 8 μm in height, along with an ectophragm, if preserved, represent additional characteristics. Cyst diameter typically measures between 85 and 105 μm across examined specimens.

Remarks: *Cassiculosphaeridia magna* can be easily distinguished from *C. reticulata* Davey (1969) by its larger size, the presence of strong processes supporting the crests, and its larger hypotract-epitract ratio (Davey, 1969).

Family **Areoligeraceae** Evitt, 1963

Genus ***Circulodinium*** Alberti, 1961

Species ***Circulodinium hirtellum*** Alberti, 1961

Plate 1, Fig. b

Age: Valanginian-Hauterivian.

Description: *Circulodinium hirtellum* exhibits a slightly longer than broad, irregularly rounded, flattened cyst shell. The surface, apart from the central parts of the dorsal and ventral sides, is adorned with short, pointed, thorn-like spines. This cyst displays a short, blunt apical horn, along with two unequal-sized rounded antapical horns. The base of the thorns varies in length and distribution. The cyst membrane is transparent and yellow brown, with dimensions for the holotype measuring at a length of 102 μm, breadth of 93 μm, thorns length of 3-4 μm, an apical horn of 7 μm, and antapical bulges of 10-12 μm.

Remarks: Fensome and Williams (2005) informally suggested the term "*Reculadinium*" to describe cysts of the areoligeracean group that exhibit low relief, granulate to denticulate ornamentation. Although similar forms have been subsequently classified within *Circulodinium* (Williams et al., 2017), the observations made in the Hornby Island section also support the original concept of "*Reculadinium*" in terms of the varying degrees of asymmetry and definition of the antapical lobe. also stated that ridges have been observed from which a series of spines originates.

Family **Gonyaulacaceae** Lindemann, 1928

Genus ***Cribroperidinium*** Neale and Sarjeant, 1962

Species ***Cribroperidinium edwardsii*** (Cookson and Eisenack, 1958) Davey, 1969

Plate 1, Fig. h

Age: Valanginian to Barremian according to (Duxbury, 1977).

Description: *Cribroperidinium edwardsii* features a nearly spherical, thick-walled cyst. Its surface displays fine granulation, with a longitudinal furrow extending towards the antapex and a helicoid, narrow girdle showing low borders. The cyst's epitheca bears a long, stiff, pointed, occasionally curved horn, while the hypotheca terminates broadly at the posterior end. The plates exhibit low ribbing with spines along their edges, more pronounced at the corners and particularly in the apical region. The cyst measures approximately 143 μm by 125 μm overall. Details regarding the archeophyle or specific structures representing it are not explicitly detailed in the available information.

Remarks: Type locality is Carnarvon Basin, W Australia from Albian-Early Turonian. The taxonomy of *Cribroperidinium edwardsii* is still under debate.

Genus ***Dapsilidinium*** Eaton & Williams, 1980

Species ***Dapsilidinium warrenii*** (Habib, 1975)

Age: Berriasian-Aptian.

The genus *Dapsilidinium* is known from the Early Cretaceous to the Recent. The species *Dapsilidinium warrenii* is known from the Upper Cretaceous of southern England (Duxbury, 2023).

Description: *Dapsilidinium warrenii* features a subcircular to elliptical cyst shape with a two-layered periblast and numerous thin, hollow cylindrical processes (60-68) extending from the periphragm, creating a circular base. The cyst's surface is microgranulate to minutely spinate. The apical archeopyle exhibits a simple, free operculum (type A). The central body measures around 23-35 microns, while process lengths range from 9-15 microns. This species stands apart from related ones due to its numerous, slender processes and the absence of a closed, recurved spinate margin at their ends, a feature seen in other similar species.

Remarks: *Dapsilidinium warrenii* is a dinoflagellate species with numerous thin, parallel-

sided processes. It can be distinguished from other species in the genus by the open distal ends of its processes. *D. warrenii* is named after John S. Warren, who first reported it from the Lower Cretaceous of California. In the western North Atlantic, *D. warrenii* ranges from the upper half of the *Biorbifera johnewingii* Zone through the *Oligosphaeridium complex* Zone, which corresponds to the Berriasian or Valanginian to Barremian geological periods (Habib, 1976).

Genus ***Dingodinium*** Cookson and Eisenack, 1958

Species ***Dingodinium albertii*** Sarjeant, 1966

Plate 2, Fig. b

Age: Early Barremian.

Description: *Dingodinium albertii* appears as a cavate dinoflagellate cyst with an irregularly ovoidal to subpolygonal shape and a thin outer shell, often deformed in various ways. It exhibits folds or ridges suggesting a tabulation and is drawn out into a short, blunt apical horn. The inner body is spheroidal, wider than long, with a smooth periphragm and a slightly granular endophragm, bearing small, conical tubercles of less than 1 μm in height. The cyst demonstrates an uncertain but possible intercalary archeopyle position on the upper epitract, possibly corresponding to an intercalary plate. It stands out from other species due to the relative shapes of the outer shell and inner body and the unique ornamentation of the inner body. Dimensions range from 50-66 μm in overall length and 37.5-52 μm in breadth across different specimens.

Remarks: The species *Dingodinium albertii* is known from the Lower Cretaceous of the Speeton Clay, Yorkshire (Sarjeant, 1966).

Genus ***Downiesphaeridium*** **(**Islam, 1993) Fauconnier and Masure, 2004

Downiesphaeridium **spp.**

Age: Early Cretaceous.

Description: *Downiesphaeridium* comprises spherical to subspherical dinoflagellate cysts that display a variety of characteristics. These cysts can be either auto or biphragmal, and they exhibit a range of surface textures such as psilate or ornamented, which includes chagrinate,

echinate, granulate, or reticulate patterns. The key characteristic is the presence of processes with similar shapes and sizes within individual specimens and an apical archeopyle tA or (tA) (Islam, 1993).

Remarks: The species *Downiesphaeridium* are difficult to distinguish from each other, and more research is needed to clarify their taxonomy (Islam, 1996). *Downiesphaeridium* spp. are found in a variety of marine environments, including the Atlantic, Pacific, and Indian Oceans (Downie, 1992; Riding, 1997).

Genus ***Exochosphaeridium*** Davey, 1966

Species ***Exochosphaeridium phragmites*** Davey, 1966

Age: Cenomanian-Early Cretaceous.

Description: *Exochosphaeridium phragmites* manifests as a subspherical to oval dinoflagellate cyst with a pitted surface and numerous acuminate processes. These processes are solid or fibrous, often broad-based, occasionally perforate, and sometimes branching medially or distally. While their arrangement typically seems haphazard, a specific alignment is observed in a single specimen where the processes run parallel to the *cingulum*. Notably, a distinctive branched apical process is present, situated near the archaeopyle, indicating the orientation. The presence of a precingular archaeopyle alongside this unique apical process distinguishes this species. The dimensions of the central body range from 33x36 μm to 49x56 μm, while process length reaches up to 22 μm (Davey, 1966).

Remarks: Type locality is Fetcham Mill, Surrey, England from Cenomanian age. The species is named after the common reed, *Phragmites australis*, which is the type locality for the species (Davey, 1966).

Genus ***Impletosphaeridium*** Morgenroth, 1966

***Impletosphaeridium* spp.**

Age: Early Cretaceous

Description*: Impletosphaeridium* spp. appears as spherical to subspherical or ellipsoidal skolochorate dinoflagellate cysts, either mono or biphragmal. Their phragma is weakly granulated or psilate, and they feature numerous nontabular solid processes that are slender,

round in cross-section or platy, slightly broader at the base, and vary in distal structure, either simple and acuminate or expanded, resembling calyxes or spatulas, or branched and ramified. The cysts possess an apical archeopyle of type tA or (tA), and the operculum is free or adnate. Notably, tabular features are absent, although groupings or alignments of processes hint at partial tabulation, potentially indicating the presence of *cingulum* and sulcus. The paratype of the "type species" specifically displays an apical archeopyle, as per Islam's description in 1993.

Remarks: Islam (1993) reported that the paratype of the "type species" has an apical archeopyle. The species *Impletosphaeridium* spp. are difficult to distinguish from each other, and more research is needed to clarify their taxonomy.

Family **Gonyaulacaceae** Lindemann, 1928

Genus ***Florentinia*** Davey, 1973

Species ***Florentinia buspina*** Davey and Verdier, 1976

Plate 2, Fig. h

Age: Barremian-Middle Maastrichtian (Duxbury, 1980; Begouen, 1993).

Description: *Florentinia buspina* presents spherical to subspherical dinoflagellate cysts with densely granular walls and thin-walled processes of variable size, approximately one per reflected plate area, and roughly equal in length. The processes are faintly striate, wider proximally, and typically truncated distally. They exhibit varying complexities, including simple, bifurcating, trifurcating, and large complex processes, mostly noticeable in the postcingular region, often divided into several truncated tubules or crowned with tubules at their distal ends. The antapical process is not distinctive. The archeopyle is formed by the loss of precingular plate 3", occasionally with incipient breakage between the apical and precingular plate series. The central body diameter ranges from 43-57 μm, with process lengths ranging from 18-27 μm. The cyst's surface contains noticeably thickened and granular areas beneath the processes, making sutural areas easily discernible.

Remarks: According to (Davey and Verdier, 1976) *Silicisphaera buspina* is very similar to *S. ferox* except that it possesses complex processes, the postcingular ones being extremely large and immediately obvious. Type locality of *Florentinia buspina is* Loffre Borehole, Nord, France from Senonian age.

Family **Gonyaulacaceae** Lindemann, 1928

Genus ***Florentinia*** Davey, 1973

Species ***Florentinia mantellii*** Davey and Williams, 1966

Plate 1, Fig. j

Age: late Cenomanian.

Description: *Florentinia mantellii* exhibits spherical to sub-spherical dinoflagellate cysts with a smooth to lightly granular central body, often more markedly granular beneath the processes. The cyst bears thin-walled, hollow, tubular processes, mainly simple and few distally bifurcating, approximately one per plate, open distally, with occasional branches or tubules. The processes are regularly arranged and exhibit a reflected tabulation of 6'', 6c, 5''', 1p, 1''''. The apical, cingular, precingular processes are relatively fine with tapering distally, ending in a small expansion or bifurcation. Postcingular processes 2''', 3''', and 4''' are exceptionally wide, either bifurcating distally or giving rise to tubules; process 5''' is smaller. The sulcal processes vary in shape, from elongate acuminate to finely tubular, and the antapical process is distinctly larger, lagenate, convex distally, sometimes bearing small spines around the convexity. The archeopyle is primarily precingular (3''), possibly with an incipient tear between the apical and precingular plates.

Remarks: *F. mantellii* is similar to *F. radiculata* but is now considered to be more closely related to F. deanei (Davey et Williams 1966). *F. deanei* does not possess compound processes but does have a combination archaeopyle and marked variation in process size. In addition, *F. deanei* is generally larger and has more massive, and sometimes lagenate, processes (Davey, 1966). Type locality of the specie is Fetcham Mill (Surrey, England) from Cenomanian age.

Family **Gonyaulacaceae** Lindemann, 1928

Genus ***Hystrichodinium*** Deflandre, 1935

Species ***Hystrichodinium pulchrum*** Deflandre, 1935

Plate 1, Fig. d

Age: Senonian – Hauterivian.

Description: Specie resembles a *Peridinium* with a helicoid furrow dividing the theca into equal-sized epitheca and hypotheca. The entire surface is adorned with long, hollow horns,

irregularly distributed but equidistant, often appearing rigid yet somewhat flexible. The membrane, with distinct ornamentation and strong punctuations, lacks visible plates and presents lines of punctuations parallel to the transverse furrow, occasionally along meridian lines (Deflandre, 1936). Dimensions range from 45-55 μm in length, 110-125 μm including horns, and 42-48 μm in width. The specific details about an archeophyle are not explicitly mentioned in the provided information (Sarjeant, 1966).

Remarks: Type locality is Silex (Le Múe Seine-et-Marne, France) from Senonian age. Deflandre provided a detailed description in 1936. According to Sarjeant in 1966, there was speculation that this species could be a younger name for *Xanthidium spinosum*, which is presently known as *Exochosphaeridium spinosum*. The preservation quality is high in the samples and abundant in the slides of the Munk Marl Bed levels.

Family **Goniodomataceae**

Genus ***Hystrichosphaeridium*** Deflandre, 1937

Species ***Hystrichosphaeridium arborispinum*** (Davey, 1966), Stover and Ewitt, 1978

Plate 3, Fig. f

Holotype: Davey and Williams 1966b, p. 61, pl. 9, Fig. 10

Age: Early-Middle Barremian

Description: The cysts of *Hystrichosphaeridium* are subspherical, featuring a smooth surface and bearing approximately 25 to 30 hollow, commonly cylindrical intratabular processes that are usually open and typically expanded at their distal ends. These processes are similar in shape and have denticulate to aculeate tips. The cysts possess a reflected tabulation pattern of 4, (-5), 6``, 6c, 5-6```, 1p, 1````` with an apical archaeopyle of the type (tA).

Remarks: The preservation of the fossils is not the best, but the processes that formed them are still recognizable. Duxbury (2023) explains that specie is effectively absent from the Hauterivian and early Barremian at Speeton Clay from England.

Family **Gonyaulacaceae** Lindemann, 1928

Genus ***Kleithriasphaeridium*** Davey, 1974

Species ***Kleithriasphaeridium corrugatum*** Davey, 1974

Plate 1, Fig. l

Age: Early Barremian (Davey, 1974)

Description: *Kleithriasphaeridium corrugatum*, has an almost spherical central body adorned with robust, faintly ribbed tubular processes that exhibit variations in both length and width, especially notable in the sulcal processes that appear notably narrow (Davey, 1974). The processes slightly broaden distally and terminate with secate or denticulate margins, while closer to the central body, the ribs become more prominent, extending radially from the base of each process. Notably, between adjacent processes, the ribs tend to adopt a vermiform appearance, occasionally linking the processes through a proximal membrane. The central body wall beneath these tubular processes is thick and coarsely granular, with a precingular archaeopyle consistently present. The surface, difficult to ascertain in detail, exhibits a complex series of ribs and corrugations among the processes, suggesting a somewhat circular arrangement, with approximately 20 to 21 large tubular processes and about 4 sulcal processes observed in the cyst (Davey, 1974).

Remarks: The morphology of the cysts can be used to infer the behavior and ecology of the dinoflagellate (Fensome, 2008). The surface of the cysts is covered in fine ridges and grooves (Duxbury, 2023; Ogg, 1994). Preservation quality high in the Munk Marl Bed samples and the processes are quite remarkable in distinguishing between the *Florentinia mantelli.*

Genus ***Kleithriasphaeridium*** Davey, 1974

Species ***Kleithriasphaeridium eoinodes*** (Eisenack, 1958), Sarjeant (1985)

Plate 3, Fig. h

Age: Barremian – Aptian.

Description: *Kleithriasphaeridium eoinodes*, initially described by Eisenack in 1958 and later emended by Sarjeant in 1985, presents a chorate, skolochorate cyst structure. The central body appears broadly ovoidal in lateral view and circular when observed apically. Its surface ranges from laevigate to granulate. The cyst features tubiform to buccinate processes, which vary in thickness, with solid sulcal processes and hollow non-sulcal processes that may exhibit very fine perforations. The processes ramify distally, terminating with a coarse secate or denticulate margin. The length of these processes is about 50% of the central body cross-measurement. A precingular archaeopyle is consistently developed, indicated as a

single-plate type formed by the loss of paraplate 3'''. The paratabulation follows a specific pattern denoted by 4'', 6''', 6c, 5-?6''''', 1p, 1''''''', ?4s. Dimensions include an overall diameter of 62-71 μm and a central body diameter of 30-35 μm (Sarjeant, 1985).

Remarks: According to Below (1982*), Kelithriasphaeridium simplicispinum* is considered to be a taxonomic junior synonym of *Kelithriasphaeridium eoinodes*. *Kelithriasphaeridium eoinodes* was originally described from the Late Aptian of Germany. The discovery of *Kelithriasphaeridium eoniodes* is important because it provides information about the marine ecosystems of the Aptian and Barremian periods (Below, 1982). It has since been found in other parts of Europe, as well as in North Africa and North America (Sarjeant, 1985). It is not abundant specie in the Munk Marl Bed samples but not hard to distinguish from *Kleithriasphaeridium corrugatum* and *Florentinia mantelli.*

Genus ***Kleithriasphaeridium*** Davey, 1974

Species ***Kleithriasphaeridium fasciatum*** Davey, 1966

Plate 3, Fig. j

Age: Barremian – Berriasian

Description: *Kleithriasphaeridium fasciatum*, as described by Davey and Williams in 1966, displays a spherical to subspherical central body. The cyst features a fibrous periphragm and a reticulate endophragm. Its processes are short, wide, smooth, or slightly fibrous, always hollow, and terminate with denticulate distal ends. Each cyst consists of 18-20 of these tubiform processes, varying in length between 12-25 μm, while the central body ranges in diameter from 35-47 μm. An apical archaeopyle is typically present, albeit challenging to determine its exact shape. The central body and process nature bear similarities to certain Hystrichosphaeridium species, hinting at potential relationships among these forms due to shared characteristics of periphragm composition. However, the exact type of archaeopyle is yet to be precisely determined. (Davey and Williams, 1966).

Remarks: The species was originally described from the Barremian of England, but it has since been found in other parts of Europe, as well as in North Africa and North America (Davey, 1966).

The periphragm on the surface of the central body and when composing the processes of *Florentinia mantelli* is very similar to *Kleithriasphaeridium fasciatum*, which may indicate a

relationship between this species (Davey, 1966; Davey, 1974).

Family **Gonyaulacaceae** Lindemann, 1928

Genus ***Kiokansium*** Below, 1982

Species ***Kiokansium unituberculatum*** Stover and Evitt, 1978

Plate 3, Fig. b

Age: Campanian – Valanginian.

Description: Specie has a subovate cyst shell with an inner ring of pointed protuberances emerging from a distinct inner band, terminating in a small knob or neck. The exterior of this band displays a fringe area featuring flexible, curved, bifurcated, or pointed processes. The cyst's diameter ranges between 33-57 μm, while the maximum diameter of the shell is about 46 μm. These solid processes exhibit proximal flaring and distal furcation into several very fine, flexuous spines, typically measuring 15-25 μm in length and around 2 μm in thickness at the base. The archeopyle is a two-plate precingular structure, and the surface presents an approximate density of 1.5 processes per 5 μm of edge (Tasch, 1964; Fensome, 1995).

Remarks: *Kiokansium unituberculatum*, initially described as *Hystrichosphaeridium unituberculatum* by Tasch in 1964 and later reclassified by Stover and Evitt in 1978. The taxonomic classification of *Kiokansium unituberculatum* has undergone a transition from its original designation within *Hystrichosphaeridium* to its current placement in *Kiokansium*. *Hystrichosphaeridium recurvatum* subsp. *polypes* is suggested to be a taxonomic junior synonym of *Kiokansium polypes* by implication, according to Duxbury (1983).

Family **Ceratiaceae** Lindemann, 1928

Genus ***Muderongia*** Cookson & Eisenack, 1958

Species ***Muderongia crucis*** (Neale & Sarjeant 1962) Monteil, 1991

Plate 1, Fig. k

Age: Valanginian – Barremian.

Description: *Muderongia crucis* exhibits an ellipsoidal cyst shape with a distinct structure: four prominent, tapered horns, including an apical, two laterals, and an antapical horn. The shell is yellowish-brown, perforate, and exhibits variable concentrations of perforations, often more concentrated within the horns. Symmetrical and two-layered, the cornucavate

pericyst is proximate to proximochorate. The tapered horns show varying thickness and features, with pointed, closed distal ends and narrow proximal ends. The periphragm, mostly scabrate with small, unorganized perforations, and the endocyst may display a protrusion at the horns' bases. The archeopyle is apical (type 4A) with an angular margin and marks the paratabulation while the perisulcal area is not observed.

Remarks: *Muderongia crucis* stands out from other species within the genus due to its unique horn length and shape. Unlike species like *Muderongia tetracantha* and *Muderongia mcwhaei*, *Muderongia crucis* lacks distinct notches on its horns. Additionally, compared to Muderongia staurota, it has narrower axial parts of lateral horns, an elongated postcingular extension, and a slender antapical pericoel, as highlighted by Neale and Sarjeant in 1962 and Monteil in 1991.

Family **Ceratiaceae** Lindemann, 1928

Genus ***Muderongia*** Cookson & Eisenack, 1958

Species ***Muderongia staurota*** **(**Sarjeant 1966) Monteil, 1991

Plate 3, Fig. e

Age: early Barremian**.**

Description: *Muderongia staurota`s* cyst shape is proximate to proximochorate, compressed dorsoventrally, possessing a two-layered structure and symmetrical pericyst characterized by four prominent tapered horns: one apical (axial), two subequal lateral (bent), and one antapical (axial). These horns, either closed and pointed or open and perforated-ragged at their distal extremities, show varying width at their proximal ends, particularly with the antapical horn consistently wider than the others. The surface, comprising the periphragm, is notably thin, ranging from smooth to scabrate and may display fine perforations in the distal portions, sometimes ornamented by processes. The endophragm appears thin, exhibiting varying textures from smooth to granulate. The archeopyle is apical in type (4A) with an angular margin and is accompanied by a marked parasulcal notch and a free operculum. Paratabulation is indicated mainly by the archeopyle and is further expressed through the distribution and types of processes, if present, signifying stages from I to IV, with a suggested pericingulum inferred from the lateral horns (Monteil, 1991). The overall dimensions of the holotype are 170µm x 93µm (length x width).

Remarks:. *Muderongia staurota* is most similar to *Muderongia mcwhaei*, but it can be distinguished by the lack of a second antapical horn (Alberti, 1961; Neale, 1962). *Muderongia simplex*, described by Alberti (1961), is from the Lower Cretaceous (Hauterivian to Valanginian) of Germany and Bulgaria. It has short, blunt, notched lateral horns and a second antapical horn. *Muderongia perforata*, also described by Alberti (1961), is from the Upper Cretaceous (Turonian) of Germany. It has extremely long and delicate horns, with the lateral horns being notched so deeply that they almost bifurcate into unequal branches. *Muderongia tomaszowensis*, described by Alberti (1961), is from the Lower Cretaceous (Valanginian) of Germany and Poland. It has stubby apical and antapical horns and blunt notched lateral horns. *Muderongia crucis*, described by Neale and Sarjeant (1962), is from the Lower Cretaceous (Hauterivian) of England.

Family **Ceratiaceae** Lindemann, 1928

Genus ***Muderongia*** Cookson & Eisenack, 1958

Species ***Muderongia tetracantha*** **(**Gocht, 1957) Monteil, 1991

Plate 2, Fig. d

Age: late Hauterivian.

Description: *Muderongia tetracantha* exhibits a dorso-ventrally compressed, symmetrical, bilaterally elongated shape characterized by four prominent, tapered horns: one apical, two subequal curved lateral horns (Type L IV), and one antapical horn (Type ATP I). The surface of the cyst displays a thin, scabrate periphragm with small, unorganized perforations and a granulate endophragm. These cysts lack ornamentation and are distinguished by their angular, apical archeopyle (Type 4A) with a marked parasulcal notch. Paratabulation, indicated solely by the archeopyle, paracingulum, and perisulcus, implies a formula of ?pr, 4', 0a, 6".

Remarks: This species differs from *Muderongia staurota* and *Muderongia crucis* in having lateral horns that are curved (Alberti, 1961). *Muderongia tetracantha* is typically found in marine sediments from all over the world, including Australia, North America, and Europe (Gocht, 1957; Morgan, 1980; Jansonius, 1982).

Family **Gonyaulacaceae** Lindemann, 1928

Genus ***Oligosphaeridium*** Davey, 1966

Species ***Oligosphaeridium abaculum*** Davey, 1979

Plate 3, Fig. g

Age: Barremian - early Albian.

Description: *Oligosphaeridium abaculum* manifests a spheroidal cyst shape with minimal dorso-ventral flattening. Its wall is two-layered and closely appressed, intraperforate, and lightly to densely scabrate or pitted. The tubiform processes exhibit distal flaring resulting in six slight flexuous spines, joined medially in some instances, with variation in stem width and length but overall approximately half the endocyst's diameter. The cyst has an apical archaeopyle, presenting a strong zigzag margin with a deep parasulcal notch. Paratabulation, primarily marked by low ridges or changes in internal wall structure, sets it apart from other species, differing notably from *Oligosphaeridium verrucosum* due to the distinctiveness of its periphragm granulation and paratabulation form. Additionally, the presence of tabulate specimens in the Lower Cretaceous of Alaska suggests a potential comparison to this species.

Remarks: *Oligosphaeridium abaculum* was first found in the Aptian of the northern Bay of Biscay by Davey (1979). Wiggins and Engelhardt also found tabulate specimens of *Oligosphaeridium* in the Lower Cretaceous of Alaska, but it is not clear if these specimens are the same species (Evitt, 1977).

Species ***Oligosphaeridium complex*** Davey, 1966

Plate 3, Fig. d

Age: latest Ryazanian-earliest Hauterivian.

Description: *Oligosphaeridium complex* exhibits a subspherical to ovoidal central body with a two-layered wall - an endophragm and a periphragm producing processes. Processes are mainly cylindrical, expanding distally with aculeate or secate margins, simple or branched, occasionally orthogonal or recurved, not exceeding 18 in number, often with an apical archaeopyle displaying a zigzag margin. The cyst size ranges from 29-58 μm for the central body and 23-47 μm in process length, presenting variations in granularity in periphragm and process characteristics across different geological periods like Cenomanian and Ypresian (Davey and Wiliams, 1966).

Remarks: The specimens of this species from the Speeton Clay (Barremian) of Yorkshire are very similar to the forms illustrated by Eisenack (1958). The periphragm of the central body is often slightly granular, and some of the processes are more deeply divided than is usual in this species. Specimens from the London Clay (Ypresian) strongly resemble the Cenomanian forms, but the processes may be a little stouter (Eisenack, 1958). The *Oligosphaeridium* complex is a common group of dinoflagellate cysts in the Mesozoic and Cenozoic eras (Davey, 1966).

Family **Gonyaulacaceae** Lindemann, 1928

Genus ***Stanfordella*** Helenes, 1997

Species ***Stanfordella fastigiata*** (Duxbury, 1977) Helenes and Lucas-Clark, 1997

Plate 2, Fig. j

Age: early Hauterivian-early Barremian.

Description: *Stanfordella fastigiata* cysts exhibit a proximate, subhexagonal body with an apical horn, characteristic of the early Hauterivian to early Barremian period. The cyst's endophragm, except under the apical horn and beneath the parasutural ridges, is usually smooth or finely granular. The periphragm forms high crests that terminate in distally denticulate elements, featuring spiny ridges defining a paratabulation conforming to that of Stanfordella. The cyst's structure is hexagonal with a prominent apical horn. The archeopyle, a precingular type P4, is formed by the loss of plate 3" in the paratabulation formula ?4", 6", ?6"""", 1p, 1pv, 1"""""". The species differs from *Rhynchodiniopsis serrata* primarily in its size and specific structural details in the denticulation and horn structure, as well as the distinct size dimensions of the cyst. The overall dimensions are within the range of 58-81 x 54-78 μm, while the equatorial diameter is about 70 μm and the apical horn's height approximately 15 μm (Helenes, 1986; Duxbury, 1977).

Remarks: It was originally described as *Gonyaulacysta fastigiata* by Duxbury (1977), but was later transferred to the genus Stanfordella by Helenes and Lucas-Clark (1997). *S. fastigiata* is a common fossil in the Early Cretaceous rocks of Europe and North America. It has been used as a zonal marker in the Berriasian and Barremian stages. The species is also found in other parts of the world, including Asia and South America (Jan du Chene, 1986).

Genus ***Scriniodinium*** Klement, 1957

Species ***Scriniodinium campanula*** Gocht, 1959

Plate 1, Fig. c

Age: Berriasian – Campanian.

Description: *Scriniodinium campanula* cysts feature a flattened, tabulated outer shell with a distinct longitudinal furrow, an epitheca resembling a helmet, a short and slightly sagged apical horn creating a bell-like shape, and a slightly elongated, rounded or blunt hypotheca at the pole. The inner body is ovoidal and laterally separated from the main body, measuring between 85-100 μm in length and 74-91 μm in width. Surface structure and the presence of processes are unspecified.

Remarks: It was originally described by Gocht (1959) as *Gonyaulacysta campanula* but was later transferred to the genus *Scriniodinium* by Riding and Fensome (2003). Jan du Chêne et al. (1986a) described the morphology of *Scriniodinium campanula*, including its paratabulation and ornamentation. Fensome et al. (1991) listed *S. campanula* as a member of the *Scriniodinium complex*, which is characterized by a complex paratabulation and a thick, smooth wall. Stover and Evitt (1978) provided a range chart for *S. campanula*, which shows that it is found in the Aptian to Albian stages of the Cretaceous. Riding and Fensome (2003) provided a revised diagnosis for *S. campanula* and discussed its taxonomic relationships with other dinoflagellate cysts. Harker and Sarjeant (1975) summarized the stratigraphic distribution of *S. campanula*, and Brideaux and McIntyre (1975) provided a detailed description of the cyst from the Aptian-Albian rocks of the Horton River in Canada.

Genus ***Spiniferites*** **(**G.A.Mantell, 1850) Sarjeant, 1970

Spiniferites **spp.**

Plate 1, Fig. f

Age: Early Cretaceous to Cenozoic.

Description: *Spiniferites* cysts display a subspherical body with proximochorate to skolochorate features and exhibit only gonal or gonal with intergonal processes. The body is characterized by the presence of parasutural ridges or septa connecting the bases of these processes, while the tips remain unconnected. Gonal processes end in trifurcations, and

intergonal ones bifurcate, with the gonyaulacacean paratabulation primarily recognized through these ridges and septa. The cyst features a precingular archeopyle, identified as Type P, and is typically subspherical in shape.

Remarks: The genus was first described by Mantell (1850) and was later revised by Sarjeant (1970). Sarjeant (1970) provided a detailed description of the morphology of *Spiniferites spp.*, including the different types of spines and the range of variation in the cyst size and shape.

Genus ***Systematophora*** **(**Klement, 1960) Riding and Helby, 2001

Systematophora spp.

Plate 2, Fig. g

Age: late Jurassic – Cenozoic.

Description: *Systematophora* cysts present a spherical to ellipsoidal central body with a smooth to granular surface. The cyst shape is typically subspherical with a moderate surface texture. Processes, penitabular to intratabular, emerge from the precingular, postcingular, and antapical paraplates, showing various levels of interconnection, forming circular or elliptical groupings. They are solid, of moderate length, featuring branching from a single bifurcation to complex, multi-branched structures. The paratabulation consists of 0-2pr, 4`, 6", 5-6c, 5-6, 1p, 1, 1-5s. The archeopyle is apical, often exhibiting a sulcal notch, indicating Type (tA). Cingular and sulcal paraplates might lack processes or showcase single isolated processes or pairs joined together proximally by a wall or ridge (Sarjeant, 1990; Riding and Helby, 2001).

Remarks: The genus was first described by Klement (1960) and was later revised by Brenner (1988). Klement (1960) described the morphology of *Systematophora* spp., including the different types of cyst wall plates and the range of variation in the cyst size and shape.

Brenner (1988) provided a detailed description of the morphology of *Systematophora* spp., including the different species and their stratigraphic distribution.

Stancliffe and Sarjeant (1990) used *Systematophora* spp. to correlate the Bathonian to Oxfordian (Jurassic) rocks of Europe. Riding and Helby (2001) studied the dinoflagellate cysts from the Late Jurassic (Oxfordian) *Wanaea spectabilis* Zone in the Timor Sea region and found that *Systematophora spp.* was one of the most common species in the sample.

Eaton et al. (2001) re-evaluated the status of the dinoflagellate cyst genus *Cleistosphaeridium*,

and found that some species of *Cleistosphaeridium* should be transferred to the genus *Systematophora*. Downie and Sarjeant (1965) provided a bibliography and index of fossil dinoflagellates and acritarchs, which includes references to *Systematophora* spp.

Genus ***Phoberocysta*** Gocht, 1957

Specie ***Phoberocysta neocomica*** (Gocht, 1957) Helby, 1987

Plate 2, Fig. f

Age: Berriasian – Aptian.

Description: *Phoberocysta neocomica* cysts exhibit a rhomboidal shape with prominent horns, including an apical horn, cingular horns, and an antapical horn. The surface features variously sized protrusions concentrated along the cyst's outline, often displaying pointed or blunt shapes. These projections may bear large, solid, capitate spines and smaller accompanying spinules. The cyst's structure is two-layered, with a rhomboidal endocyst closely appressed to the pericyst. The archeopyle is apical, showing a zigzag suture and a left-sided parasulcal notch. The surface also shows variable textures from smooth to scabrate, with some perforations in the periphragm. A transverse feature, the paracingulum, is evident across the dorsal surface onto the paracingular horns. The parasulcus is sinuous, offset to the left ventral position on the epicyst from the midventral position on the hypocyst (Helby, 1987).

Remarks: The ovoid dinoflagellate cyst was originally described as Wetzeliella? neocomica by Gocht (1957). It was subsequently transferred to the genus *Phoberocysta* by Millioud (1969) and emended by Helby (1987) to include a more detailed description of the thecal plates. It is a taxonomic junior synonym of *Muderongia tomaszowensis*, but this synonymy has not been generally followed. The cyst is known from the Hauterivian strata of Europe, North Africa, Asia, and Australia.

Genus ***Ptrerodinium*** Eisenack, 1958

Specie ***Pterodinium alectrolophum*** Eaton, 1976

Plate 1, Fig. 1

Age: Middle Barremian.

Description: *Pterodinium alectrolophum* cysts possess an ovoidal theca without an apical horn and exhibit a polygonal appearance due to high, delicate crests along the plate boundaries. The pericoel surface displays a coarse granulation with regularly spaced granules. These thin, high crests often have smooth or occasionally finely denticulate edges. The cyst contains seven clear cingular plates with a prominent, long, and narrow sulcus extending almost from the apex to the antapex. The archaeopyle in the paratype is well-developed, formed by the loss of plate 3'', while it's absent in the holotype (Sarjeant, 1966).

Remarks: *Pterodinium alectrolophum* is a dinoflagellate cyst that was first described by Sarjeant (1966b). Typical locality is Speeton Clay (Heslerton, England) from Middle Barremian age. According to (Sarjean, 1966) it is named: *Leptodinium alectrolophum*. It is distinguished from all described species by its combination of crest and thecal morphology and tabulation. Jan du Chêne et al. (1986a) provided a detailed description of the morphology of *Pterodinium alectrolophum*, including the different types of spines and the range of variation in the cyst size and shape. They also discussed the stratigraphic distribution of the species, and its use as a biostratigraphic marker in the Jurassic rocks of the world. It is also a potential indicator of environmental conditions, as it is found in a variety of marine environments, including shallow and deep water (Below, 1982; Sarjeant, 1966).

Family **Ceratiaceae** Lindemann, 1928

Genus ***Pseudoceratium*** Gocht, 1957

Species ***Pseudoceratium pelliferum*** (Gocht, 1957) Dörhöfer and Davies, 1980

Plate 2, Fig. a

Age: Valanginian-late Hauterivian

Description: *Pseudoceratium pelliferum* cysts are asymmetrically triangular, longer than wide, and exhibit a strong apical horn along with two shorter, unevenly sized antapical horns. The cyst surface is densely adorned with short, rounded-obtuse, bristle-like processes, which may stand alone or connect at the base, covering the cyst more or less uniformly. The cyst measures between 92-173 μm in length and 52-70 μm in width, with the apical horn around 35 μm, the larger antapical horn about 25 μm, and the smaller antapical horn about 12 μm. The species now includes two anterior intercalary plates forming part of the operculum, an archaeopyle (4A2I), and numerous short penitabular and intratabular processes, possibly

following latent sutures between fused plates. The cyst surface between the processes appears finely corrugated-reticulate, while a slight left postcingular bulge suggests a possible fourth horn position (Dörhöfer and Davies, 1980; Gocht, 1957).

Remarks: Typical locality is Well Ruehlertwist 3 (Emsland, NW Germany) from Valanginian-Hauterivian age.

Family **Gonyaulacaceae** Lindemann, 1928

Genus ***Tanyosphaeridium*** Davey, 1966

Species ***Tanyosphaeridium* spp.**

Plate 2, Fig. e

Age: late Jurassic-early Cretaceous

Description: *Tanyosphaeridium* spp. exhibits distinct features. The cyst's shape is elongate ellipsoidal, characterized by a central body composed of endophragm and periphragm, where the latter forms the tubular processes. These processes, either nontabular or intratabular, are typically open and not interconnected at their distal ends, arranged in a more or less circular manner around the central body. The cyst displays a smooth or faintly ornamented periphragm or autophragm between processes, with no parasutural features. An apical archaeopyle of type (tA) is observed, often accompanied by a free operculum, and the cysts are described as skolochorate, lacking interconnected distal connections among processes. This distinctive structure sets *Tanyosphaeridium* apart from similar genera like *Prolixosphaeridium*, *Peridictyocysta*, and *Distatodinium*, mainly due to the absence of complexly branched or trabeculae-connected processes and the unique arrangement of the archeopyle at the apical end (Davey, 1966).

Remarks: *Tanyosphaeridium* spp. is a significant genus of dinoflagellate cysts first characterized by Davey and Williams in 1966. The type species, *Tanyosphaeridium variecalamum*, dates back to the late Jurassic and early Cretaceous.

Family **Gonyaulacaceae** Lindemann, 1928

Genus ***Tanyosphaeridium*** Davey, 1966

Species ***Tanyosphaeridium xanthiopyxides*** (Wetzel, 1933) Sarjeant, 1985

Plate 2, Fig. c

Age: Campanian – Thanetian.

Description: *Tanyosphaeridium xanthiopyxides* is a small, ellipsoidal to elongate-ellipsoidal cyst characterized by its distinct features. The cyst possesses an elongated, thin-walled structure with a surface that appears feebly granulated. It is adorned with approximately 50-60 widely spaced, slender, and hollow processes, each exceeding one-third of the longest diameter of the complete cyst. These processes take on a trumpet-like shape at their distal ends, with weakly denticulate or smooth edges. The cyst is identified by its apical archaeopyle of the type (tA), which typically consists of a free operculum or opercular pieces.

Remarks: The species initially described by Wetzel in 1933 as *Hystrichosphaera xanthiopyxides* was later renamed *Hystrichosphaeridium xanthiopyxides* due to the non-valid publication of the former genus name. This species has been reassigned under various genera including *Baltisphaeridium*, *Prolixosphaeridium*, and *Tanyosphaeridium*. It spans Late Maastrichtian to Danian periods, displaying consistent features, hinting at a Maastrichtian origin for its type material and indicating possible evolutionary ties to earlier forms found in the Albian of the Paris basin (Stover, 1978; Sarjeant, 1985; Dietz, 1999).

Family **Gonyaulacaceae** Lindemann, 1928

Genus ***Rhynchodiniopsis*** G.Flandre, 1935

Species ***Rhynchodiniopsis aptiana*** (Deflandre, 1935) Sarjeant, 1982

Plate 1, Fig. a

Age: Hauterivian – Albian.

Description*:* *Rhynchodiniopsis aptiana*, exhibits a distinct morphology characterized by an irregularly hexagonal to rounded-hexagonal cyst shape with an apical mamelon or horn of varying length. The cyst consists of an epitract and hypotract, both almost equal in size and resembling steep-sided cones truncated at approximately half to two-thirds of their height. The flanks of these tracts are typically planar to convex, sometimes shallowly concave, with the epipericoel primarily situated on the horn or occasionally restricted to the horn tip. The complex tabulation showcases marked ridges or crests of variable characteristics, typically denticulate to echinate, accompanied by gonal spinules longer than the crests. The cyst's

paratabulation features distinct plate arrangements (2pa, 4", 1-2a, 6"", 6c, 6"""", 1p, ?0pv, 1"""") while the archaeopyle is a single-plated precingular structure formed through the loss of paraplate 3"", with a reduced operculum (Lindemann, 1928; Sarjeant, 1982).

Remarks: The species *Rhynchodiniopsis aptiana*, first described by Deflandre in 1935, has had differing taxonomic placements. Lentin and Williams (1973) upheld its status in Rhynchodiniopsis, while Below (1981) proposed it as Gonyaulacysta fimbriata, a view challenged by Sarjeant (1982). There was confusion about Stover and Evitt (1978) emending the species, which they didn't. The holotype is shown in Deflandre's illustrations (1935, 1936b). Originally labeled *Rhynchodiniopsis aptiana*, it was also linked to the genus Gonyaulacysta. This species originates from the Senonian stage in the Cretaceous period and has been found in various marine and lacustrine settings, as mentioned by Sarjeant (1982) and Jan du Chene (1986).

5.3 Spores and Pollen

Regarding their explanation and defining taxonomically the morphology played a crucial role to help separate them by their shape.

Genus: ***Bisaccate*** Potonié and Kremp, 1954

Plate 5, Fig. a

Description and remarks: *Bisaccate* pollen grains are characterized by the presence of two sacci. In polar view, the outline of the sacci appears disconnected from the outline of the corpus, giving the grains the appearance of consisting of three distinct, oval-shaped parts. This unique feature distinguishes *bisaccate* pollen grains from other types of pollen (Punt et al., 2007; Hughes, 1989).

This is usually rounded with different sacci sizes. The exines are thin and finely granulated. Their sacci are coarsely grained with size ranging between 25-30μm. The sacci are between 10-15μm for the types identified (Adojoh et al., 2019). These pollen types belong to the gymnosperm group.

Genus: ***Callialasporites*** Sukh Dev, 1961

Plate 4, Fig. h

Description and remarks: Typically, these spores exhibit a monolete structure and possess a circular to subcircular shape. They commonly feature a granulate or finely perforate surface ornamentation (Sukh Dev, 1961).

Genus: ***Cicatricosisporites*** Potonié & Gelletich, 1933

Plate 4, Fig. j

Description and remarks: *Cicatricosisporites* is a genus of fossil spores in the Schizaeaceae (tree ferns). It was first described by Potonié and Gelletich in 1933 and is characterized by its tuberculate (warty) ornamentation. *Cicatricosisporites* have a wide geographic and stratigraphic range, having been found the Middle Jurassic to the Early Cretaceous.

Genus: ***Cibotiumspora*** Chang, 1965

Plate 4, Fig. c

Description and remarks: These spores are generally tetrahedral or trilete, often in the size range of 20 to 40 micrometers. The spores possess a well-defined exine, the outer layer, which can exhibit reticulate, granulate, or striate surface ornamentations (Raine et al., 2011; Zhang et al., 2021)**.** *Cibotiumspora* is a genus of fossil spores in the *Cibotiaceae* (tree ferns). It was first described by Chang in 1965.

Genus: ***Classopollis*** Pflug 1953 emend. Pocock & Jansonius, 1961

Plate 5, Fig. c

Description: Spherical to circular in equatorial section. Monoporate with a circular distal pore. Exine ornamented by striate band or girdle surrounding the equator, intexine thin, laevigate, occasionally showing a small trilete mark at the proximal pole, rays of trilete mark about 3 μm long (Fig.14). Dimension**:** maximum diameter 35 (32) 31 μm

The sub-equatorial aperture that encircles pollen grains of the *Classopollis* group.

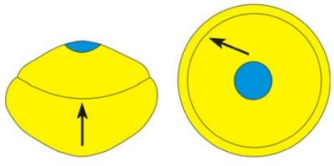

Figure 14. Rimula draw from (Punt et al., 2007).

Remarks: The genus *Classopollis* is a genus of fossil pollen in the Coniferales (conifers) family Cheirolepidaceae. It was first described by Pflug in 1953 and is characterized by its spherical shape, subequatorial circumpolar canal, and thickened equatorial band. *Classopollis* has a wide geographic and stratigraphic range, having been found in rocks from the Upper Triassic to the Eocene. It was an important component of the plant communities of the Mesozoic and Cenozoic Eras and has been reported from localities as diverse as Greenland, China, Argentina, and Australia (Balme, 1995; McLoughlin, 2009).

Genus: ***Chasmatosporites*** Nilsson, 1958

Plate 4, Fig. e

Description and remark: The type species of *Chasmatosporites* is *Chasmatosporites hians*, which was described by Nilsson in 1958. *Chasmatosporites hians*, characterized by its non-trilete, monosaccate, and stratified exine, represents this genus. The sporopollenin wall features a prominently folded surface and a thickening layer, rendering it distinct and easily identifiable. Chasmatosporites is typically spherical or subspherical in shape, displaying a reticulate pattern on the surface (Balme, 1995; Taylor, 2009).

Genus: ***Cyathides*** Couper, 1953; Jarzen, 1982

Plate 4, Fig. a

Description and remarks: *Cyathides* spores possess distinctive morphological characteristics: they are typically ellipsoidal to nearly spherical in shape, ranging from approximately 25 to 60 micrometers in size. Their exine, the outer layer of the spore, is notably thick and often ornamented with various patterns such as granulate, reticulate, or striate textures. It was first described by R.A. Couper in 1953 and was originally placed in the Family Lycopodiaceae. In 1994, Potonié proposed a new classification for the genus *Cyathidites*. He divided the genus into two subgenera: *Cyathidites* and *Australites*.

Genus: ***Cyathides***

Cyathides australis Couper, 1953

Plate 4, Fig. g

Description and remarks*:* *Cyathidites australis* is a fossil spore that was first described by R.A. Couper in 1953. The spore is characterized by its spherical shape, trilete aperture, and finely reticulate ornamentation. The name *Cyathidites australis* is derived from the Greek words "cyathos" (cup) and "idion" (peculiar), and the Latin word "australis" (southern). This is because the spore was first described from Australia. In 1968, Venkatachala suggested that the spore should be placed in a new genus, *Australites*. However, this proposal was not widely accepted, and *Cyathidites australis* remains the accepted name for the spore. In recent years, there have been a number of studies that have further characterized *Cyathidites australis*. In 2022, Vera et al. studied the spore from the Late Triassic of Argentina and found that it was morphologically similar to spores from the Early Jurassic of Australia. This suggests that *Cyathidites australis* may have had a wider geographic distribution than previously thought.

In 2023, Perez Loinaze et al. studied the spore from the Early Cretaceous of Argentina and found that it was morphologically similar to spores from the Late Triassic of Australia. This suggests that *Cyathidites australis* may have persisted for a longer period than previously thought.

Genus: ***Deltoidospora*** **(**Miner, 1935) Van Buggenum, 1985

Plate 5, Fig. b

Description and remarks: Trilete spore, triangular shape with slightly concave sides. Exine smooth to weakly punctuate punctate, 1.5-2 μm thick. Laesura at least 2/3 spore radius.

Dimension: Maximum equatorial diameter 53 (57) 62 μm.

Potonié (1956) first described the genus *Deltoidospora*, a genus of fossil spores in the *Lycopodiophyta* (clubmosses). It is characterized by its deltoid (triangular) shape and thick, tuberculate walls. Potonié (1956) described the genus and its type species, *Deltoidospora deltoidospora*, based on specimens from the Early Carboniferous of Germany. Kedo (1964) studied the occurrence of *Deltoidospora* in the Early Carboniferous of the Soviet Union, and Taylor et al. (2009) reviewed the fossil record of *Deltoidospora*, reporting it from Greenland, China, Argentina, and Australia. These localities represent a wide range of paleoenvironments, from tropical to temperate to polar, suggesting that *Deltoidospora* was a versatile plant that could adapt to a variety of conditions.

Genus: ***Densoisporites*** Weyland & Krieger, 1953

Plate 4, Fig. f

Description and remarks: These spores are typically spherical or near-spherical, ranging in size from approximately 20 to 60 micrometers in diameter. *Densoisporites* spores are characterized by their thick, tuberculate walls. They are typically found in association with fossilized plants of the Selaginellaceae Family. Dettmann (1963) first described the genus *Densoisporites*, a genus of fossil spores in the *Lycopodiophyta* (clubmosses). It is characterized by its thick, tuberculate walls and is typically found in association with fossilized plants of the Selaginellaceae Family.

Genus: ***Dictyophyllidites*** Couper, 1958 emend. Dettmann, 1963

Plate 4, Fig. b

Description and remarks: Trilete spore, amb triangular with slightly concave sides. Laesura distinct, reaching the equator with raised lips bounded by parallel labra. Dimension: Maximum diameter: 42 (44.5) 47 μm. *Dictyophyllidites* is distinguished from *Deltoidospora* by laesura enclosed within membranous elevated lips (Dettmann, 1963). It was first described by Bolkhovitina in 1953 and is characterized by its dictyoxylic (reticulate) ornamentation.

Genus: ***Fungal spore*** Fries, 1821

Plate 4, Fig. l

Description and remarks: Based on the morphology of fungal spores divided into three main groups: basidiospores, ascospores, and conidia.

Genus: ***Retitriletes*** Pierce, 1961

Plate 4, Fig. k

Description and remarks: The genus *Retitriletes* was first described by R.L. Pierce in 1961. It is a genus of fossil spores that are characterized by their trilete aperture and reticulate ornamentation.

Genus: ***Staplinisporites*** Pocock, 1962

Plate 4, Fig. i

Description and remarks: The genus based on the characteristic trilete aperture and finely reticulate ornamentation of the spores. The genus has been revised several times since it was first described, and in 2021, Zhang et al. proposed that *Staplinisporites* should be synonymized with the genus *Lycopodiumsporites*.

6

RESULTS

A total of 1877 spores and pollen were counted, and 14 *taxa* have been identified. The *Bissacates*, *Deltoidospora*, and *Dictyophyllidites* are the most abundant *taxa* across the studied the samples. The dinoflagellate cyst fauna is composed of 17 genera and 21 species across the 1753 counted specimens. The most dominant dinoflagellate cysts are *Batioladinium longicornutum, Cribroperidinium edwardsii, Hystrichodinium pulchrum* and *Pseudoceratium pelliferum* (See Appendix). Only one taxon of acritarch (*Micrhystridium* sp.) was recorded through the upper part of the log.The high-resolution sampling across the Munk Mark interval and the identification of this fossil assemblage provides additional insights to define this stratigraphic interval and allows the possibility of better correlation across other wells in the region. The MMB is not always easy to define in wireline logs or composite well logs due to the similar or locally higher gamma marls, so the biostratigraphy plays an important role to help geologists understand the subsurface in higher detail. A detailed examination of an 8 m section of the wellbore, which is a part of the Early Barremian Åsgard Formation, was conducted within the scope of this study. The studied section from the well, between 1918 m-1926 m, includes MMB levels in the middle parts of the section. The lowermost parts of the section were barren of fossils and organic matter. Dinoflagellate cysts were nearly absent, but fragments of terrestrial palynomorphs were observed. Abundant fossil content was observed in the samples analyzed from 1922-1923 m. The species *Muderongia crucis, Kleithriasphaeridium corrugatum, Kleithriasphaeridium eoinodes, Hystrichosphaeridium arborispinum* are more abundant than *Pseudoceratium pelliferum, Florentinia mantellii, Circulodinium hirtellum, Ryhcnıopsis aptiana, Batioladinium longicornutum, Muderongia tethracantha.* Sample from 1921.73 m were generally barren and had low organic matter content. However, the *Kiokansium unituberculatum* was dominant only in the upper level of the MMB, where the first two samples were taken. Samples were taken from the interval of drilling core between 1920-1921 m. They all were recovered for this interval (Fig.15). These

species are consistent with the Early Barremian age. These samples rarely contained only this species, had poor preservation quality, and the concentration of organic matter was observed to be quite low. Therefore, the immediate upper levels of these levels were observed as 1920 m and the first 30-40 cm above them as barrens but then, when it reaches 1919 m, *Stanfordella fastigiata*, *Cassiculosphaeridia magna, Hystricodinium pulchrum* are recorded.

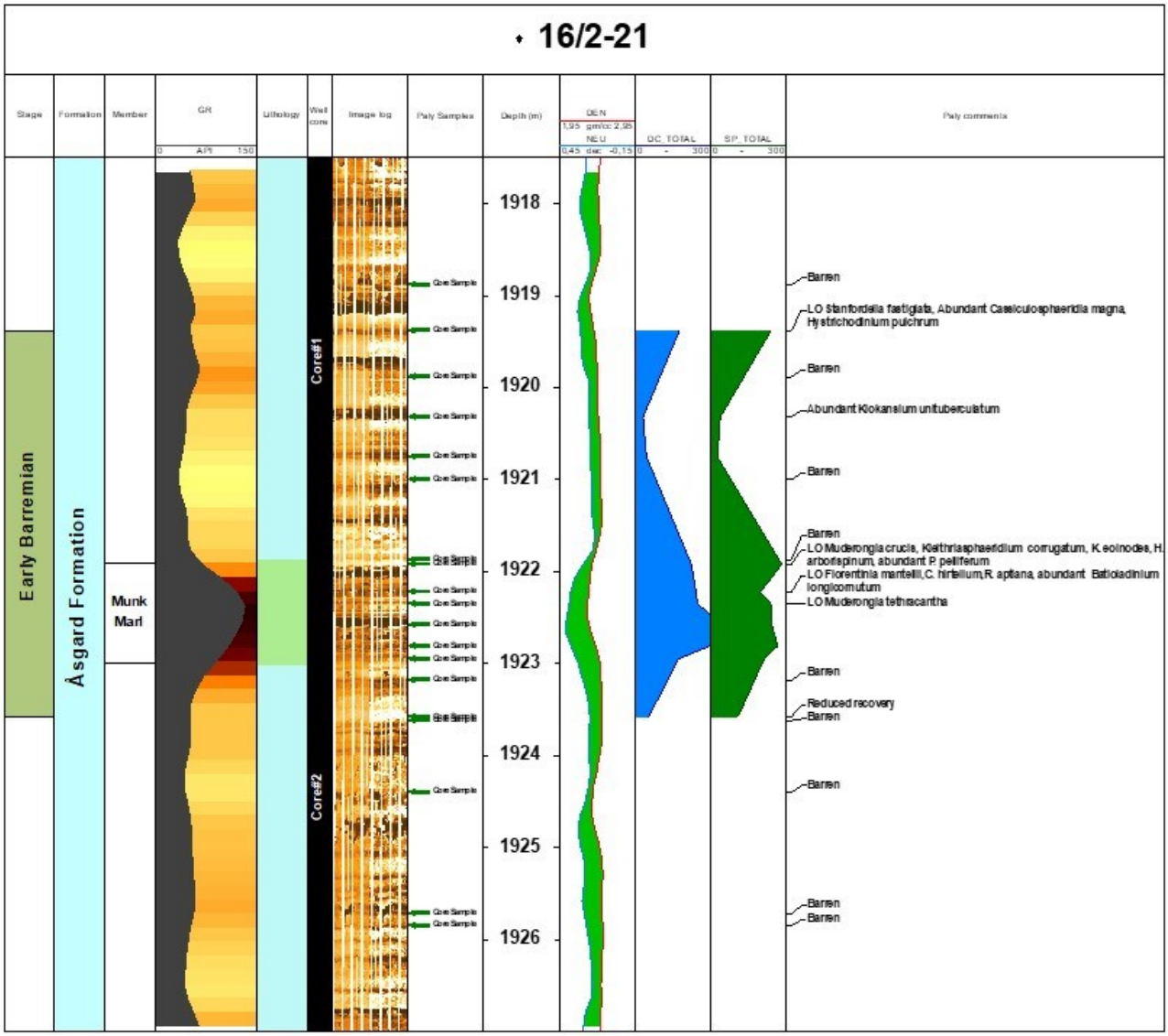

Figure 15. General biostratigraphical section chart of the Munk Marl Bed.

The uppermost level of the section was very poorly preserved and was observed to be barren of palynomorphs and organic content. This is likely due to the fact that this level is transitional to the Late Barremian and may have experienced different environmental conditions than the underlying levels. The lack of organic matter in the samples taken from the first levels of the section may also be due to these different environmental conditions.

Additionally, these levels may also be characterized by lithological differences, or differences in the composition of the rocks. For these reasons, the data specific to the MMB did not provide consistent results at these levels.

Figure 16 presents the distribution of dinoflagellate fossils in the analyzed core samples. The fossil assemblage are diverse in the MMB interval, with a variety of species found. Also, Figure 17 presents the distribution of spores and pollen found in the core samples from the MMB interval. The spores and pollen distribution are also diverse, with a variety of species found. The observed variations in fossil content within the stratigraphic interval offer invaluable insights into environmental changes and the transition between the Early and Late Barremian age.

The occurence of *Stanfordella fastigiata*, *Cassiculosphaeridia magna,* and *Hystricodinium pulchrum*, particularly in the lower part of the MMB, suggests a transitional phase, indicating shifts in environmental conditions and potential lithological variations impacting the preservation of palynomorphs. Moreover, the scarcity of palynomorphs in certain levels, the probable consequence of differing environmental conditions or lithological disparities, necessitates a more nuanced interpretation. Understanding these intricacies is crucial for refining the biostratigraphic context and reconstructing the paleoenvironmental dynamics of the Munk Marl Bed. The data obtained from the examination of the Munk Marl Bed's fossil assemblage plays a pivotal role in refining the characterization of this stratigraphic interval, particularly in situations where wireline logs or composite well logs might struggle to distinctly delineate the MMB due to similar lithological features.

Additionally, the study sheds light on environmental changes, preservation qualities, and variations within the Munk Marl Bed. The transitional phase between Early and Late Barremian is recognized, allowing for better comprehension of the changes in environmental conditions and how they might have impacted the preservation and distribution of palynomorphs. Furthermore, the lithological differences and their impact on fossil preservation are highlighted, providing crucial context for interpreting data specific to different stratigraphic levels.

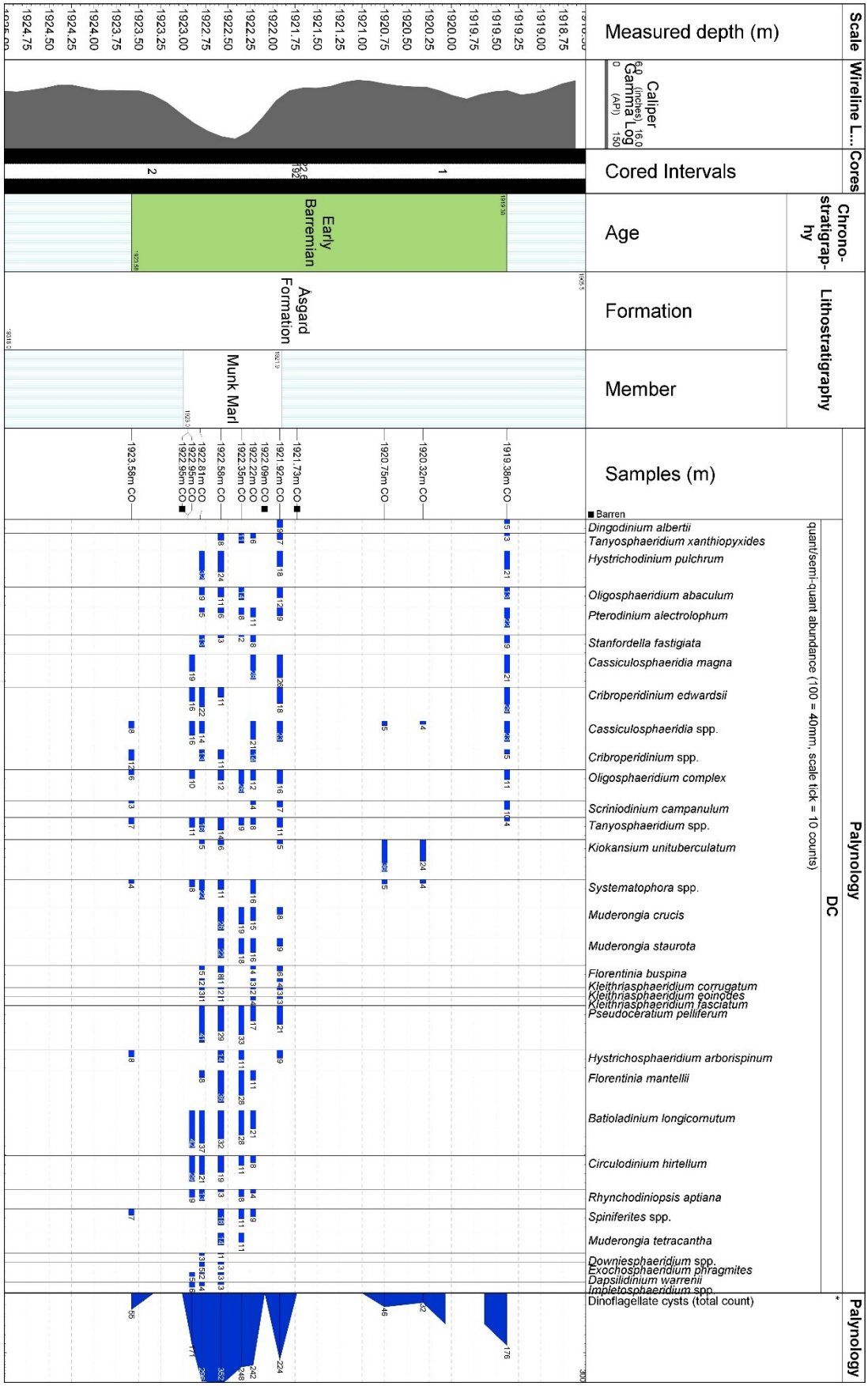

Figure 16. Dinoflagellate distribution chart of the 16-2-21 Well.

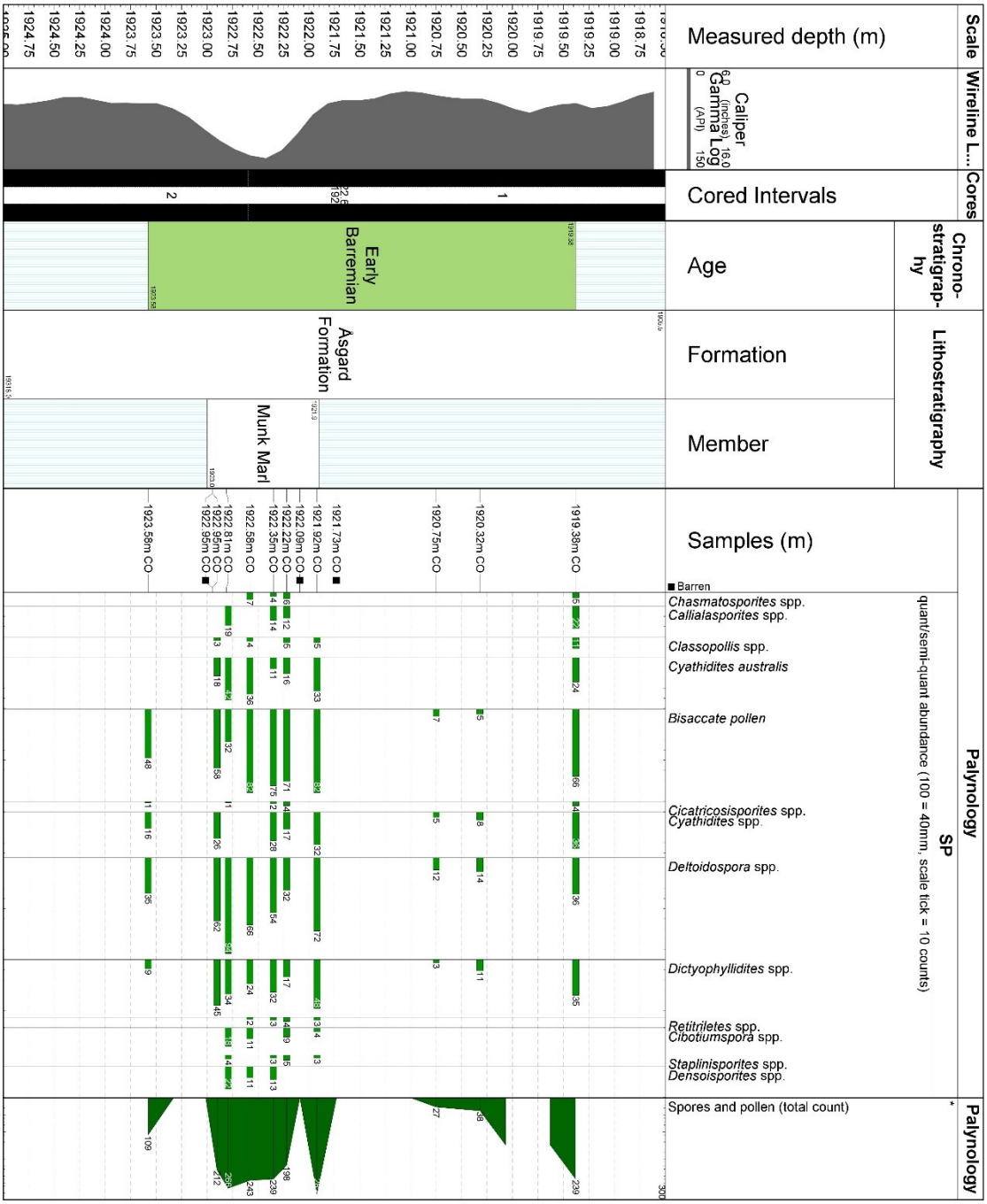

Figure 17. Spores and pollen distribution chart of the 16-2-21 Well.

7

PALYNOSTRATIGRAPHY

7.1. Discussion and Correlation

Hauterivian to Barremian interval

In this study the most relevant age diagnostic taxa are: *Stanfordella fastigiata, Muderongia crucis, Kleithsphaeridium corrugatum.* These 3 species have been recorded as a highly potential stratigraphic markers of the Early Barremian age for the Munk Marl Bed. These taxa are observed across the North Sea Basin within the same age interval and extensively used in the industry as markers for penetration of Early Barremian sediments.

Focusing on key species recorded in the MMB, the occurrence of *Pseudoceratium pelliferum* and *Batioladinium longicornutum* have notable abundance. The *Pseudoceratium pelliferum*. show a marked decrease in the abundance upsection of early Barremian, and disappear in the late Barremian. These features were also recognised by Erba (1996) and Davey and Verdier (1974), who established that the last occurrence of *Pseduceratium pelliferum* is at the Barremian–Aptian boundary in Mediterranean regions of Tethys. Elsewhere, *Pseudoceratium pelliferum* is recognized in the North Sea, generally in older strata, with first (Habib and Drugg, 1983; Jardiné et al., 1984) and last occurrences during the late Barremian (Poulsen and Riding, 2003). Therefore, the last occurrence of *Pseudoceratium pelliferum* is in accordance with the age assigned by the other maker taxa. Likewise, the first occurrence of *Cribroperidinium edwardsii* is used as a stratigraphic marker for the Barremian-Aptian boundary in Europe. It has been consistently recorded in the Barremian of England (Sarjeant, 1966; Davey et al., 1966) and occurs in the Aptian in Germany (Eisenack, 1958) and the Albian in Romania (Baltes, 1967). More recently, this interval was highlighted in Italy (Torricelli, 2000) and in northern Africa, northern Egypt (Tahoun & Led, 2018). It includes the following key taxa for the Hauterivian–Barremian interval: *Cribroperidinium* spp., *Pseudoceratium pelliferum, Hystrichodinium ramoides, Subtilisphaera perlucida, Subtilisphaera*

scabrata, Odontochitina operculata and Cribroperidinium? tenuiceras.

These *taxa* are also known in northeastern European regions, such as: England (Erba, 1996), Galicia (Masure, 1998), North Sea (Davey, 1979 and Verreussel et al., 2021) and North-East Greenland (Nohr-Hansen et al., 2019), emphasizing the cosmopolitan nature of this assemblage. Nevertheless, the northestern European zonal schemes and dinoflagellate cyst events are based on other groups of *taxa* of boreal influence (for instance, *Aptea* spp., *Batioladinium* spp., *Canningia* spp., and *Nexosispinum* spp.).

In northern Egypt, *C. edwardsii* is a key taxon for the Early Barremian to the Aptian (Tahoun and Led, 2018). Accordingly, the occurrence of *C. edwardsii* supports Barremian age, not excluding a younger age. Erba (1996) and Leereveld (1997) suggested that the first occurrence of *Cribroperidinium? tenuiceras* indicates proximity to the Barremian-Aptian boundary. Stover and Williams (1987) provided a range chart for *Spiniferites* spp., which shows that the genus is found in the Mesozoic and Cenozoic rocks of the world. Edwards (1996) used *Spiniferites* spp. to correlate the Marlboro Clay and Nanjemoy Formation of Virginia and Maryland. Schiøler (2005) found that *Spiniferites* spp. was one of the most common species in the sample of dinoflagellate cysts and acritarchs from the Oligocene-Lower Miocene interval of the Alma-1X well, Danish North Sea. *Spiniferites* spp. are found in a wide range of marine environments, including shallow and deep water. The genus *Spiniferites* is a useful fossil for biostratigraphic correlation. The different species of *Spiniferites* can be used to identify specific time intervals, and the genus as a whole can be used to identify the general age of a rock unit. In the samples analysed for this study wasn't possible to recognize any particular *Spiniferites* species that could be used for biostratigraphy.

Habib (1978) suggests that the *Dapisilidinium warrenii* occurence in the *Phoberocysta neocomica* Subzone may be comparable to the results from well (16-2/21).

The papers by Davey (1979), Verreussel et al. (2021), and Nohr-Hansen et al. (2019) all identify dinoflagellate cysts that can be used to date sedimentary rocks from the Hauterivian to Barremian interval. The dinoflagellate cyst *Pseudoceratium pelliferum* is found in the papers by Davey (1979) and Verreussel et al. (2021) and is considered a key marker for the early Barremian.

The presence of *Cribroperidinium* spp. and *Pseudoceratium pelliferum* in the MMB suggests that the bed was deposited during the Hauterivian to Barremian interval, with the upper part of

the bed being deposited during the early Barremian.

In (Nøhr-Hansen, 1994) original work, the lower boundary of the zone was redefined from the first occurrence (FO) of *Muderongia australis* to the slightly younger FO of *Batioladinium longicornutum*. This adjustment was made based on the belief that *Batioladinium longicornutum* serves as a more reliable marker for this boundary. According to Leereveld, (1997) it indicates relatively cool sea-surface conditions.

Within the context of the Munk Marl Bed, *Stanfordella fastigiata, Muderongia crucis*, and *Kleithsphaeridium corrugatum* stand out as crucial species aiding in stratigraphic dating within the Hauterivian to Barremian interval. Notably, *Stanfordella fastigiata* serves as a reliable marker for the Early Barremian age, as supported by prior studies such as Erba (1996) and Davey and Verdier (1974) which have identified its significance in delineating the Barremian-Aptian boundary within the Tethys Mediterranean regions. Its disappearance towards the Late Barremian aligns with its proposed role as an indicator for this age boundary. Similarly, *Muderongia crucis* has been identified as a pivotal species indicative of the Early Barremian, highlighted through its proposed transition from the first occurrence of *Muderongia australis* to the slightly younger first occurrence of *Batioladinium longicornutum*, reinforcing its role in stratigraphic dating within the Munk Marl Bed as seen in Nøhr-Hansen (1994). Although specific citations for *Kleithsphaeridium corrugatum* in relation to the Munk Marl Bed were not explicitly provided, its recognition in the Hauterivian to Barremian interval aligns with its importance as a species aiding in defining the Early Barremian age within this stratigraphic context. These species collectively contribute to establishing temporal boundaries and assisting in aligning the age characterization of the Munk Marl Bed with previous studies and zonal schemes, particularly emphasizing their significance in dating this specific interval. Hence, as depicted in Figure 18, the species *Kleithisphaeridium corrugatum* shows correlation potential with findings in the Central Graben Denmark region (Verreussel et al., 2021). Moreover, the presence of *Batioladinium longicornutum* within the Munk Marl Bed (MMB) aligns with discoveries in the Greenland region. While the Greenland findings suggest a somewhat more recent age, overlaps during the initial phases of the Late Barremian age are feasible (Nøhr-Hansen et al., 2019).

Figure 18. Comparision chart of the Hauterivian-Barremian interval biostratigraphy.

The Munk Marl Bed

Munk Marl is a unit of organic-rich mudstone found in the North Sea Basin. It was originally thought to be a flooding surface; however, recent studies have shown that it is more likely to be a lowstand system tract. The palynological evidence from the North Jens-1 MMB indicates an intra-*fissicostatum* age, probably equivalent to a position within Speeton unit LB2. The presence of the saccate miospore species *Ruguvesiculites rugosus* in the early Barremian is unusual and might reflect brief climatic change (? warming), associated with the production of rich lowland miospore assemblages (Duxbury, 2023; Williams, 2006; Jeremiah, 2000). However, recent studies have shown that *Pseudoceratium anaphrisum* can also occur in lowstand systems tracts. This suggests that MMB may not be a flooding surface after all, but rather a lowstand system tract (Abbink, 1998; Jeremiah, 2000).

The palynological evidence from the North Jens-1 MMB indicates an intra-*fissicostatum* age, which is younger than the *rarocinctum* age of Copestake et al. (2003, *op. cit.*) assigned to it. However, Copestake et al. (2003, *op. cit.*) was correct in considering it to be older than the Hauptblatterton of Germany (and Speeton) (Fig.19). This suggests that the MMB may be a separate unit from the Hauptblatterton and that it may have been deposited under different environmental conditions (Copestake et al., 2003; van Buchem et al., 2017).

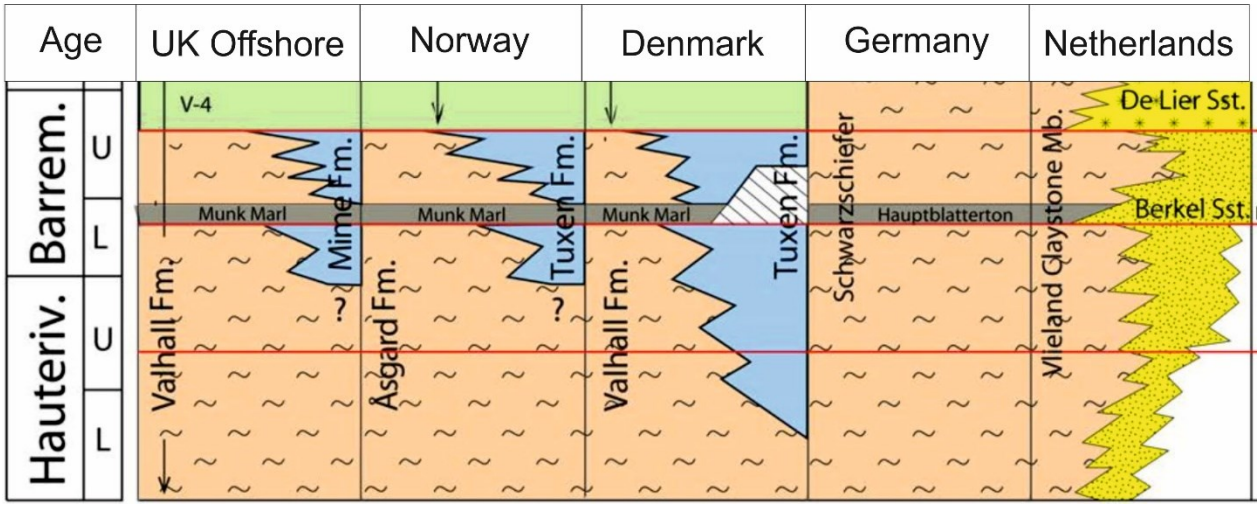

Figure 19. Chronostratigraphic scheme for the upper part of the Lower Cretaceous in the North Sea Basin (adapted from van Buchem et al., 2017).

Copestake (2003) discussed the age relationship of the MMB to two lithologically similar units. He stated that the top of the MMB occurs within the Lower Barremian, below the first dinoflagellate occurrence of *Kleistriasphaeridium corrugatum*, which defines the top of the

Lower Barremian palynologically. The study also stated that biomarker events occur close to basal Barremian markers of *Gorgonisphaera barremiana* and *Odontochitina operculata*), suggesting a position within the *Rarocinctum* Ammonite Zone (Duxbury, 2023). Van Buchem et al. (2017) estimated that the Munk Marl is of late early Barremian age, based on the occurrence of the ammonite *Hoplocrioceras fissicostatum*. This is younger than the earliest Barremian age that Copestake et al. (2003) reported. Van Buchem et al. also stated that the Munk Marl is time-equivalent to the Berkel Sandstone Member, which is also of late early Barremian age. However, this contradicts the findings of Rawson and Mutterlose (1983), who assigned an upper *fissicostatum* to elegans ammonite Zone age to Speeton division LB1 (Hauptblatterton), which is equivalent to the MMB (Duxbury, 2023).

The presence of organic-rich deposits in the MMB and other intra-Barremian units is a puzzling phenomenon. The reason for their occurrence is unclear, but it may be due to a combination of factors, including a very warm and arid climate, low nutrient influx, and reduced terrigenous run-off. These factors may have led to the development of anoxic conditions in the water column, which would have promoted the preservation of organic matter (Copestake, 2003; Jeremiah, 2000). Møller et al. (2019) suggested that the MMB was deposited during a period of very warm and arid climate. This climate would have reduced ocean mixing and enhanced stratification of the water column, leading to anoxia in the bottom waters. The low nutrient influx and reduced terrigenous run-off would have further contributed to the anoxic conditions. However, this explanation does not fully account for the presence of so much lowland organic material in the MMB. It is possible that the lowland material was transported to the MMB by rivers during periods of flooding. Alternatively, it is possible that the lowland material was deposited in the MMB by windblown dust (Moller et al., 2019; van Buchem, 2017; Duxbury, 2023).

Muderongia tetracantha, Circulodinium hirtellum and Oligospharedium abaculum are consistent with MMB results. Although the presence of *Muderongia tetracantha* and *Circulodinium hirtellum* suggests an age of *Fissicostatum*, but the presence of *Oligospharedium abaculum* indicates that the Speeton clay is from the base of the Early Barremian. Therefore, when correlating with the MMB, it is more appropriate to compare the MMB to species other than *Oligospharedium abaculum*. This suggests that the MMB could also be of *Fissicostatum* age. This is supported by the view of Buchem et al. (2017), who suggest that the MMB corresponds to the lower levels of the *Fissicostatum* age (Fig.20).

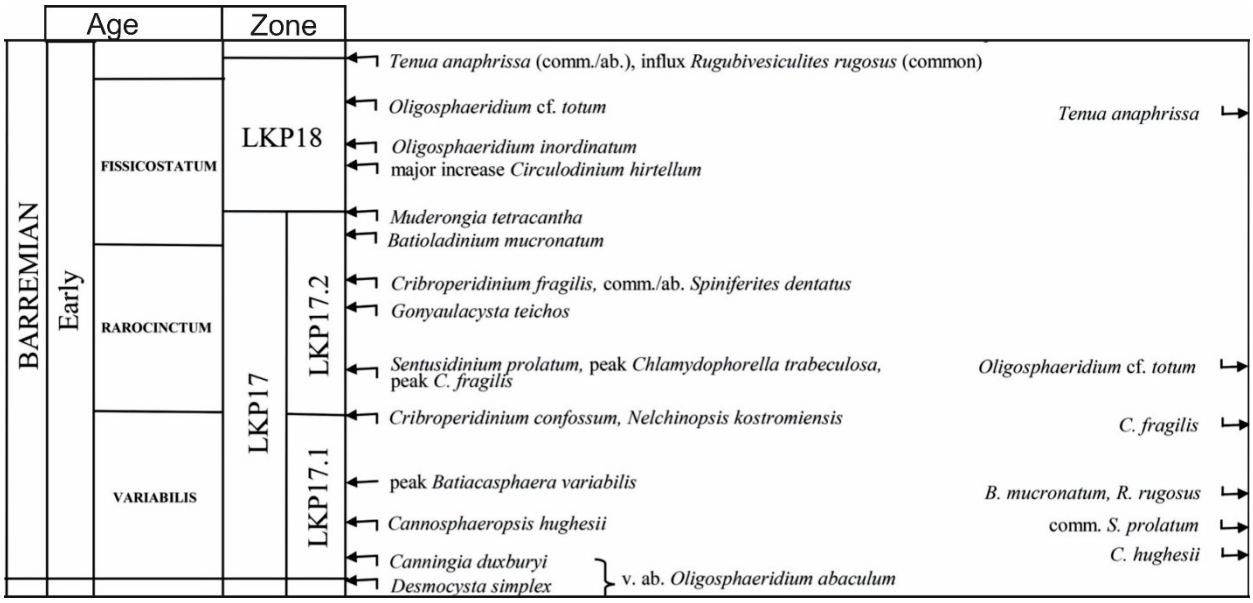

Figure 20. Palynofloral zonation chart from Speeton outcrop (adapted from Duxbury, 2001).

8

ARTIFICIAL INTELLIGENCE APPLICATIONS

The recent expansion of artificial intelligence and machine learning techniques has facilitated their widespread adoption by most of scientific areas, in particular petroleum and natural gas companies, enabling geoscientists to utilize these technologies with greater ease.

8.1 Introduction

In this study, the aim is to assess the application of deep learning techniques for the automatic detection and recognition of dinoflagellate cysts of a specific species, *Batioladinium longicornutum.*

This study aims to investigate the use of Convolutional Neural Networks (CNN) for species classification and understand how accuracy can be improved using different datasets. CNNs are a small part of the broader field of artificial intelligence (AI), and in nomenclature terms, CNNs are a type of deep learning neural network, which falls under the umbrella of machine learning methodologies (Fig. 21).

Manual species identification is a time-consuming and error-prone process, and with the advancement of machine learning techniques, it becomes possible to automate this process and enhance its accuracy. Several studies have already demonstrated the effectiveness of these techniques in the identification of microfossils and palynomorphs in various environments (e.g., Carlson et al., 2022; Gonçalves et al., 2022; Gorur et al., 2022; Viertel & König, 2022).

The study evaluated the validated application of these methods in the automatic detection of dinoflagellate cysts, using the species *Batioladinium longicornutum* as an example, based on a dataset of 1,453 images collected to train three independent models using the TensorFlow library in Python. These models, built on a Convolutional Neural Network (CNN) architecture, were tested with a separate test dataset to assess their performance in

classifying the target species. The species examined in this study were retrieved from ten core samples (well 16/2-21) collected throughout the MMB, which is part of the Åsgard Formation drilled in the Norwegian North Sea.

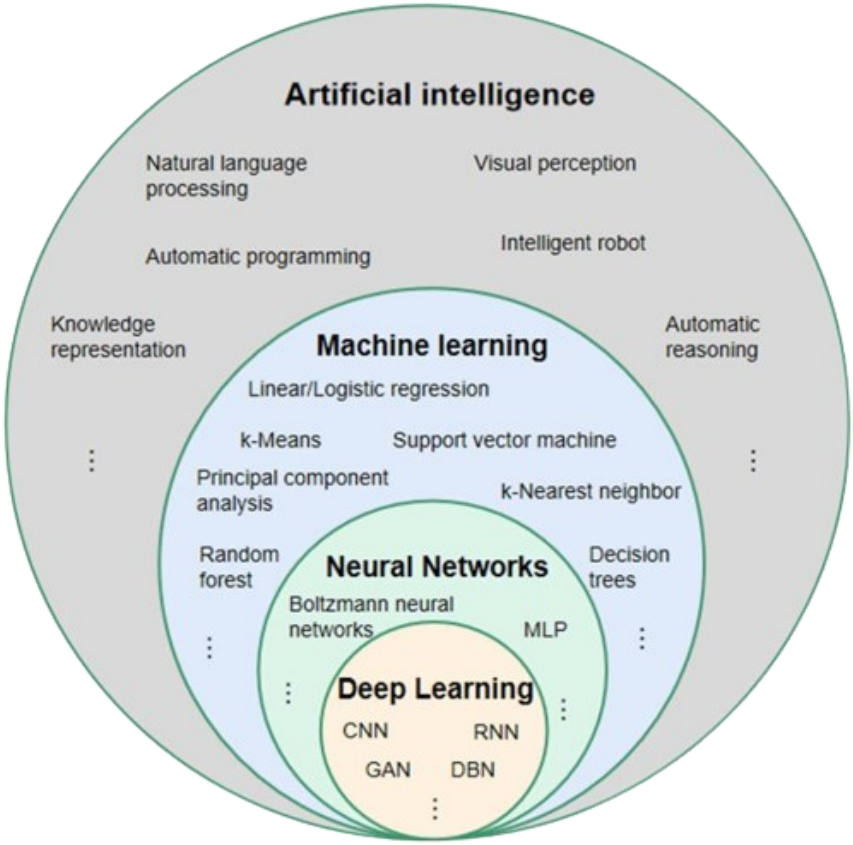

Figure 21. Chart of the Deep Learning and AI relation adapted from (Li et al., 2021).

8.2 Methodology

All models are trained based on a pre-trained model of the 'mobilenet' type, which reduces the images to a resolution of 320x320 pixels, and propagates them through its structure, during 2000 learning cycles (Fig.22). In methodological terms, the study proceeded in 3 phases: (i) processing and classification of the set of training images; (ii) training of deep learning models; (iii) testing the models and building the forecast model. The images were pre-classified, identifying *B. longicornutum* and other species of palynomorphs, using a specific labeling algorithm in Python for the application of artificial intelligence methods. To increase the accuracy and detail of the study, the first set of images was subjected to two further classification steps (Fig.23). The second step distinguishes full-body specimens from fragmented specimens, while the third step focuses on specific features such as the body, apical horn, and antapical horns. These classified image sets are the basis for refining the model's ability to recognize and classify various aspects of the target species. The training of the models took place in 3 steps, each step resulting in a different detection model (Fig.24).

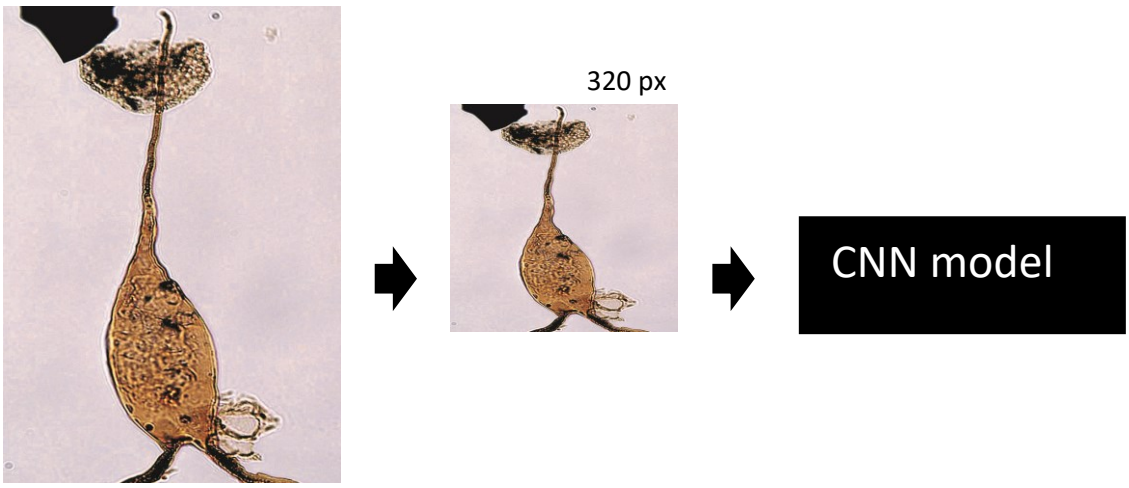

Figure 22. The model automatically reduced the images to a standard 320 x 320 automatically in the algorithm.

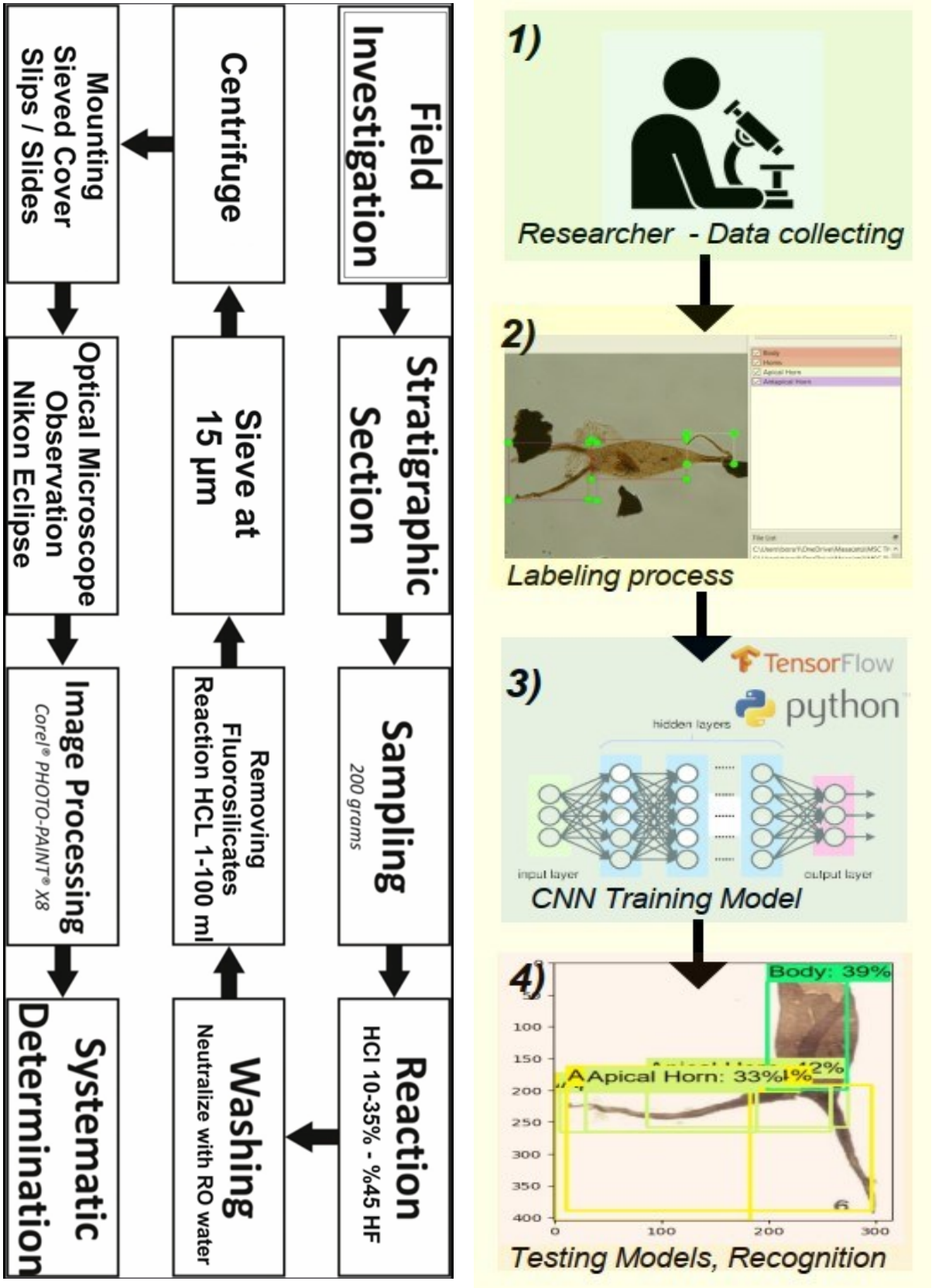

Figure 23. Flowchart of the deep learning methodology from scratch.

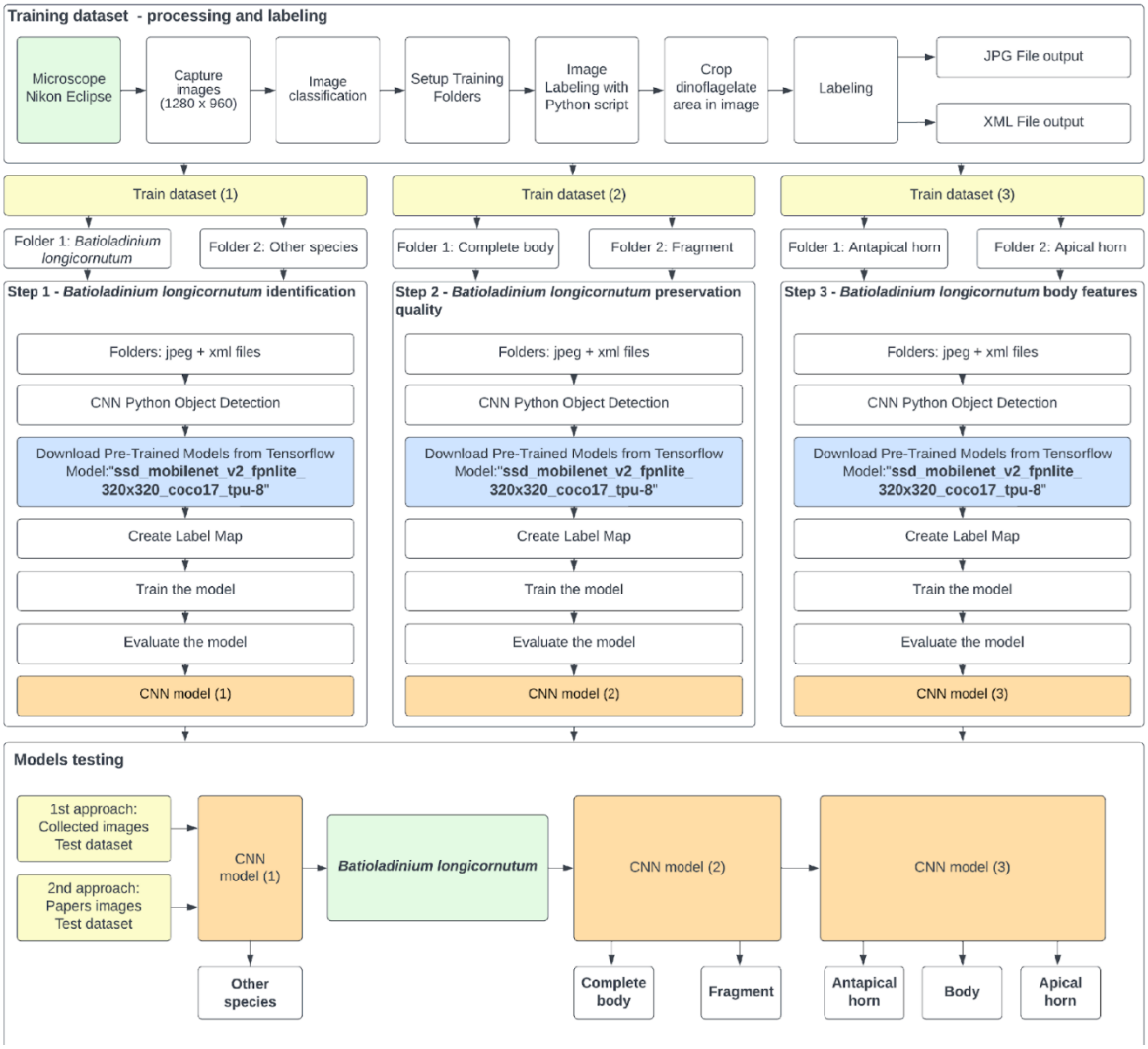

Figure 24. Flowchart of the deep learning methodology from scratch.

Each model has a set of corresponding images, classified in the previous phase. The 1st training stage results in a model that detects in the image the area corresponding to a palynomorph and classifies it into *B. longicornutum* and another species. The 2nd training stage results, in turn, in an assessment of the quality of preservation of the specimen, when corresponding to a *B. longicornutum*, classifying it as `Complete' or `Fragmented'. The last trained model focuses on species-specific features, identifying the areas on the images that correspond to the body, apical horn and antapical horns.

8.2.1. Create Training Sets

Creating training datasets for object detection involves several steps and considerations. Here's a breakdown of the process, addressing each of the points.

1. Equipment Used:

Microscope: The microscope is a critical tool for capturing high-resolution images of microscopic samples. It allows for magnification and precise examination of the samples.

Camera or Imaging Device: An imaging device, often integrated with the microscope, is used to capture digital images of samples. The camera should have the capability to capture clear and detailed images.

2. How Images Were Captured:

Microscopic Imaging: The process begins with microscopic imaging. Slides are placed under the microscope, and images are captured using the attached camera. The camera settings, such as resolution and focus, are adjusted to ensure high-quality images.

3. How Images Were Classified:

Classification Criteria:

Model 1: For the first model, images are classified based on the species of interest and all other typical species found in the sample.

Model 2: The second model classifies images based on whether the species is complete or fragmented.

Model 3: The third model classifies images based on specific morphological characteristics of the species.

4. Labeling Process and Python Script Identification:

Labeling Images: The labeling process involves annotating the images to define the regions of interest (e.g., the species) within each image. Each annotated region is assigned a class label.

Python Script for Labeling: Python scripts are commonly used for image labeling. These scripts allow annotators to draw bounding boxes around the regions of interest and specify the corresponding class labels. The script also generates label maps and TFRecord files that are used for training the models. The specific Python script used for labeling and TFRecord generation is identified in the code, such as generate_tfrecord_1.py.

5. Jupyter Notebook, Folder Structure, and Workflow:

Jupyter Notebook: Jupyter Notebook is an interactive environment that can be used to run Python scripts, visualize data, and perform labeling tasks. It provides a flexible platform for managing and processing images.

Folder Structure:

workspace1/ is the root directory for organizing the datasets and project files.

annotations/: This directory holds the TFRecord files, label maps, and other annotation-related files. images/: Images are stored in this directory, organized into subdirectories such as 'train' and 'test' for training and testing data.

models/: The 'models' directory includes subdirectories for each custom model (1, 2, 3). Each model directory contains its pipeline configuration and checkpoint files.

scripts/: The 'scripts' directory houses Python scripts used for various tasks, including generating TFRecord files and other utilities.

The folder structure is designed to keep data, scripts, and model-related files organized and easily accessible within the workspace. It simplifies the workflow and allows for a systematic approach to data preparation and model training. Considering the training datasets, the 1st model (1) inputs are 2 different datasets: one for the species of interest and another set for all other typical species in the sample. The other 2 model's inputs are also the species-specific datasets, but with different labelling procedures (Fig.25). The 2nd model (2) is labeled based on whether the species is complete or fragmented. And the 3rd model (3) is labeled based on morphological characteristics of the species.

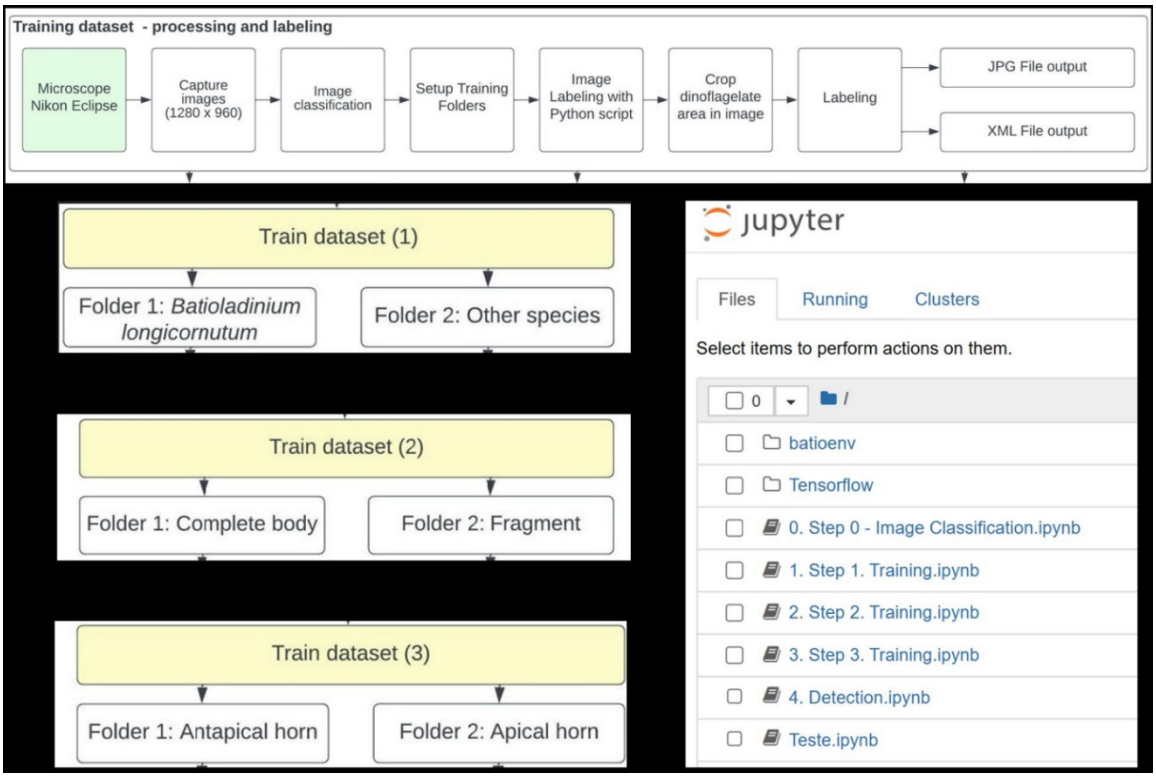

Figure 25. Training datasets table.

8.2.2. Train model Step 1

Setup Paths:

In this initial step of the code, the following actions are taken to set up the workspace and directory structure:

Workspace and Directory Paths: Several paths are defined to organize the project, such as the workspace, script, API model, annotation, image, model, pretrained model, checkpoint, output, TensorFlow.js (TFJS), and TensorFlow Lite (TFLite) paths. These paths are used to manage different aspects of the object detection project.

Files Dictionary: A dictionary called files is created, which contains file paths for the pipeline configuration, TF record script, and label map.

Path Creation: The code iterates through the paths defined and checks if the corresponding directories exist. If the directories do not exist, the code creates them using the mkdir command. The specific directory structure is essential for organizing and managing the data and files associated with the object detection project.

In this step, the WORKSPACE_PATH is particularly highlighted, as it represents the main directory where the project's workspace is set up. This directory will contain various subdirectories for images, annotations, models, and more, making it the central location for managing the project's files and data. This step establishes the necessary directory structure and paths for organizing and running an object detection project. The `workspace1` directory is the core workspace for this project. And just it will change for the next Step 2 and Step 3.

Download TF Models Pretrained Models from Tensorflow Model Zoo and Install TFOD:

This step in the code performs the following tasks:

Installs the wget package (if running on Windows) and imports it. Checks if the TensorFlow Object Detection API repository doesn't exist in the specified path. If it doesn't exist, it clones the official TensorFlow models repository from GitHub to the specified path. Installs the TensorFlow Object Detection API by running the appropriate commands based on the operating system. It installs the required dependencies, compiles the protocol buffers, and copies the necessary setup files to the research directory. Downloads the pretrained model from the provided URL and extracts it to the specified directory. Upgrades TensorFlow to

the latest version and also upgrades or installs protobuf and matplotlib packages to ensure compatibility with the TensorFlow Object Detection API. Finally, it verifies the installation by running a verification script. This step is crucial in setting up the environment and installing the necessary packages and models for object detection with TensorFlow.

Create Label Map:

In this step of the code, a label map is created. A label map is a text file that defines a mapping between class names and their corresponding integer IDs. Each line in the label map file represents a class and its ID.

It defines a list of labels, where each label is represented as a dictionary with a "name" and an "id." In this step 1 we have only 2 different set as a: [{'name':'Batioladinium_longicornutum', 'id':1}, {'name':'Other species', 'id':2}]. It opens the label map file specified by the files['LABELMAP'] path in write mode. It iterates through the list of labels and writes the label information into the label map file in a specific format. Each label is written as a block of text enclosed in "item {...}" with the "name" and "id" fields set accordingly. The resulting label map file will be used in the object detection pipeline to map class names to integer IDs, which is essential for training and inference.

Create TF Records:

In this step of the code, the TF (TensorFlow) record files are generated for training and testing data. TF records are a binary format used for efficient storage and retrieval of data in TensorFlow.

It checks if there is an archive file at the specified path (ARCHIVE_FILES) and, if it exists, extracts its contents. This step is optional and is used for extracting image data if it's archived.

It checks if the TF record generation script doesn't exist in the specified path, and if so, it clones the script repository from GitHub. It runs the TF record generation script twice:

The first command generates TF records for training data (train.record). It takes images from the 'train' directory, uses the label map file to map class names to IDs, and saves the resulting TF records in the annotation directory. The second command generates TF records for testing data (test.record) in a similar manner, using images from the 'test' directory. It installs the pytz library, which is used for time zone support. This step prepares the training and

testing data in a format suitable for use with TensorFlow Object Detection models. The generated TF record files are used during the model training process.

Copy Model Config to Training Model:

In this step of the code, the pipeline configuration file of a pre-trained model is copied to the training folder. The pipeline configuration file contains important settings and configurations for the object detection model, including hyperparameters, training data paths, and other parameters. It checks the operating system type (POSIX for Linux/Unix, NT for Windows). If the operating system is POSIX (Linux/Unix), it uses the cp command to copy the pre-trained model's pipeline configuration file from the specified source path to the training checkpoint directory (CHECKPOINT_PATH). If the operating system is NT (Windows), it uses the copy command to achieve the same copy operation. This step is important because it ensures that the pipeline configuration file is available in the training folder, so it can be used during the training process to configure and fine-tune the pre-trained model for specific object detection tasks.

Update Config for Transfer Learning:

In this step, the configuration for transfer learning is updated. The code modifies the pipeline configuration for the object detection model, specifically for transfer learning.

It reads the existing pipeline configuration from the specified pipeline configuration file using TensorFlow's config_util.get_configs_from_pipeline_file function.

It creates a TrainEvalPipelineConfig object and populates it by parsing the existing pipeline configuration from the file. It updates various settings in the pipeline configuration to customize it for transfer learning. These updates include:

Setting the number of classes to the total number of labels in the label map. Adjusting the batch size for training. Specifying the fine-tune checkpoint from the pre-trained model. Setting the fine-tune checkpoint type to "detection." Configuring the label map path and input paths for both training and evaluation data. It converts the modified pipeline configuration back to text format and writes it to the pipeline configuration file, overwriting the existing configuration.

This step is crucial for configuring the model for transfer learning, where you adapt a pre-trained model to a new object detection task using a specific dataset and labels.

Train the Model:

In this step, the actual training of the object detection model takes place. The model is being fine-tuned to recognize and classify objects belonging to two specific classes: "Batioladinium_longicornutum" and "Other species."

During training, the model is presented with a large dataset containing images of these objects, where each object is labeled with its corresponding class. The model learns to identify and distinguish between the two classes by adjusting its internal parameters, also known as weights. The training process involves multiple iterations (in this case, 2000 steps) where the model evaluates its predictions, calculates errors, and updates its weights to improve its accuracy. As the training progresses, the model becomes better at recognizing objects of the specified classes. The final trained model can then be used for object detection in new, unseen images, helping to identify and classify objects as "Batioladinium_longicornutum" or "Other species" based on the features it has learned during the training.

Evaluate the Model:

In this step, the trained object detection model is undergoing an evaluation process to assess its performance and accuracy. The model has been fine-tuned to recognize and classify objects from two specific classes: "Batioladinium_longicornutum" and "Other species."

Evaluation Setup: The code prepares the necessary setup for evaluating the model's performance. It specifies the directory where the trained model checkpoints are stored (model_dir), the pipeline configuration file that defines the model and evaluation parameters (pipeline_config_path), and the checkpoint directory, which contains the trained model's checkpoints.

Model Assessment: During the evaluation, the model is tested on a separate dataset that it hasn't seen during training. This dataset likely contains images of objects from the two classes: "Batioladinium_longicornutum" and "Other species."

Performance Metrics: The evaluation process measures the model's accuracy, precision, recall, and other performance metrics. These metrics indicate how well the model can correctly identify and classify objects from the specified classes.

Validation of Object Detection: The evaluation is critical to validate the model's ability to detect and classify objects accurately. It helps assess whether the model is capable of

distinguishing between "Batioladinium_longicornutum" and "Other species" in real-world scenarios.

Quality Assurance: The results of the evaluation are used for quality assurance and to determine whether the model meets the desired level of accuracy and reliability. This step is essential to ensure that the model is ready for deployment in practical applications, such as automated object detection and classification.

Load Train Model from Checkpoint:

In this step, the code is loading a trained object detection model from a checkpoint file, which allows the model to be used for making predictions on new and unseen data. The model has been fine-tuned to detect objects from two specific classes: "Batioladinium_longicornutum" and "Other species."

Loading Configuration: The code loads the pipeline configuration that defines the model's architecture, hyperparameters, and other settings. This is necessary to construct the same model architecture as during training.

Building the Detection Model: The code uses the loaded configuration to construct a detection model. This model is designed for object detection tasks and is configured for inference, which means it's ready to make predictions on new images.

Restoring Checkpoint: The trained model's checkpoint, which contains the learned weights and parameters, is restored. This checkpoint file was created during the training process and is located in the CHECKPOINT_PATH. The checkpoint is essential for initializing the model with the learned knowledge from the training phase.

Detect Function: The code defines a function detect_fn that takes an input image and processes it through the detection model. This function handles image preprocessing, model prediction, and post-processing of the predictions to obtain detected objects and their properties.

Object Detection: With the loaded and initialized model, it is now capable of detecting objects within images. In the context of your two-class data (Batioladinium_longicornutum and Other species), the model can take an image as input and identify whether any objects in the image belong to either of these two classes.

This step prepares the model for real-world usage, allowing it to analyze new images and identify objects based on its training on "Batioladinium_longicornutum" and "Other species."

Detect from Image:

In this step, the code demonstrates how to use the previously loaded and trained object detection model to detect objects in a specific image. The model has been fine-tuned to detect objects from two classes: "Batioladinium_longicornutum" and "Other species

Loading the Image: The code loads an image for object detection. In one of specific example, the image is named "Dinocysts-marker-of-Early-Cretaceous-age-earliest-Hauterivian-Barremian-and-Aptian_W640.jpg."

Preparing the Image: The loaded image is preprocessed and converted into a format suitable for the model. This includes resizing, data type conversion, and creating a tensor that the model can process.

Object Detection: The model is applied to the image using the detect_fn function. The model analyzes the image and produces predictions regarding the presence, class, and location of objects within the image.

Visualization: The code uses the predictions to draw bounding boxes around detected objects in the image and labels them with their respective classes. The visualization includes information such as the class name, confidence score, and the position of the detected objects.

Displaying the Result: The code then displays the annotated image with the bounding boxes and labels using the matplotlib library.

In the context of your two-class data ("Batioladinium_longicornutum" and "Other species"), this step demonstrates how the model can take an input image and identify and visually highlight any instances of these two classes present in the image. The model's predictions and annotations are overlaid on the image for visual inspection and analysis.

8.2.3. Train model Step 2

All the necessary steps and codes are the same as in this Step 1. Just the difference in the beginning using workspace2 while setup the paths. Then in the 2nd phase when creating label maps, it will include the names of following classes: labels = [{'name':'Complete', 'id':1}, {'name':'Fragment', 'id':2}]

8.2.4. Train model Step 3

All the necessary steps and codes are the same as in this Step 1. Just the difference in the beginning using workspace3 while setup the paths. Then in the 2nd phase when creating label maps, it will include the names of following classes: labels = [{'name':'Body', 'id':1}, {'name':'Antapical Horns', 'id':2}, {'name':'Apical Horn', 'id':3}]

8.2.5. Model testing

Setup Paths:

In this step, the project is preparing to work with multiple custom object detection models and label maps. This suggests that the project is becoming more complex and likely involves different stages or iterations of model development.

Custom Model Names: The project is now using three different custom model names (CUSTOM_MODEL_NAME_1,CUSTOM_MODEL_NAME_2, and CUSTOM_MODEL_NAME_3).

This implies that the project is evolving and possibly experimenting with multiple versions or iterations of object detection models. Each custom model may have specific objectives or requirements.

Label Map Names: Three label map names (LABEL_MAP_NAME_1, LABEL_MAP_NAME_2, and LABEL_MAP_NAME_3) are defined. Label maps are crucial for mapping class names to integer IDs for the model. The presence of multiple label maps suggests that different versions of the model may have varying sets of classes to detect. Pre-trained Model: The project continues to use a pre-trained model (PRETRAINED_MODEL_NAME) as a starting point. This pre-trained model likely provides a solid foundation for further customization and fine-tuning. TF Record Script: The use of TF_RECORD_SCRIPT_NAME indicates that the project will continue generating TF record files to prepare and organize the training and testing data for each model version. In summary, this step reflects an advanced stage of the object detection project, where multiple model versions and label maps are being managed. Each version of the model may have

unique training objectives or may target different classes, expanding the project's capabilities and versatility.

Load Train Model from Checkpoint:

In this step, the code is focused on loading and preparing multiple trained object detection models, with each model corresponding to a different version or iteration. These models have been trained on various datasets and are intended to collectively address the object detection tasks.

TensorFlow and Protobuf Installation: The code starts by upgrading TensorFlow and installing a specific version of Protobuf (Protocol Buffers). These are essential dependencies for working with object detection models and configurations.

Loading Multiple Detection Models:

The code loads pipeline configurations (configs1, configs2, configs3) from different pipeline configuration files (files['PIPELINE_CONFIG_1'], files['PIPELINE_CONFIG_2'], files['PIPELINE_CONFIG_3']) for three distinct object detection models. Each configuration corresponds to a different model version with unique settings, architectures, and possibly datasets. Detection models (detection_model_1, detection_model_2, detection_model_3) are built based on the loaded configurations using the model_builder.build function. These models are set up for inference (is_training=False).

Restoring Model Checkpoints: The code restores the checkpoints for each model (ckpt_1, ckpt_2, ckpt_3) from their respective checkpoint directories (paths['CHECKPOINT_PATH_1'], paths['CHECKPOINT_PATH_2'], paths['CHECKPOINT_PATH_3']). The checkpoints contain the trained weights and parameters of the models, allowing them to make predictions.

Detection Functions: The code defines three detection functions (detect_fn_1, detect_fn_2, detect_fn_3) for each model. These functions preprocess input images, use the models to make predictions, and post-process the predictions to obtain detected objects and their properties.

In summary, this step is crucial for setting up and loading multiple object detection models, each trained on different datasets or with different objectives. These models are prepared and ready to make predictions on new images, collectively covering a broader range of object detection tasks.

Detect from Image:

In this step, the code demonstrates the detection process using three different object detection models, each associated with a specific dataset or objective. These models are applied to the same image, and the resulting detections are visualized. Here's the situation with all three datasets: Loading Categories and Images:

Three sets of categories (category_index_1, category_index_2, category_index_3) are created based on their respective label maps (files['LABELMAP_1'], files['LABELMAP_2'], files['LABELMAP_3']), which map class names to integer IDs. These label maps are crucial for interpreting the model's output. An image (pala5.jpg) from the test dataset is loaded for object detection. This image is shared among all three models.

Object Detection with Model 1:

The first model (detect_fn_1) processes the input image and makes predictions.

The code extracts detection results, including bounding boxes, classes, and scores. These results are then processed for visualization. Detected objects from Model 1 are visualized on the image using the matplotlib library. This visualization includes the bounding box, class label, and confidence score for the most confident detection. The parameters used for visualization are configured to show all detected objects (max_boxes_to_draw=1) regardless of their confidence score.

Object Detection with Model 2:

The second model (detect_fn_2) processes the same input image and makes predictions. Similar to Model 1, detection results are processed and visualized for Model 2. The visualization settings for this model are adjusted, displaying only objects with a confidence score of at least 0.1 (min_score_thresh=.1).

Object Detection with Model 3:

The third model (detect_fn_3) processes the image and makes predictions. Detection results from Model 3 are processed and visualized with specific settings for this model. Here, up to three detected objects are shown (max_boxes_to_draw=3) with a minimum confidence score of 0.1 (min_score_thresh=.1). Visualization: After applying all three models to the same image, the final result is displayed as a series of images, each showing the original image with detected objects highlighted according to the settings and label maps specific to each model. The visualizations include bounding boxes, class labels, and confidence scores for the detected objects.

This step illustrates how multiple models, trained on different datasets or with varying objectives, can be applied to the same image, allowing for diverse and targeted object detection tasks within a single scenario.

8.3 Pre-trained Models Training

The training of the three models based on pretrained models and their purposes:

Training Pretrained Models:

Model Purpose:

Three models were trained, each serving a specific purpose:

Model 1: The first model's primary objective is to classify and detect the species of interest, which, in this case, is Batio (B. longicornutum).

Model 2: Model 2 is designed to assess the conservation state of Batio specimens, categorizing them as 'complete body' or 'fragmented.'

Model 3: Model 3 specializes in characterizing Batio by identifying unique morphological characteristics, such as body shape, the presence of apical or antapical horns, and other specific features.

Folder Structure:

The models are trained based on a specific folder structure within the project workspace. This structure includes directories for annotations, images, models, and scripts. The images are organized into subdirectories, such as 'train' and 'test,' to separate training and testing data.

CNN (Convolutional Neural Network) Type: MobileNet:

All three models are based on Convolutional Neural Networks (CNNs) using the MobileNet architecture. MobileNet is chosen for its efficiency and effectiveness in image classification tasks.

Rescaling Images to 320x320px:

To create a standard dimension for training and testing, all images are rescaled to a size of 320x320 pixels. This standardization allows the algorithm to compare patterns between images consistently and create mathematical rules that apply uniformly to all images.

Training Until Minimum Error Accepted:

The models undergo a training process using a dataset of labeled images. Training continues iteratively until the model achieves a minimum acceptable error rate. This process involves adjusting the model's parameters to enhance its accuracy in classifying and detecting the species or other specific attributes.

Resulting CNN Algorithm:

The outcome of training is a CNN-based algorithm that can analyze new and independent images. When presented with a new image, the algorithm compares the patterns in the image with patterns associated with each variable. It provides a range of confidence scores that indicate how likely the new image corresponds to the variable being assessed. In the case of Model 1, the variable of interest is the species Batio.

The three pretrained models, based on the MobileNet architecture, are purpose-built for classifying, evaluating the conservation state, and characterizing microscopic samples of Batio. These models use standardized image sizes, are trained until an acceptable error rate is reached, and provide confidence scores for accurate assessments. Each model has a specific role in the comprehensive analysis of Batio samples, from species detection to conservation state evaluation and detailed morphological characterization.

8.4 Preliminary Results

Process of testing independent images with the resulting trained models, especially focusing on Model 1 and its subsequent application to Models 2 and 3.

Testing Independent Images with Trained Models:

Initial Testing with Model 1:

Independent images of microscopic samples are subjected to the initial testing phase using Model 1. The primary objective is to detect the presence of the species of interest, in this case, Batio (B. longicornutum). The performance of Model 1 in classifying and detecting Batio relies heavily on the quality of the labeling process and the diversity of images in the "other species" dataset. A well-annotated and diverse "other species" dataset is essential to train Model 1 effectively.

Conditional Application to Models 2 and 3:

If Model 1 successfully identifies the species as Batio, the image is conditionally passed to Models 2 and 3 for further evaluation. Model 2 assesses the conservation state of the Batio specimens. It categorizes them as either 'complete body' or 'fragmented.' Model 3 specializes in characterizing Batio by focusing on unique characteristics such as body shape, the presence of apical or antapical horns, and other specific morphological features (Fig.26).

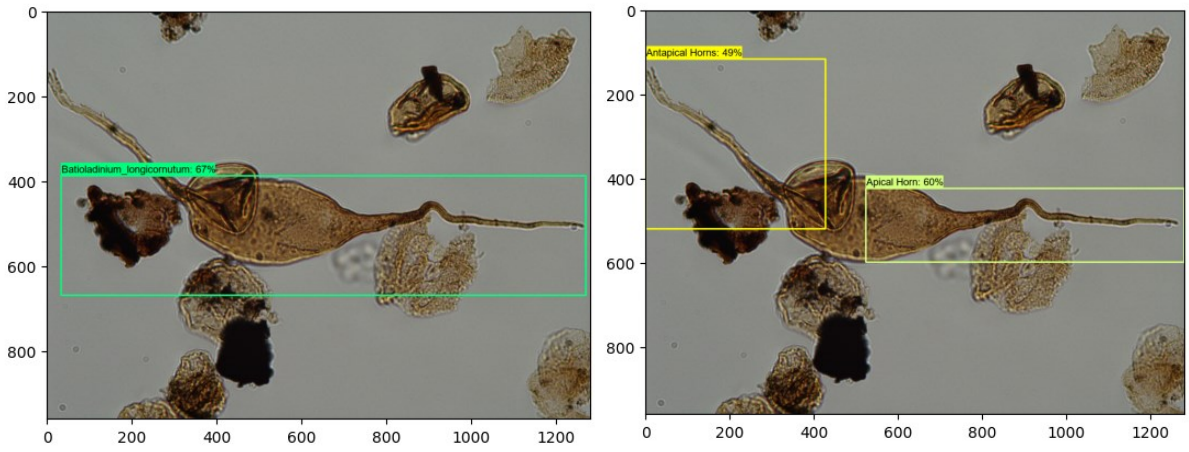

Figure 26. The “Preservation status” and “Species characteristics” model are only applied if the condition species *B. longicornutum* is respected.

Key Points to Consider:

Quality of Labeling Process: The accuracy and effectiveness of Model 1 in identifying Batio are heavily influenced by the quality of the labeling process. Accurate annotations and a diverse "other species" dataset are crucial. Diversity of "Other Species" Dataset: To ensure the robustness of Model 1, it's important to have a diverse set of images in the "other species" dataset. This diversity helps the model distinguish Batio from other species effectively.

Conservation State Assessment: Model 2 is designed to assess the conservation state of the Batio specimens. This is crucial for evaluating the quality of the specimens and their preservation.

Detailed Morphological Characterization:

Model 3 specializes in characterizing Batio based on specific morphological features. This model goes beyond basic detection and aims to provide more detailed insights into the species' unique characteristics.

Sequential Application: The sequential application of Models 1, 2, and 3 allows for a progressive and targeted evaluation of the samples. This approach maximizes the information extracted from the images.

This testing process ensures that the detection and classification of B. longicornutum are comprehensive and accurate. It highlights the importance of robust training datasets and specialized models for the in-depth analysis of microscopic samples.

The classification and detection of the *B. longicornutum* (1) will highly depend on the labelling process quality and the number and diversity of images in the "other species" dataset (2) distinguish the conservation state of the specimens and is trained using the same architecture as model (1) and labelled as 'complete body' or 'fragmented' (3) is designed to be more specific in the characterization of the *B. longicornutum* by focusing with unique characteristics, such as shape of the body, the presence of apical or antapical horns, allows the model to learn more detailed features of the species (Fig.27). Mixed total results of the detection shows variable differences between different pictures (Fig.28).

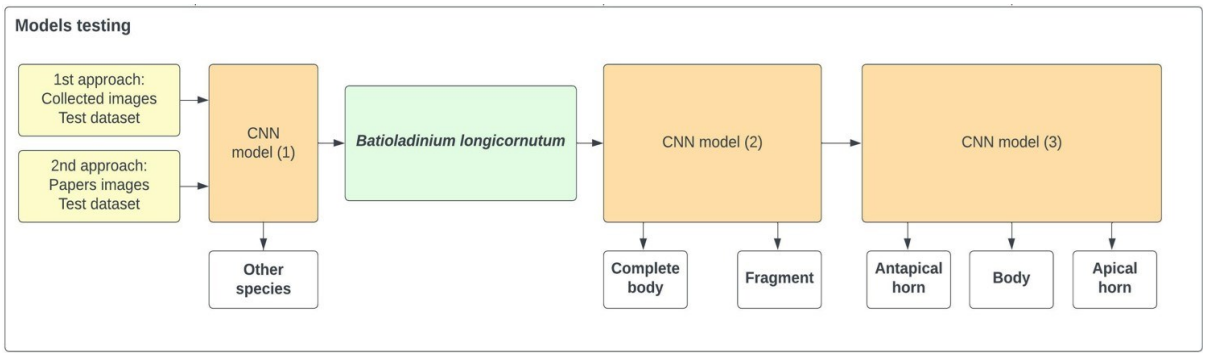

Figure 27. Flowchart of the result section.

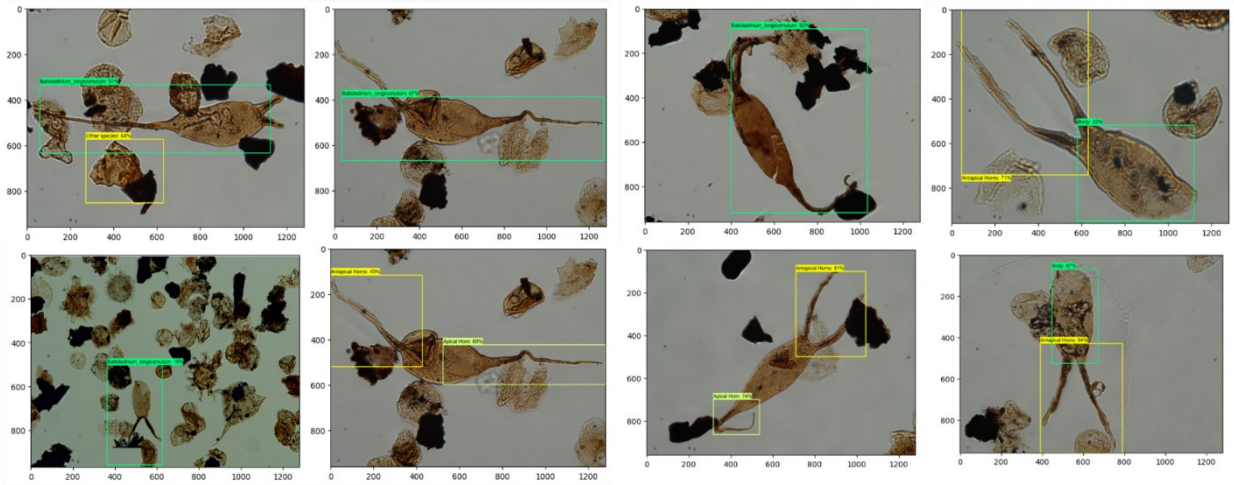

Figure 28. Obtained results by the detection algorithm in the Jupyter Notebook with the Python scripts.

8.5 Discussion

The methodology allows an automatic detection approach of the species *B. longicornutum*, its conservation status and some morphological characteristics.

The classification and detection of *B. longicornutum* depends on the quality of the training set labeling process and the number and variety of the image set that feeds the "other species" class. The model that distinguished the state of conservation ("complete body" or "fragmented") was the model with the most unstable prediction. This can be explained by noise in the training set, labeling process, or inadequacy of the pre-trained model (Fig.30).

The morphological features model is a detailed object detection model that focuses on a single morphological feature (body, apical horn, or antapic horns). This was the model with the best prediction performance. The results obtained by testing the previously published dinoflagellate cysts match our CNN models with high accuracy (Fig.29).

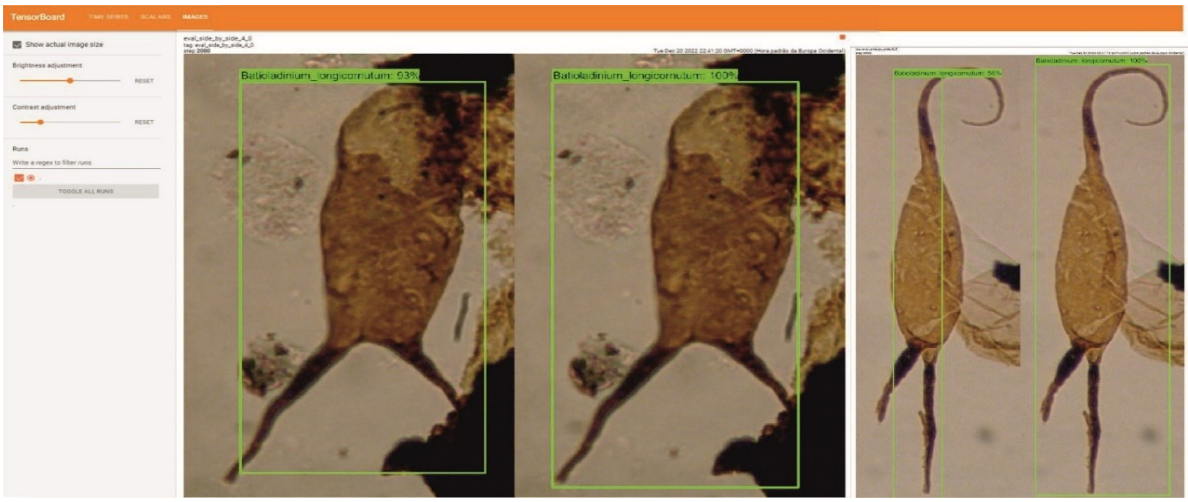

Figure 29. Evaluation phase results from the pre-published Early Cretaceous palynology articles. Batioladinium longicornutum (Nohr-Hansen, 1998).

Some examples illustrating the capabilities and performance of the methodology:

Incomplete Specie Detection:

In our research, we found that the methodology exhibits a remarkable capability to identify *B. longicornutum*, even when the specimen is not fully visible in the image. For instance, in

microscopic images where only a part of the species is within the frame or when the specimen's boundaries are not clearly defined, the algorithm can still recognize and classify it as *B. longicornutum*. However, it's important to note that in such situations, the algorithm's confidence level may vary. The confidence score provided by the algorithm reflects the degree of certainty it has in classifying the specimen. In cases of incomplete or partially visible specimens, the confidence score may be lower due to the reduced amount of information available in the image.

Apical Horn Identification:

Our research revealed that the methodology is highly adept at identifying specific morphological features, such as the apical horn of *B. longicornutum*, even when the horn is not well-preserved or is partially obscured in the image. This is a significant finding, as it demonstrates the methodology's robustness in characterizing specific attributes of the species. Whether the apical horn is damaged, partially hidden, or not clearly distinguishable, the algorithm can still recognize and classify it as a defining characteristic of *B. longicornutum*.

Multi-Species Environments:

In real-world applications, our methodology excels at identifying *B. longicornutum* in complex environments where images contain multiple species. We conducted tests using images with diverse collections of microscopic specimens, often including tens of different species. The results were impressive, as the methodology consistently and accurately pinpointed and identified *B. longicornutum*, even in the presence of a multitude of other species. The algorithm's ability to distinguish the target species from a complex background of other species is a testament to its accuracy and adaptability.

These detailed descriptions and examples emphasize the methodology's versatility and precision in species detection, even in challenging and varied research scenarios. They offer valuable insights into the methodology's capabilities and can be included in your research article to support your findings.

To improve the models' accuracy and reliability, it is essential to continue developing more specific and detailed models that can capture unique morphological and structural characteristics of dinoflagellate cysts. This would enable more precise classification and identification of the species of interest, enhancing the models' overall performance (Fig.30).

Therefore, future research should focus on developing more comprehensive and diverse

datasets specifically on the Train dataset (1) and make it able to detect other species separately with their original names. Also, to focus on the picture of whole palynology slide to run algorithm in one time.

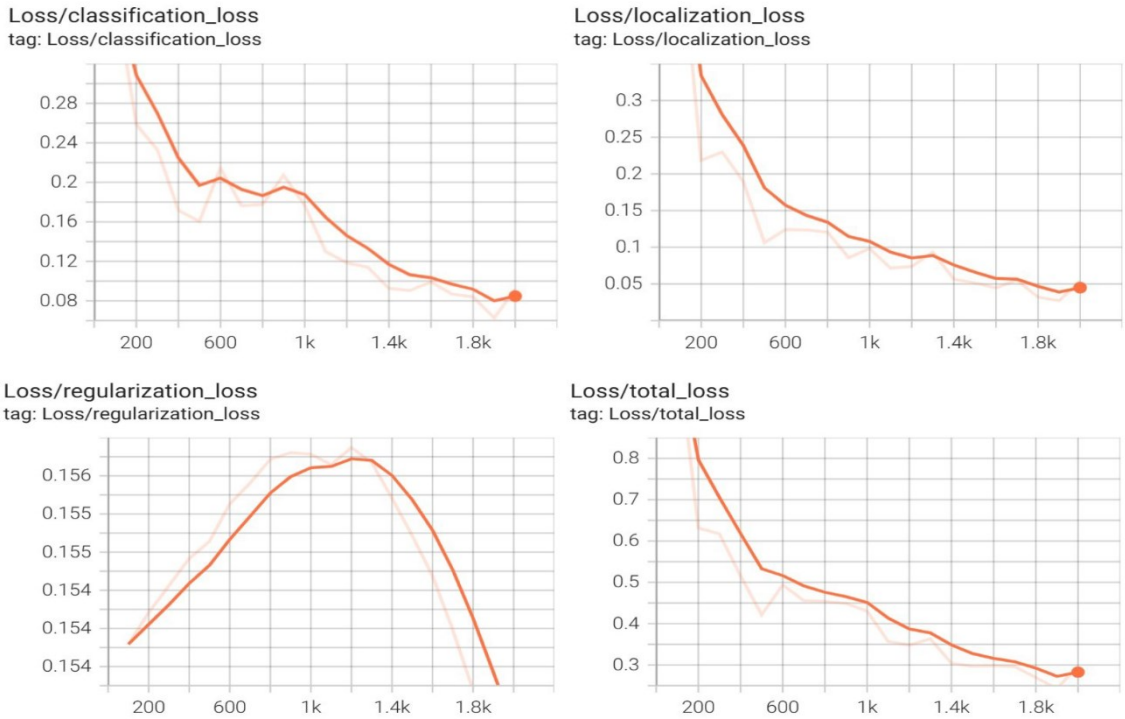

Figure 30. Loss graphs through the training process. Created in Tensorboard

8.6. Conclusion

The methodology allows for an automatic detection approach of the species *B. longicornutum,* its conservation status and some morphological characteristics.

The classification and detection of *B. longicornutum* depends on the quality of the training set labeling process and the number and variety of the image set that feeds the "other species" class.

The model that distinguished the state of conservation ("complete body" or "fragmented") was the model with the most frightening prediction. It can be justified by noise in the training set, labeling process, or inadequacy of the pre-trained model.

The morphological features model is a detailed object detection model that focuses on a single morphological feature (body, apical horn, or antapical horns). It was the model with the best prediction performance.

Algortihm shows in the that the can be weak when there are more data of a similar nature around the object, the size of the object decreases in the photo, and the consistency of the algorithm decreases (Fig.31).

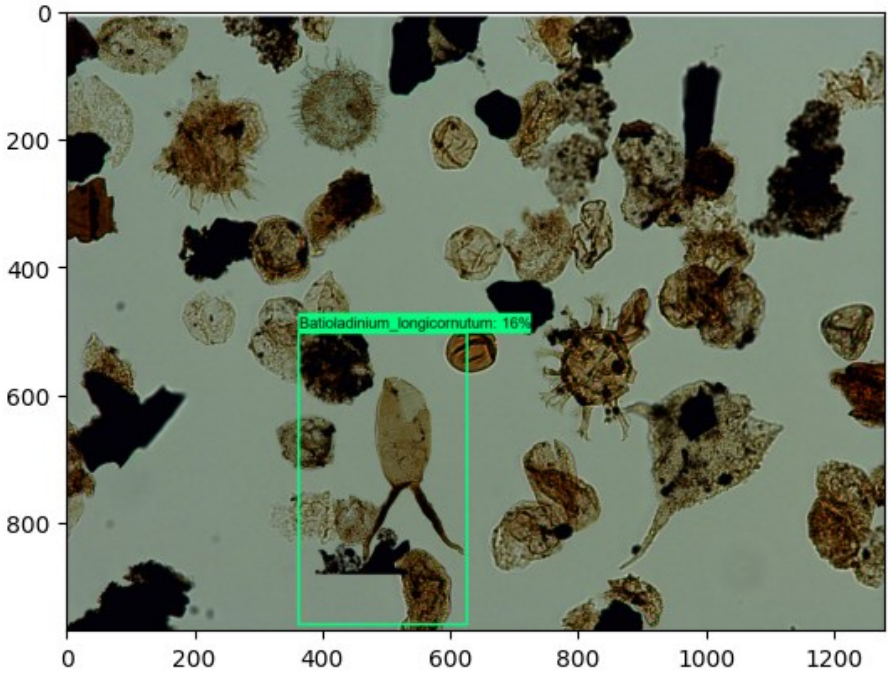

Figure 31. The detection result of the focused species from the 20x magnification slide view.

9

CONCLUSION

The examination of the Munk Marl Bed (MMB) through detailed palynological analysis and the assessment of various fossils has significantly contributed to understanding its stratigraphic placement within the Hauterivian to Barremian interval. Key species such as *Stanfordella fastigiata, Muderongia crucis, Kleithsphaeridium corrugatum*, alongside other identified taxa, serve as crucial markers defining the Early Barremian age within this geological context. Their presence and distribution, along with dinoflagellate cysts, spores, and pollen diversity within the MMB, offer valuable insights into environmental changes and transitions occurring in this interval. These variations indicate shifts in environmental conditions and potential lithological differences influencing palynomorph preservation and distribution.

However, there are exist discrepancies in the literature concerning the exact age and environmental conditions associated with the MMB. Some studies propose varying interpretations, suggesting deposition during the early Barremian, potentially extending into the late Barremian, and hinting at environmental shifts within this stratigraphic interval.

The debate regarding whether the MMB represents a flooding surface or a lowstand system tract adds complexity to its interpretation. Recent studies challenge the traditional concept of the MMB as a flooding surface, instead proposing it as a lowstand system tract. These conflicting interpretations underscore the necessity for further research to gain a more nuanced understanding of the environmental factors contributing to the MMB's deposition.

The presence of organic-rich deposits raises intriguing questions about prevailing climatic conditions, potential anoxic environments, and the mechanisms responsible for accumulating such abundant organic material. While factors such as climate and terrigenous run-off are suggested to contribute, the precise deposition mechanism remains under ongoing investigation.

In summary, the examination of the Munk Marl Bed is a complex endeavor characterized by identifying key stratigraphic markers, exploring diverse fossil assemblages, and ongoing debates surrounding its precise age, depositional environment, and factors responsible for the abundant

organic-rich material. Addressing these complexities will enhance our understanding of stratigraphy and paleoenvironmental dynamics within the Hauterivian to Barremian interval in the North Sea Basin. Interdisciplinary studies and refined analyses are necessary to unravel the intricacies surrounding the MMB.

Moreover, the intensive analysis of composited drilling core samples from well 16/2-21 has enabled ultra-high-resolution age-dating through palynostratigraphy. Comparison of identified key diagnostic palynomorphs with an established reference zonation scheme enhances biostratigraphic accuracy, emphasizing the rich and diverse palynomorph assemblage in the region. This research underscores the significance of palynostratigraphy in age-dating and reconstructing paleoenvironments in marine sedimentary deposits. These findings have implications for regional correlation efforts and in comprehensively understanding the geological formations in the Utsira High area.

The presence of species like *Stanfordella fatigiata, Kleitosphaeridium corrugaum*, and *Muderongia crucis* as definitive markers enables the delineation of the Early Barremian age. The high-resolution sampling within the Munk Mark Bed offers additional information for defining this stratigraphic interval and has implications for regional correlation efforts and enhancing our understanding of the geological formations in the Utsira High area. Further studies on other Munk Marl cores across the North Sea Basin would facilitate direct age comparison and provide a more comprehensive regional perspective.

BIBLIOGRAPHY

Abbink, O. A. (1998). Dinoflagellate cysts from the Hauterivian–Barremian (Lower Cretaceous) of the Lusitanian Basin, Portugal. Palaeontographica, Abteilung B, 251(1-6), 1-82.

Ainsworth, N. R., Riley, L. A., & Gallagher, L. T. (2000). An Early Cretaceous lithostratigraphic and biostratigraphic framework for the Britannia Field reservoir (Late Barremian-Late Aptian), UK North Sea. Petroleum Geoscience, 6(4), 345–367. https://doi.org/10.1144/petgeo.6.4.345

Alberti, G. (1961). Zur Kenntnis mesozoischer und altertiärer Dinoflagellaten. Neues Jahrbuch für Geologie und Paläontologie, Abhandlungen, 112, 1–58.

Baltes, N. (1967). Dinoflagellate cysts from the Albian of the Rumanian Plain. Revista Española de Micropaleontología, 19(2), 375-391.

Barclay, R., McElwain, J., Dilcher, D., & Sageman, B. (2007). The cuticle database: Developing an interactive tool for taxonomic and paleoenvironmental study of the fossil cuticle record. CFS Courier Forschungsinstitut Senckenberg, 258, 39–55.

Below, R. (1982). Kiokansium, eine neue Dinoflagellaten-Gattung aus dem Cenomanian von England. Geologisches Jahrbuch, A62, 33-36.

Bercovici, A., & Vellekoop, J. (2017). Methods in Paleopalynology and Palynostratigraphy: An Application to the K-Pg Boundary. An Application to the K-Pg Boundary. In Terrestrial Depositional Systems: Deciphering Complexities through Multiple Stratigraphic Methods (Issue December). https://doi.org/10.1016/B978-0-12-803243-5.00003-0

Bercovici, Antoine. (2017). Methods in Paleopalynology and Palynostratigraphy : An Application to the K-Pg Boundary (Issue April 2018). https://doi.org/10.1016/B978-0-12-803243-5.00003-0

Blok, C. N., Ineson, J., Anderskouv, K., Fantasia, A., Sheldon, E., Thibault, N., Jelby, M. E., Adatte, T., & Bodin, S. (2022). Latitude-dependant climate changes across the Aptian Oceanic Anoxic Event 1a. Palaeogeography, Palaeoclimatology, Palaeoecology, 601(June), 111085. https://doi.org/10.1016/j.palaeo.2022.111085

Bøe, R., Fossen, H., & Smelror, M. (2010). Mesozoic sediments and structures onshore Norway and in the coastal zone. NGU Bulletin, 450(January), 15–32.

Bøe, R., Smelror, M., Davidsen, B., & Walderhaug, O. (2008). Nearshore Mesozoic basins off Nordland, Norway: Structure, age and sedimentary environment. Marine and Petroleum Geology, 25(3), 235–253. https://doi.org/10.1016/j.marpetgeo.2007.07.004

Brideaux, M.-T. (1975). Taxonomic studies of the Mesozoic dinoflagellate genera Batioladinium and Oligosphaeridium. Geological Survey of Canada Bulletin, 244, 1–84.

Buchem, F. S. P. van, Hantschel, T., & Weitschat, W. (2017). Biostratigraphy of the Lower Cretaceous (Berriasian–Barremian) of the Boreal and Tethys realms. Cretaceous Research, 73, 14-30.

Bujak, J. P., & Foundation, T. A. (2018). Microfossils: Palynology. June. https://doi.org/10.1007/978-3-319-02330-4

Cookson, I. C., & Eisenack, A. (1958). Microplankton from the Australian Lower Cretaceous. Proceedings of the Linnean Society of New South Wales, 83, 103-120.

Copestake, P. (2003). Palynology of the Hauterivian–Barremian (Lower Cretaceous) of the North Sea Basin: correlation and palaeoenvironmental implications. Cretaceous Research, 24(2), 185-211.

Crittenden, S., Cole, J., & Harlow, C. (1991). the Early To "Middle" Cretaceous Lithostratigraphy of the Central North Sea (Uk Sector). Journal of Petroleum Geology, 14(4),

387–416. https://doi.org/10.1111/j.1747-5457.1991.tb01033.x

Davey, R. J. (1966). Some dinoflagellates from the English Chalk. Bulletin of the British Museum (Natural History), Geology, 11, 483-533.

Davey, R. J. (1969). Non-calcareous microplankton from the Cenomanian of England and northern France. Bulletin of the British Museum (Natural History), Geology, 17, 1–200.

Davey, R. J. (1974). *Cassiculosphaeridia magna* n. sp. from the Cenomanian of England. Geoscience and Man, 10, 11–14.

Davey, R. J. (1979). Dinocysts from the Boreal Lower Cretaceous (Berriasian–Aptian). Palaeontographica, Abteilung B, 168(1-4), 73-120.

Davey, R. J. (2001). A summary of the palynology of the lower Hauterivian (Lower Cretaceous) from Speeton, east England. Neues Jahrbuch Für Geologie Und Paläontologie - Abhandlungen, 219(1–2), 83–93. https://doi.org/10.1127/njgpa/219/2001/83

Davey, R. J., & Verdier, A. (1974). Dinocysts from the uppermost Jurassic and lowermost Cretaceous of the Paris Basin. Palaeontology, 17(3), 609-664.

Davey, R. J., & Verdier, J. (1976). Dinoflagellate cysts from the Turonian of the Paris Basin and their implications for dinoflagellate classification. Palaeontology, 19, 731-772.

Davey, R. J., & Williams, G. L. (1966). The genus Hystrichosphaeridium and its allies. Bulletin of the British Museum (Natural History), Geology, 13, 103-168.

Deflandre, G. (1935). Considérations biologiques sur les microorganismes d'origine planctonique conservés dans les sédiments anciens. Annales de la Société Géologique de France, 109, 123-151.

Deflandre, G. (1939). Microplancton du Jurassique supérieur du Calvados. Bulletin de la

Société Linnéenne de Normandie, 8, 203–220.

Dettmann, M. E. (1963). Triassic palynology of the Clarence-Moreton Basin, New South Wales. Australian Journal of Botany, 11(3), 285–349.

Downie, C. (1973). Observations on the nature of the acritarchs.

Downie, R. A. (1973). Acritarchs and the continental sedimentary record. In The Precambrian, 327–356.

Duxbury, M. (2023). The Munk Marl Bed (Lower Cretaceous) of the North Sea Basin: a review of its palynology, age and depositional environment. Earth-Science Reviews, 233, 104124.

Duxbury, S. (1977). A palynological investigation of the type section of the Dunvegan Formation (Upper Jurassic) at the Grand Rapids of the Athabasca River, Alberta. Geological Survey of Canada Bulletin, 261, 1-62.

Duxbury, Stan. (2023). Organic-walled marine microplankton from the Hauterivian and early Barremian of the North Sea Region-biostratigraphy and taxonomy. Micropaleontology, 69(2), 113–258. https://doi.org/10.47894/mpal.69.2.01

Duxbury, Stanley. (1977). A palynostratigraphy of the Berriasian to Barremian of the Speeton Clay of Speeton, England. Palaeontographica, Abteilung B, 160(1–3), p.17-67, pl.1–15.

Eisenack, A. (1958). Microplankton aus dem norddeutschen Apt. Neues Jahrbuch für Geologie und Paläontologie, Abhandlungen,106, 383-422.

Eisenack, A. (1958). Mikroplankton aus dem Norddeutschen Apt. Geologisches Jahrbuch, 77, 3-18.

Erba, E. (1996). Dinoflagellate cysts from the Hauterivian–Barremian interval of the western

Tethys. Bollettino della Società Paleontologica Italiana, 35(2), 271-338.

Evitt, W. R. (1985). Sporopollenin dinoflagellate cysts: their morphology and interpretation. Amer Assn of Stratigraphic.

Faegri, K., & Iversen, J. (2000). Textbook of pollen analysis 4th ed.). Springer.

Fensome, R. A., Taylor, F. J. R., Norris, G., Sarjeant, W. A. S., Wharton, D. I., & Williams, G. L. (1993). A classification of living and fossil dinoflagellates. Micropaleontology, 38, 81–216.

Francine, M. (1993). ACRITARCHS: A REVIEW. Biol. Rev., 68, 475–538.

Glad, A. C., Amour, F., Welch, M. J., Clausen, O. R., Anderskouv, K., Ineson, J. R., Sheldon, E., & Nick, H. M. (2022). Natural fractures and discontinuities in a Lower Cretaceous chalk-marlstone reservoir, Valdemar Field, Danish North Sea. Marine and Petroleum Geology, 136(November), 105445. https://doi.org/10.1016/j.marpetgeo.2021.105445

Gocht, H. (1957). Mikroplankton aus dem nordwestdeutschen Wealden. Geologisches Jahrbuch, 74, 59-188.

Gocht, H. (1959). Mikroplankton aus dem Alb von Lehrte (bei Hannover). Geologisches Jahrbuch, 76, 1-100.

Gowland, S., Taylor, A. M., & Martinius, A. W. (2018). Integrated sedimentology and ichnology of Late Jurassic fluvial point-bars – facies architecture and colonization styles (Lourinhã Formation, Lusitanian Basin, western Portugal). Sedimentology, 65(2), 400–430. https://doi.org/10.1111/sed.12385

Graversen, O. (2016). Upper Triassic – Cretaceous stratigraphy and structural inversion offshore SW Bornholm , Tornquist Zone ,. December 2004. https://doi.org/10.37570/bgsd-2004-51-08

Habib, D. (1975). Neocomian Dinoflagellate Zonation in the Western North Atlantic. Micropaleontology, 21(4), 373. https://doi.org/10.2307/1485290

Habib, D. (1978). Dinoflagellate cysts from the Upper Jurassic and Lower Cretaceous sediments of the offshore Gippsland Basin, Southeast Australia. Palaeontographica, Abteilung B, 168(1-4), 121-194.

Habib, D., & Drugg, W. S. (1983). *Kallosphaeropsis* and associated dinoflagellate cysts from the Upper Jurassic and Lower Cretaceous of the North Sea. Palynology, 7, 1-27.

Helenes, J. (1997). Stanfordella fastigiata gen. et sp. nov., a new dinoflagellate cyst from the Late Cretaceous of the Great Valley Sequence, California. Journal of Paleontology, 71, 951-953.

Hoppenrath, M. (2017). Dinoflagellate taxonomy — a review and proposal of a revised classification. Marine Biodiversity, 47(2), 381–403. https://doi.org/10.1007/s12526-016-0471-8

Horikx, M., Heimhofer, U., Dinis, J., & Huck, S. (2014). Integrated stratigraphy of shallow marine Albian strata from the southern Lusitanian Basin of Portugal. Newsletters on Stratigraphy, 47(1), 85–106. https://doi.org/10.1127/0078-0421/2014/0041

Hughes, N. F. (1989). Geological Magazine, 126(2), 205–206. https://doi.org/10.1017/s0016756800006440

Ineson, J. R., Lauridsen, B. W., Lode, S., Sheldon, E., Sørensen, H. O., Wisshak, M., & Anderskouv, K. (2022). A condensed chalk–marl succession on an Early Cretaceous intrabasinal structural high, Danish Central Graben: Implications for the sequence stratigraphic interpretation of the Munk Marl Bed. Sedimentary Geology, 440, 106234. https://doi.org/https://doi.org/10.1016/j.sedgeo.2022.106234

Ineson, J. R., Petersen, H. I., Andersen, C., Bjerager, M., Jakobsen, F. C., Kristensen, L., Mørk, F., & Sheldon, E. (2022). Early Cretaceous stratigraphic and basinal evolution of the Danish

Central Graben: a review. Bulletin of the Geological Society of Denmark, 71(September), 75–98. https://doi.org/10.37570/bgsd-2022-71-05

Isaksen, D., & Tonstad, K. (1989). NPD-BULLETIN NO 5: A revised cretaceous and tertiary lithostratigraphic nomenclature for the Norwegian North Sea, 1–79.

Islam, M. A. (1993). Downiesphaeridium, a new dinoflagellate genus from the Cretaceous of Bangladesh. Micropaleontology, 39, 353-356.

Jakobsen, F., Ineson, J. R., Kristensen, L., & Stemmerik, L. (2004). Characterization and zonation of a marly chalk reservoir: The Lower Cretaceous Valdemar field of the Danish Central Graben. Petroleum Geoscience, 10(1), 21–33. https://doi.org/10.1144/1354-079303-584

Jardiné, S., Tambareau, Y., Magniez-Jannin, F., & Leffingwell, H. C. (1984). Dinoflagellate cysts from the Upper Jurassic and lowermost Cretaceous of the Purbeck Formation of southern England. Journal of Micropalaeontology, 3(1), 47-77.

Jelby, M. E., Ineson, J. R., Thibault, N., Bodin, S., Blok, C. N., Edvardsen, N., Clemmensen, T. S., Buls, T., & Anderskouv, K. (2022). Facies and depositional processes of Lower Cretaceous carbonates, Danish Central Graben. Bulletin of the Geological Society of Denmark, 71(August), 51–74. https://doi.org/10.37570/bgsd-2022-71-04

Jensen, T. F., Holm, L., Frandsen, N. and Michelsen, O. (1986). Jurassic-Lower Cretaceous lithostratigraphic nomenclature for the Danish Central Trough. Danmarks Geol. Underssogelse, 12 (Series A), 7–65.

Jeremiah, J. A. (2000). Palynology of the Hauterivian–Barremian (Lower Cretaceous) of the North Sea Basin: Implications for correlation and palaeoenvironment. Unpublished PhD thesis, University of Aberdeen.

Kemp & Cook. (1997). Paleopalynology. Oxford University Press.

Klement, K. (1957). Über einige neue und interessante Dinoflagellaten-Gattungen aus dem Jura. Geologisches Jahrbuch, 73, 57-66.

Klement, K. (1960). Systematophora, eine neue Dinoflagellatengattung aus dem Jura. Geologisches Jahrbuch, 77, 101-104.

Kofoid, C. A. (1907). The plates of Ceratium with a note on the unity of the genus.

Lauridsen, B. W., Lode, S., Sheldon, E., Frykman, P., Anderskouv, K., & Ineson, J. (2022). Lower Cretaceous (Hauterivian–Aptian) pelagic carbonates in the Danish Basin: new data from the Vinding-1 well, central Jylland, Denmark. Bulletin of the Geological Society of Denmark, 71, 7–29. https://doi.org/10.37570/bgsd-2022-71-02

Leereveld, H. (1997). Dinoflagellate cysts from the Hauterivian and Barremian (Lower Cretaceous) of the Tethyan region: systematics and biostratigraphy. Mededelingen Rijks Geologische Dienst, 58, 1-39.

Leereveld, H. (1997). Upper Tithonian – Valanginian (Upper Jurassic – Lower Cretaceous) dinoflagellate cyst stratigraphy of the western Mediterranean, 1, 385–420.

Mantell, G. A. (1850). On the vegetable structure of some fossil ferns from the coal strata of Tasmania. Papers and Proceedings of the Royal Society of Tasmania,1, 293-297.

Martinsen, O. J., & Dreyer, T. (2001). Sedimentary environments offshore Norway. Palaeozoic to Recent: an introduction, 1–5.

Masure, E. (1998). Dinoflagellate cysts from the Hauterivian–Barremian (Lower Cretaceous) of the Lusitanian Basin, western Portugal. Palaeontographica, Abteilung B, 251(1-6), 1-82.

Miljeteig, K. I. (2016). Late Triassic (early Carnian) palynology of the shallow stratigraphic core 7830/3-U-1, offshore Kong Karls Land, Northern Barents Sea.

Møller, J. M., Jenkyns, H. C., Riding, J. B., Leng, M. J., & Duarte, L. V. (2019). Organic-rich mudstones in the Hauterivian–Barremian (Lower Cretaceous) of the Boreal realm: Implications for climate and ocean redox conditions. Palaeogeography, Palaeoclimatology, Palaeoecology, 514, 58-79.

Moore et al. (1991). Pollen Analysis. 2nd Edition. Blackwell.

Morgenroth, P. (1966). Neue Dinoflagellaten und Hystrichosphaeren aus dem Emscher und Untersenon von NW-Deutschland. Geologisches Jahrbuch, 75, 241-279.

Mutterlose, J., & Harding, I. C. (1987). Phytoplankton from the anoxic sediments of the Barremian (Lower Cretaceous) of North-West-Germany. In Abhandlungen der Geologischen Bundesanstalt, vol. 39.

Neale, J. W., & Sarjeant, W. A. S. (1962). Microplankton from the Cretaceous of the Canadian Arctic. Bulletin of the Geological Survey of Canada, 83, 1–57.

Neale, J. W., & Sarjeant, W. A. S. (1962). Microplankton from the Cretaceous of the Canadian Arctic. Bulletin of the Geological Survey of Canada, 83, 1-57.

Nøhr-Hansen, H. (1994). Dinoflagellate cyst stratigraphy of the Barremian to Albian, Lower Cretaceous, North-East Greenland - a summary. Rapport Grønlands Geologiske Undersøgelse, 160, 68–72. https://doi.org/10.34194/rapggu.v160.8234

Nohr-Hansen, H., Damsté, J. S. S., & Fietz, S. (2019). Dinoflagellate cysts, biomarkers and palaeoenvironments of the Hauterivian–Barremian (Lower Cretaceous) succession of the Jameson Land Basin, East Greenland. Palaeontology, 62(3), 469-501.

Nohr-Hansen, H., Piasecki, S., & Alsen, P. (2020). A Cretaceous dinoflagellate cyst zonation for NE Greenland. In Geological Magazine, vol. 157, Issue 10. https://doi.org/10.1017/S0016756819001043

Ogg, G. (1994). Dinoflagellate cysts of the Early Cretaceous North Atlantic Ocean. Marine Micropaleontology, 23(3), 241–263. https://doi.org/10.1016/0377-8398(94)90015-9

Olsen, H., Briedis, N. A., & Renshaw, D. (2017). Sedimentological analysis and reservoir characterization of a multi-darcy, billion barrel oil field – The Upper Jurassic shallow marine sandstones of the Johan Sverdrup field, North Sea, Norway. Marine and Petroleum Geology, 84, 102–134. https://doi.org/10.1016/j.marpetgeo.2017.03.029

Oosting, A. M., Leereveld, H., Dickens, G. R., Henderson, R. A., & Brinkhuis, H. (2006). Correlation of Barremian-Aptian (mid-Cretaceous) dinoflagellate cyst assemblages between the Tethyan and Austral realms. 27. https://doi.org/10.1016/j.cretres.2006.03.012

Ottesen, S., Selvikvåg, B., Scott, A. S. J., Meneguolo, R., Cullum, A., Amilibia-Cabeza, A., Vigorito, M., Helsem, A., & Martinsen, O. J. (2022). Geology of the Johan Sverdrup field: A giant oil discovery and development project in a mature Norwegian North Sea basin. AAPG Bulletin, 106(4), 897–936. https://doi.org/10.1306/11042120037

Palsys (2023). https://palsys.org/genus

Paolillo, M. A., Guler, M. V., Lazo, D. G., Pazos, P. J., Ottone, E. G., & Aguirre-Urreta, B. (2018). Early Cretaceous Dinoflagellate Cysts from the Agrio Formation at Its Type Locality (Neuquén Basin, Argentina) and Their Biostratigraphic Implications. Ameghiniana, 55(5), 554–570. https://doi.org/10.5710/AMGH.26.04.2018.3176

Pearce, M. A., Jarvis, I., Ball, P. J., & Laurin, J. (2020). Palynology of the Cenomanian to lowermost Campanian (Upper Cretaceous) Chalk of the Trunch Borehole (Norfolk, UK) and a new dinoflagellate cyst bioevent stratigraphy for NW Europe. Review of Palaeobotany and Palynology, 278. https://doi.org/10.1016/j.revpalbo.2020.104188

Poulsen, N. E., & Riding, J. B. (2003). Dinoflagellate cyst biostratigraphy of the type Berriasian (Lower Cretaceous) of southeastern France. Cretaceous Research, 24(2), 125-155.

Punt, W., Hoen, P. P., Blackmore, S., Nilsson, S., & Le Thomas, A. (2007). Glossary of pollen

and spore terminology. Review of Palaeobotany and Palynology, 143(1–2), 1–81. https://doi.org/10.1016/j.revpalbo.2006.06.008

Quattrocchio, M. E., Martínez, M. A., Pavisich, A. C., & Volkheimer, W. (2006). Early Cretaceous palynostratigraphy, palynofacies and palaeoenvironments of well sections in northeastern Tierra del Fuego, Argentina. Cretaceous Research, 27(4), 584–602. https://doi.org/10.1016/j.cretres.2005.11.012

Rasmussen, C. M. Ø., Jenkyns, H. C., Forster, A., Halimeda, G. P., & Riding, J. B. (2017). Environmental and biological changes across the Hauterivian–Barremian (Early Cretaceous) boundary in the Boreal realm. Palaeogeography, Palaeoclimatology, Palaeoecology, 485, 1-24.

Rawson, P. F., & Mutterlose, J. (1983). Ammonite biostratigraphy of the Lower Cretaceous in northwestern Europe. Zeitschrift der Deutschen Geologischen Gesellschaft, 134(1), 1-81.

Retallack, G. J. (2001). A 300-million-year record of atmospheric carbon dioxide from fossil plant cuticles. Nature, 411(6835), 287–290. https://doi.org/10.1038/35077041

Riding, J. B., & Crame, J. A. (2002). Aptian to Coniacian (Early-late Cretaceous) palynostratigraphy of the Gustav Group, James Ross Basin, Antarctica. Cretaceous Research, 23(6), 739–760. https://doi.org/10.1006/cres.2002.1024

Riding, J. B., Pound, M. J., Hill, T. C. B., & Stukins, S. (2012). The John Williams Index of Palaeopalynology Susanne Feist-Burkhardt Published by Taylor & Francis , Ltd . on behalf of the American Association of Stratigraphic Palynologists Stable URL : https://www.jstor.org/stable/41811780 REFERENCES Linked reference. 36(2), 224–233.

Rønnevik, H. C., Jørstad, A., & Lie, J. E. (2017). The discovery process behind the giant johan sverdrup field. AAPG Memoir, 113(January), 195–220. https://doi.org/10.1306/13572008M1133687

Sarjeant, W. A. S. (1966). Dinoflagellate cysts from the Lower Cretaceous of the Speeton Clay, Yorkshire. Paleontology, 9, 210–211.

Sarjeant, W. A. S. (1966). Dinoflagellate cysts from the Purbeck Beds (Upper Jurassic) of southern England. Palaeontology, 9(4), 631-672.

Sarjeant, W. A. S. (1966). Dinoflagellate cysts with gonyaulacoid archeopyle, Part I: Cenozoic and Mesozoic forms. Proceedings of the Royal Society of London B: Biological Sciences, 164, 1-36.

Silva, I. P., Barreiros, N., & Pereira, P. (2020). Dinoflagellate cysts from the Hauterivian–Barremian (Lower Cretaceous) boundary interval of the Lusitanian Basin, Portugal: implications for biostratigraphy and palaeoenvironment. Cretaceous Research, 104514.

Skupien, P., & Mohamed, O. (2008). Campanian to Maastrichtian palynofacies and dinoflagellate cysts of the Silesian Unit, Outer Western Carpathians, Czech Republic. Bulletin of Geosciences, 83(2), 207–224. https://doi.org/10.3140/bull.geosci.2008.02.207

Tahoun, S. A., & Led, J. (2018). Dinoflagellate cyst stratigraphy of the Hauterivian–Barremian interval in northern Egypt: implications for palaeoenvironment and regional correlation. Cretaceous Research, 85, 20-40.

Traverse, A. (2007). Paleopalynology. 2nd Edition.

Tyson, R. V. (1985). Palynology of the early Cretaceous (Barremian) Munk Marl Bed, Danish North Sea. Palaeontology, 28(4), 809–842.

Tyson, R. V. (1985). Palynofacies and sedimentology of some Late Jurassic sediments from the British Isles and northern North Sea. PhD Thesis, 1–623. https://doi.org/10.21954/ou.ro.0000de4f

Upchurch, G. R. (1995). Dispersed angiosperm cuticles: Their history, preparation, and

application to the rise of angiosperms in Cretaceous and Paleocene coals, southern western interior of North America. International Journal of Coal Geology, 28(2–4), 161–227. https://doi.org/10.1016/0166-5162(95)00018-6

Van Buchem, F. S. P., Smit, F. W. H., Buijs, G. J. A., Trudgill, B., & Larsen, P. H. (2018). Tectonostratigraphic framework and depositional history of the Cretaceous-Danian succession of the Danish Central Graben (North Sea)-new light on a mature area. Petroleum Geology Conference Proceedings, 8(1), 9–46. https://doi.org/10.1144/PGC8.24

Wesenlund, F. (2016). The Petroleum Geochemistry of the Johan Sverdrup Field, Southern Utsira High, Norwegian North Sea. 294.

Williams, G. L. (1975). Dinoflagellate cysts from the Wealden Beds (Early Cretaceous) of Southern England. Palaeontographica, Abteilung B, 153(1-4), 148-206.

Williams, G. L. (2006). Palynology of the Hauterivian–Barremian (Lower Cretaceous) of the North Sea Basin: implications for correlation and palaeoenvironment. Cretaceous Research, 27(1), 1-32.

Zwaan, F. (2019). Lower Cretaceous reservoir development in the North Sea Central Graben, and potential analogue settings in the Southern Permian Basin and South Viking Graben. January. https://doi.org/10.1144/SP469.3

APPENDIX

Plate 1

Scale bar is same for all figures and represent 20 μm

a. *Rhynchodiniopsis aptiana* Deflandre, 1935 (sample 1922.81 m CO).

b. *Circulodinium hirtellum* Alberti, 1961 (sample 1922.95 m CO).

c. *Scriniodinium campanula* Gocht, 1959 (sample 1919.38 m CO).

d. *Hystrichodinium pulchrum* Deflandre, 1935 (sample 1922.81 m CO).

e. *Stanfordella fastigiata* Duxbury, 1977 (sample 1922.81 m CO).

f. *Spiniferites* spp. Mantell, 1850 (sample 1922.58 m CO).

g. *Cassiculosphaeridia magna* Davey, 1974 (sample 1921. 92 m CO).

h. *Cribroperidinium edwardsii* Davey, 1969 (sample 1919.38 m CO).

ı. *Pterodinium alectrolophum* Eaton, 1976 (sample 1919.38 m CO).

j. *Florentinia mantellii* Davey & Williams, 1966 (sample 1922. 58 m CO).

k. *Muderongia crucis* Neale & Sarjeant 1962 (sample 1922.81 m CO).

l. *Kleithriasphaeridium corrugatum* Davey, 1974 (sample 1921.92 m CO).

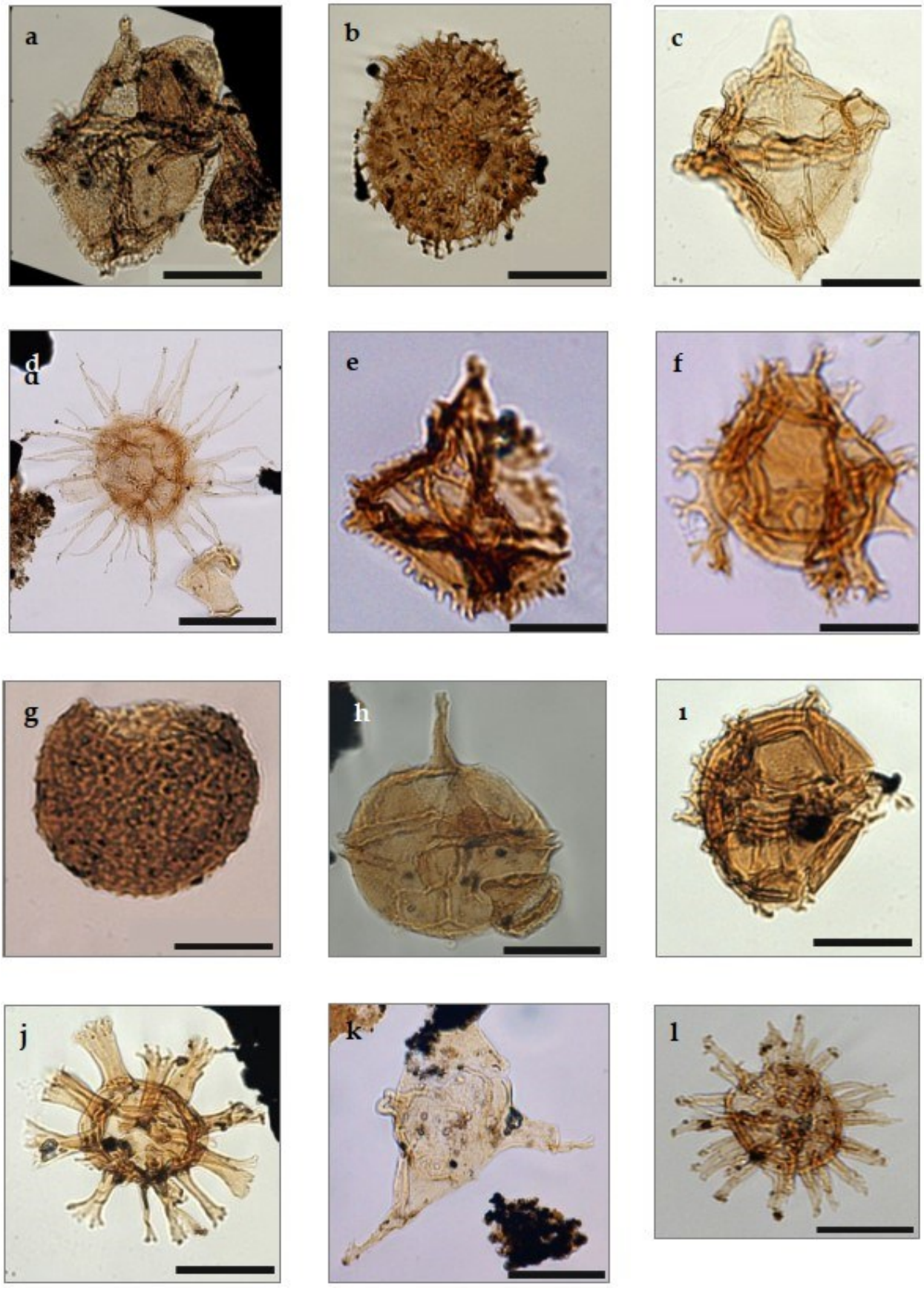

Plate 1

Scale bar is same for all figures and represent 20 μm

Plate 2

Scale bar is same for all figures and represent 20 μm

a. *Pseudoceratium pelliferum* Davies, 1980 (sample, 1922.81 m CO).

b. *Dingodinium albertii* Sarjeant, 1966 (sample, 1919.38 m CO).

c. *Tanyosphaeridium xanthiopyxides* Stover, 1978 (sample, 1922.35 m CO).

d. *Muderongia tetracantha* Gocht, 1957 (sample, 1922.58 m CO).

e. *Tanyosphaeridium spp.* Davey, 1966 (sample, 1922.81 m CO).

f. *Phoberocysta neocomica* Gocht, 1957 (sample, 1922.81 m CO).

g. *Systematophora spp.* Klement, 1960 (sample, 1922.81 m CO).

h. *Florentinia buspina* Davey & Verdier, 1976 (sample, 1922.58 m CO).

j. *Stanfordella fastigiata* Duxbury, 1977 (sample 1922.81 m CO).

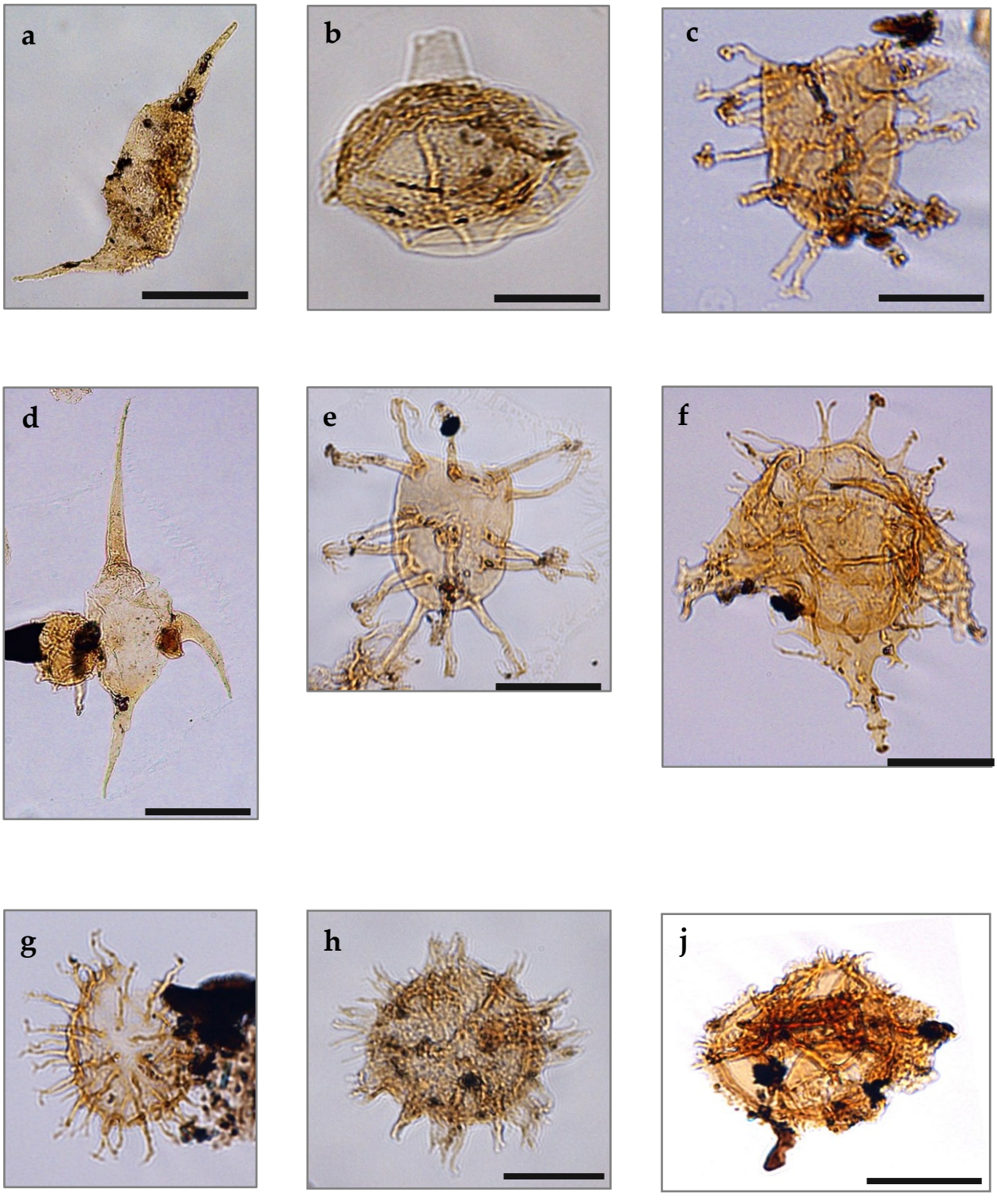

Plate 2

Scale bar is same for all figures and represent 20 μm

Plate 3

Scale bar is same for all figures and represent, 20 μm

a. *Batioladinium longicornutum* Brideaux, 1975 (sample 1922.81 m CO).

b. *Kiokansium unituberculatum* Stover & Evitt, 1978 (sample 1920.75 m CO).

c. *Pseudoceratium pelliferum* Davies, 1980 (sample 1922.81 m CO).

d. *Oligosphaeridium complex* Davey, 1966 (sample 1922.35 m CO).

e. *Muderongia staurota* Sarjeant, 1966 (sample 1922.58 m CO).

f. *Hystrichosphaeridium arborispinum* Davey, 1966 (sample 1922.58 m CO).

g. *Oligosphaeridium abaculum* Davey, 1979 (sample 1922.35 m CO).

h. *Kleithriasphaeridium eoinodes* Davey, 1974 (sample 1922.22 m CO).

j. *Kleithriasphaeridium fasciatum* Davey, 1966 (sample 1922.22 m CO).

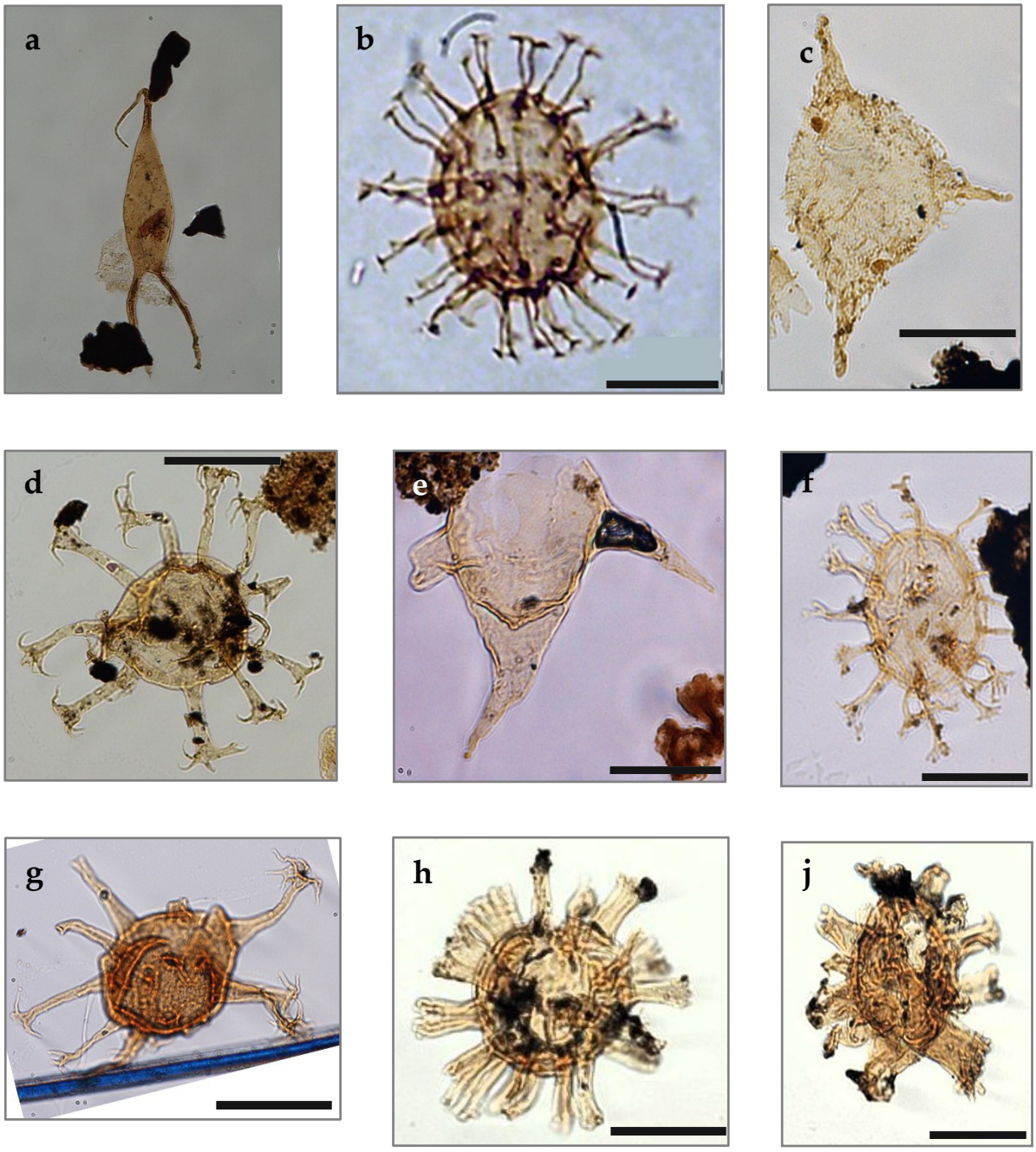

Plate 3

Scale bar is same for all figures and represent 20 μm

Plate 4

Scale bar is same for all pictures and represent, 20 μm

a. *Cyathides minor* Couper, 1953 (sample 1922.81 m CO).

b. *Dictyophyllidites* Couper, 1958 (sample 1921.92 m CO).

c. *Cibotiumspora* Chang, 1965 (sample 1922.81 m CO).

d. *Cyathides minor* Couper, 1953 (sample 1922.81 m CO).

e. *Chasmatosporites* Nilsson, 1958 (sample 1922.58 m CO).

f. *Densoisporites* Weyland & Krieger, 1953 (sample 1922.81 m CO).

g. *Cyathides australis* Couper, 1953 (sample 1922.81 m CO).

h. *Callialasporites* S. Dev, 1961 (sample 1919.38 m CO).

i. *Staplinisporites* Pocock, 1962 (sample 1922.22 m CO).

j. *Cicatricosisporites* Potonié & Gelletich, 1933 (sample 1919.38 m CO).

k. *Retitriletes* Pierce, 1961 (sample 1922.22 m CO).

l. Fulgal spore Fries, 1821 (sample 1919.38 m CO).

m. *Micrhystridium* sp. Deflandre, 1939 (sample 1922.95 m CO).

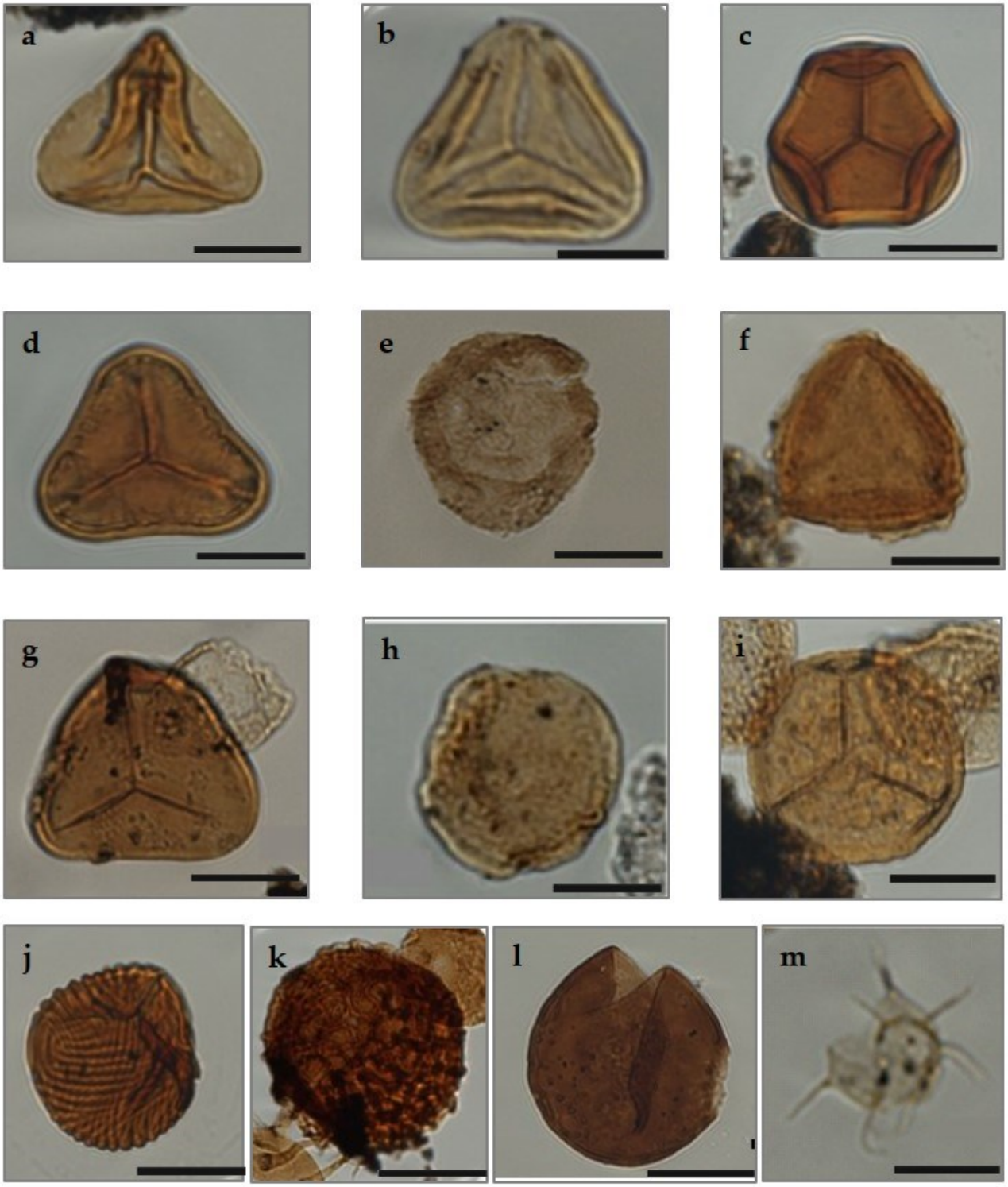

Plate 4

Scale bar is same for all figures and represent 20 μm

Plate 5

Scale bar is same for all figures and represent, 20 μm

a. *Bisaccat**e pollen*** Potonié and Kremp, 1954 (sample 1919.38 m CO).

b. *Deltoidospora* Miner, 1935 (sample 1922,81 m CO).

c. *Classopollis* Pflug 1953 (sample 1919.38 m CO).